Experimental Study of the Melting and Reduction Behaviour of Ore Used in the HIsarna Process

PhD thesis

Yingxia Qu

This research described in this thesis was performed in the department of Materials Science and Engineering of Delft University of Technology in the Netherlands.

Delft University of Technology

This research was carrier out under project number M41.5.09327 in the framework of the Research Program of the Materials Innovation Institute M2i in the Netherlands (www.m2i.nl).

Materials innovation institute

Experimental Study of the Melting and Reduction Behaviour of Ore Used in the HIsarna Process

Proefschrift

ter verkrijging van de graad van doctor
aan de Technische Universiteit Delft;
op gezag van de Rector Magnificus prof. ir. K.C.A.M. Luyben;
voorzitter van het College van Promoties
in het openbaar te verdedigen op 3 september 2013 om 10:00 uur

door

Yingxia Qu

Master of Engineering in Ferrous Metallurgy
Northeastern University, Shenyang, China
geboren te Liaoning, China

Dit proefschrift is goedgekeurd door de promotor:
Prof. dr. R. Boom

Copromotor: Dr. Y. Yang

Samenstelling promotiecommissie:

Rector Magnificus,	voorzitter
Prof. dr. R. Boom,	Technische Universiteit Delft, promotor
Dr. Y. Yang,	Technische Universiteit Delft, copromotor
Prof. dr. P. Taskinen,	Aalto University, Finland
Prof. dr. ir. J. Sietsma,	Technische Universiteit Delft
Prof. dr. J. H.W. de Wit,	Technische Universiteit Delft
Dr. C. Zeilstra,	Tata Steel, Netherlands
Prof. dr. S. Seetharaman,	Warwick University, United Kingdom
Prof. dr. I. Richardson,	Technische Universiteit Delft (Reserve)

Keywords: smelting reduction, smelting cyclone, iron-making, fine iron ore, thermal decomposition, individual particle, iron ore reduction,

ISBN: 978-90-6562-330-0

Copyright ©2013, by Yingxia Qu
quyingxia800@163.com

All rights reserved. No part of the material protected by this copyright notice may be reproduced or utilized in any form or by any means, electronic or mechanical, including photocopying, recording or by any information storage and retrieval system, without permission from the author.

Printed in the Netherlands

To my family…

Contents

Contents i

Chapter 1 Introduction 1

1.1 Background to the present study 1
1.2 Current status of the ironmaking and steelmaking processes 2
1.2.1 Blast furnace ironmaking process 4
1.2.1.1 Conventional blast furnace 4
1.2.1.2 Top gas recycling blast furnace (TGRBF) with CO_2 capture and storage (CCS) 6
1.2.2 Non-blast furnace ironmaking technology 7
1.3 Basic reactions and thermodynamics of the gas solid iron oxide reduction 18
1.3.1 The sequence of reduction of iron oxides with gases 19
1.3.2 Equilibrium between iron oxides and reducing gases 19
1.4 Kinetics of reduction of iron oxides with gases 22
1.4.1 Rate law 22
1.4.2 Reaction rate of iron ore reduction 24
1.5 Determination of rate controlling steps of iron ore reduction 28
1.5.1 Model–fitting methods 29
1.5.2 Model–free methods 33
1.5.2.1 Standard method 33
1.5.2.2 Friedman's method 33
1.6 Objectives and layout of the thesis 34
References 36

Chapter 2 Experimental Apparatus and Analysis Methods 39

2.1 Introduction 39
2.2 High temperature drop tube furnace 41
2.2.1 The furnace 44
2.2.2 The syringe pump feeder 44
2.2.3 Injection probe 45
2.2.4 Sampling probe 50
2.2.5 Sample collector 51
2.2.6 Pre-tests before the experiment 51
2.2.6.1 Syringe pump particle feeder 51
2.2.6.2 Temperature profile and cooling effect in the reactor 52
2.3 TGA – DSC 55
2.4 Electrically heated horizontal furnace 56
2.5 Analysis methods 57
References 59

Chapter 3 Experimental Study on the Thermal Decomposition Behaviour of Iron Ore Particles 61

3.1 Introduction 61
3.2 Theoretical evaluation 63
3.3 Experimental 66
3.3.1 Experimental strategy 66
3.3.2 Materials 67
3.3.3 Experimental conditions 68
3.3.3.1 Thermal decomposition of iron ore in the TGA-DSC 68
3.3.3.2 Thermal decomposition of iron ore in the horizontal furnace 68
3.3.3.3 Thermal decomposition of iron ore in the HDTF 69
3.4. Results and discussion 72
3.4.1 Experimental results with TGA-DSC 72
3.4.1.1 Thermal decomposition of hematite ore 72
3.4.1.2 Thermal decomposition of hematite 77
3.4.2 Experimental results in the horizontal furnace 80
3.4.2.1 Effect of holding time 80
3.4.2.2 Effect of temperature 81
3.4.3 Experimental results in the HDTF 83
3.4.3.1 Effect of temperature and gas 84
3.4.3.2 Effect of residence time 86
3.4.3.3 Effect of particle size 88
3.4.4 Reproducibility tests 89
3.4.5 Summary of the main results 91
3.5 Conclusions 92
References 94

Chapter 4 Reduction Behaviour of Individual Iron Ore Particles in the High Temperature Drop Tube Furnace 95

4.1 Introduction 95
4.2 Experimental procedures 95
4.3 Experimental conditions 96
4.4 Experimental objective and strategy 99
4.5 Experimental results of the iron ore reduction 100
4.5.1 Reduction degree of hematite ore 100
4.5.1.1 Reproducibility testing 100
4.5.1.2 Effect of PCR and H_2 content of the reducing gas 101
4.5.1.3 Effect of particle size 104
4.5.1.4 Effect of experimental temperature 105
4.5.1.5 Discussion 106
4.5.2 Phase changes in the hematite ore 110
4.5.3 Morphological and structural changes during reduction 112
4.5.3.1 Morphology of reduced particles 112

4.5.3.2 Morphology of a single particle 116
4.5.3.3 Internal structure and phase distribution in a single particle: analysis with optical microscope 119
4.5.3.4 Structural changes and phase distribution in a single particle: analysis with SEM-EDS 122
4.6 Conclusions 125
References 127

Chapter 5 Kinetic Modelling of Pre-reduction of Iron Ore Particles 129

5.1 Introduction 129
5.2 Reaction mechanism of iron ore reduction 130
5.2.1 Reduction process 131
5.2.2 Kinetic analysis 133
5.2.2.1 Reduction mechanism of gas-solid particle reduction 133
5.2.2.2 Reduction mechanism of mixed reduction and gas-molten particle reduction 139
5.2.2.3 Effect of partial pressure of reducing gas on the reaction rate constant 141
5.2.2.4 Forward reaction rate constant 144
5.3 Conclusions 146
References 148

Chapter 6 Conclusions and Outlook 151

6.1 Conclusions 151
6.2 Outlook 153

SUMMARY 155

SAMENVATTING 159

APPENDIX A: XRD Pattern 163

ACKNOWLEDGEMENTS 171

CURRICULUM VITAE 173

Chapter 1 Introduction

1.1 Background to the present study

Global warming caused by greenhouse gas has been recognized as a serious environmental issue facing the world in the 21st century. Up to now, the greenhouse gas emissions still increase every year in the world as a total. This increase was primarily caused by an increase in economic output that increased energy consumption across all sectors. Carbon dioxide (CO_2) is one of the five most abundant greenhouse gases in Earth's atmosphere. According to the survey of Orth et al. [1], the iron and steel industry is emitting about 650 million tonnes CO_2 per year and is the largest industrial source of CO_2 emissions due to the energy intensity of steel production and its reliance on carbon-based fuels and reductants. The large volume of steel produced was over 1510 Mt in 2012 [2]. With the growing concern about climate change, steelmakers are faced with the challenge of finding ways of lowering CO_2 emissions without seriously undermining process efficiency or considerably adding to cost.

The ULCOS (Ultra–Low Carbon dioxide (CO_2) Steelmaking) is large research program [3] within the steel industry worldwide, which is looking for solutions to the threat of global warming. It is created by a consortium of 48 European companies and organizations from 15 European countries that have launched a cooperative research & development initiative to enable drastic reduction in CO_2 emissions from steel production. The consortium consists of all major EU steel companies, of gas suppliers and engineering partners, research institutes and universities, and is supported by the European commission. The aim of the ULCOS program is to reduce the CO_2 emissions with today's the most promising ironmaking routes by at least 50 % in 2050. Considerable research has been carried out in the ULCOS program since its start-up in 2004. In order to achieve the ambitious aims of the project, the research program is divided into several stages. The first stage is an initial feasibility study. Within this study over 80 technologies were investigated. This has led to identifying several promising breakthrough technologies that will enable a significant CO_2 reduction in making steel. Finally, in 2006, the decision was taken to focus on the four iron making processes that could lead to a reduction of CO_2 emissions. The four breakthrough technologies identified are:

- Top Gas Recycling Blast Furnace (TGRBF) with CO_2 capture and storage (CCS)
- HIsarna with CCS, a new smelting reduction process (SR)
- ULCORED with CCS, advanced direct reduction
- Electrolysis of iron ore

For the TGRBF, HIsarna and ULCORED, the aim of a 50 % reduction of CO_2 emissions can only be reached if each of these technologies is combined with Carbon Capture and Storage technology. Electrolysis requires the availability of CO_2-free electricity in large quantities. Another option that might reduce the amount of CO_2 emissions in producing steel is the use of carbon from sustainable biomass. Up to now, TGRBF, HIsarna and ULCORED are in the pilot plant phase. Electrolysis of iron ore is the least developed process route currently being studied in ULCOS and it is in the laboratory study phase [4].

1.2 Current status of the ironmaking and steelmaking processes

For the time being, iron production occurs by three routes: namely, blast furnace, direct reduction (DR) and smelting reduction (SR). In 2012, around 1100 Mt/a of hot metal is produced globally by blast furnaces, while worldwide direct reduced iron (DRI) production is about 55.4 Mt/a [2]. It can be seen that about 95 % of pig iron is produced by the blast furnace. Table 1.1 shows the production of hot metal and crude steel in different regions in the world in 2002 and 2012, respectively.

Table 1.1 Pig iron and crude steel production in different region in the world [2]

Region	Pig Iron (PI) and Crude Steel (CS) production in 2002 (Mt/a)			Pig Iron (PI) and Crude Steel (CS) production in 2011 (Mt/a)		
	PI	CS	PI/CS	PI	CS	PI/CS
EU	89.7	158.6	0.56	91.3	169.4	0.54
Other Europe	22.9	45.0	0.51	9.7	37.9	0.26
C.I.S	77.9	99.9	0.78	81.8	111.2	0.74
North America	52.9	123.6	0.43	44.5	121.9	0.37
South America	33.4	40.9	0.82	30.6	46.9	0.65
Africa	7.1	15.7	0.45	4.9	12,9	0.38
Mid-East	2.2	11.9	0.18	2.1	21,6	0.10
Asia	308.9	381.9	0.81	831.4	982.7	0.85
China	169.1	181.7	0.93	654.3	708.8	0.92
Oceania	6.7	8.3	0.81	4.4	5.8	0.76
Total	603.9	885.8	0.68	1754.9	2253.5	0.78
Total DRI	45.1	--------		55.4	--------	

The production of iron is the most energy intensive step in the steelmaking process. Currently, two fundamental routes can be used in steelmaking: an integrated steel plant or a mini-mill. In the integrated steel plant, iron ore is reduced in blast furnaces by coke. For economic and environmental reasons, coal and other fuels

are increasingly injected directly into the blast furnace to replace coke. In the mini-mill, recycled steel and scrap are melted in an Electric Arc Furnace (EAF) and further processed into final products without an iron production step. However, products derived from direct reduction of iron ore without melting (e.g. DRI, HBI (Hot Briquetted Iron)) or cast pig iron may be utilized as feed in addition to scrap steel. EAFs can also be fed with molten iron. Therefore, the product of the smelting reduction process can be fed to mini-mills or integrated plants. Smelting reduction process usually produces hot metal from ore at molten-state without using blast furnace. That's why it is also called alternative iron-making process. Figure 1.1 shows these two routes and the use of the production of SR and DR clearly [5].

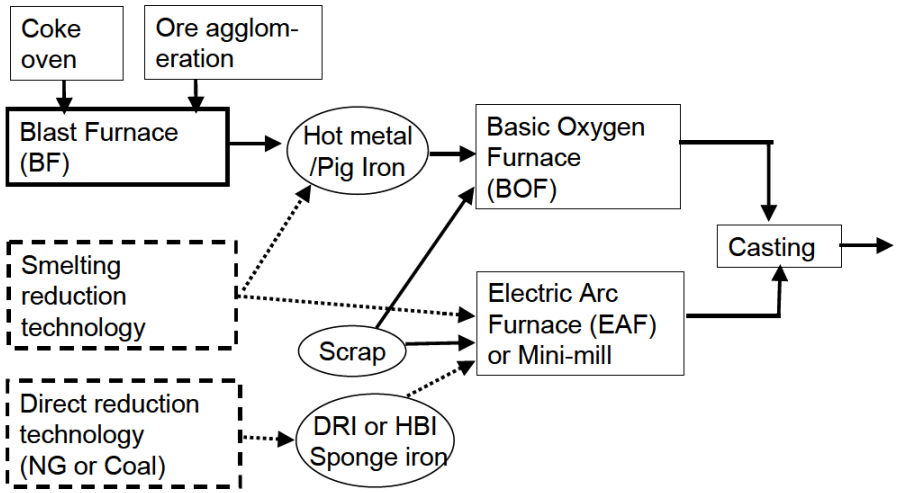

Figure 1.1 Two major routes for producing iron and steel: integrated and mini-mills [6]

Despite the apparent environmental advantages of the new ironmaking technologies, the blast furnace is still predicted to be the single largest process for ironmaking from iron ore until 2050. However, the proportion of blast furnace (BF) - basic oxygen furnace (BOF) steelmaking could drop to 40 % in 2050 from the current level of 60 % as the blast furnace ironmaking proportion falls from around 95 % to 60 % of the iron ore processed [5]. To put the ironmaking sustainability problem into perspective, breakthrough process technologies based on new routes will be required in the long term leading up to 2050. These may involve, for example, the increased use of hydrogen for reduction of iron ore, smelting reduction processes, and low carbon fuels such as natural gas (NG). Figure 1.2 gives the forecast of the share of different technologies for ironmaking which could be in place in 2050, with an assumed total global steel production in excess of 2300 Mt/a .

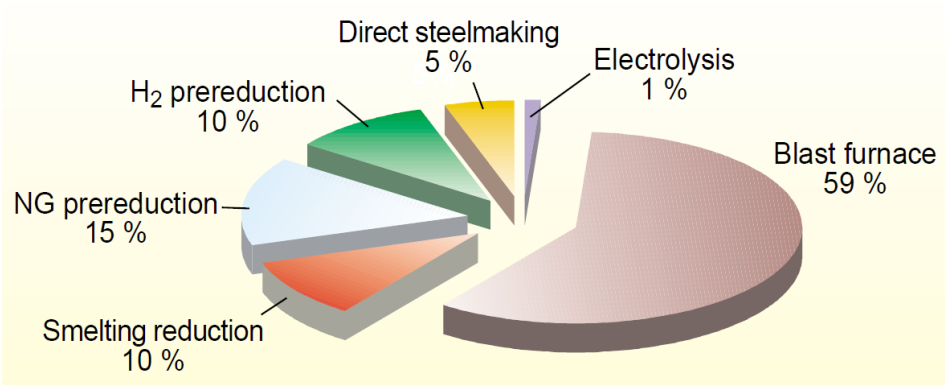

Figure1.2 Predicted proportion of ironmaking routes in 2050 [6]

1.2.1 Blast furnace ironmaking process

1.2.1.1 Conventional blast furnace

The conventional blast furnace [7-9] is a counter-current packed bed reactor for the reduction of iron ore to produce liquid iron (hot metal). Figure 1.3 shows a typical cross section of an ironmaking blast furnace.

Pellet, sinter or lump iron ore, coke particles and flux bearing materials such as limestone, dolomite or BOF slag are charged into the top of the furnace by either a bell type distributor or bell-less type charging system. The raw iron ore materials are composed mostly of hematite (Fe_2O_3) or magnetite (Fe_3O_4). These materials undergo a series of chemical and physical reactions while descending to the bottom of the furnace. The upper section of the blast furnace is a long shaft counter-current packed bed reactor. Hot reducing gases rising from the bottom of the furnace, react with the down coming bed of iron oxides, coke and flux material. As the iron oxides react during their descent in the furnace, they begin to soften, melt and finally trickle as liquid iron and slag through the coke to the bottom or hearth of the furnace. In the shaft, the hematite charged is reduced to iron by two different mechanisms: “indirect reduction”, with carbon monoxide and hydrogen as the reducing agents, and “direct reduction” by the direct contact of molten wüstite (FeO) with carbon. Iron, wüstite and the slag forming components start to get molten in the bosh which is the lower part of the shaft. The iron oxides soften and melt during their passage through the furnace in a region named the “cohesive zone”. The upward flowing gases flow through this zone, which consists of softened layers of ore alternating with layers of permeable coke. Coke must be of sufficient quality in this zone in terms of permeability (size and voidage) to provide

stable furnace operations. The molten drops leave the bosh and move through the very hot combustion zone above the slag layer. And then the drops of the molten metal and slag enter the hearth zone, where they are separated into two distinct layers as the less dense slag layer will be floating on top of the hot metal bath. The hearth allows the final exchange of minor components between the hot metal and the slag. Coke quality is very important in the hearth. Here, liquid slag at high viscosity must flow through the coke bed and, again, the permeability of the coke bed is of importance in dictating stability, tapping characteristics and productivity of the furnace. The central part of the furnace is occupied by a rather inactive and impermeable agglomerate of coke particles, which is called “deadman”. It extends up into the bosh and lower stack zones of the furnace.

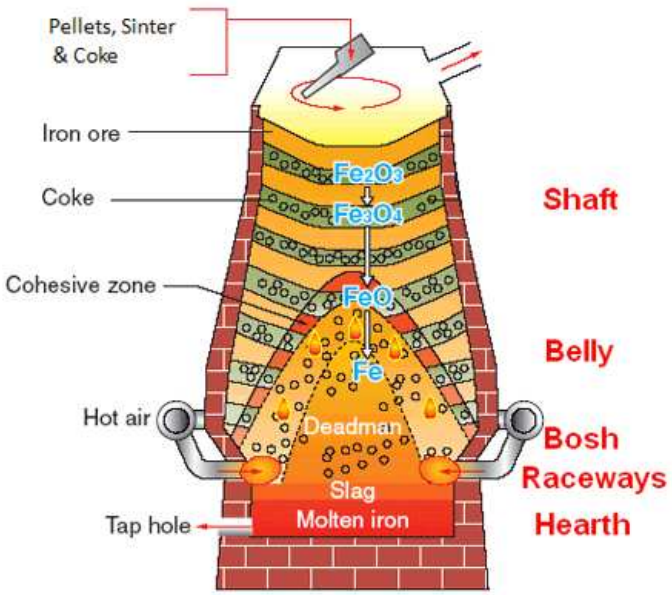

Figure 1.3 Concept of the conventional blast furnace [10]

These ascending gases are the product of the exothermic partial combustion of coke and fuel oil or fuel gas, and the endothermic reaction of coke with CO_2 and blast moisture. The oxygen and moisture necessary for the above reactions are supplied by the hot air blast. Additional oxygen and moisture to the air may be added. This blast has been heated at the hot stoves after being compressed. It enters the furnace below the packed bed, through a series of nozzles called tuyeres. The fuels react with oxygen to form carbon monoxide and hydrogen in front of the tuyeres in the combustion zone. These are then the reducing agents which enter the packed bed above the combustion zone and supply the major part of the heat requirements for the further reactions.

The conventional ironmaking technology of the blast furnace has a long history, which existed in China from about 5th century BC [11] and it was introduced to England in 1491. So far, the blast furnaces have evolved into highly efficient reactors. However, there are many difficulties that can't be overcome by blast furnaces which require coke, and coke plants are expensive and have many environmental problems associated with their operation. Thus, it would be beneficial from an economical and environmental point of view to produce iron without the use of coke. Nowadays, nearly all blast furnaces reduce their coke consumption significantly by means of reductant injection through the tuyeres. However, coke can never be fully replaced in a blast furnace because of its burden supporting function. The minimum blast furnace coke rate is assumed to be approximately 200 kg/t pig iron [12]. The top gas, exhausted at about 100-200 ^{o}C, contains typically 20-28 % CO, 17-25 % CO_2, 1-5 % H_2, and inert compounds such as N_2 50-55 %. Top gas is normally used as a combustible for the coke oven or to produce electricity. The operation of the blast furnace results in the emission of about 1.5 tonne of CO_2 per tonne hot metal produced. It is a big source of global greenhouse gas. The conventional blast furnaces have been improved all the time and new concepts of blast furnaces are generated regularly. The top gas recycling blast furnace is one of the outcomes.

1.2.1.2 Top gas recycling blast furnace (TGRBF) with CO_2 capture and storage (CCS)

The concept of the top gas recycling blast furnace in the ULCOS program (Figure 1.4) relies on removing the carbon dioxide from the top gas [4]. The useful components of the top gas can then be recycled back into the blast furnace at the tuyeres as reducing agent. This would reduce the amount of coke needed in the furnace. It also decreases the CO_2 emissions in the blast furnace by benefiting from the reducing power of the recycled gas, which contains a substantial amount of reducing agents (CO and H_2) not used in the conventional blast furnace, as well as the increasing opportunity of CO_2 storage. Moreover, the heat demand is sensibly reduced and the productivity (t/d) is improved by up to 20 %. The captured CO_2-rich stream may either be used, e.g. for EOR (Enhanced Oil Recovery) or stored geologically, e.g. in saline aquifers. In addition, the concept of injecting oxygen (O_2) into the furnace instead of preheated air, removes unwanted nitrogen (N_2) from the gas, facilitating CO_2 capture and storage.

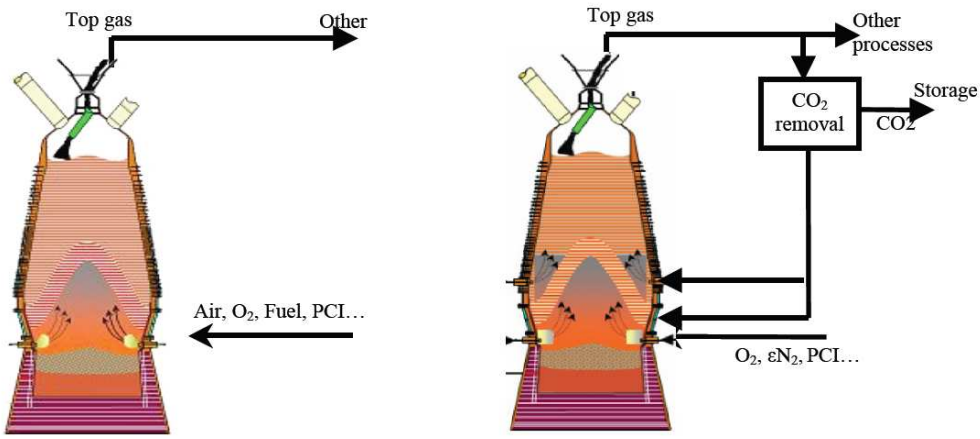

Figure 1.4 Comparison of conventional and the top gas recycling blast furnace [13]

The pilot experimental blast furnace of MEFOS at Lulea, Sweden, has been modified and operated with top gas recycling for an ULCOS program campaign in 2007 [14]. The trials were successfully done in 6 weeks. Comparing the results with the conventional blast furnace, it was found that the technology could achieve a good hot metal quality, a carbon saving ratio of about 24 % and a reduction of the CO_2 emission of about 76 % with the CCS system. The VPSA (Vacuum Pressure Swing Adsorption) plant processed up to 97 % of the blast furnace top gas without failure. The CO recovery was 88 %. [15] During the 6 weeks operation, the CO_2 removal unit was smooth and reliable. What is even more gratifying is that no safety issue has been recorded of the TGRBF. Currently, a pilot plant with top gas recycling facilities is building at Eisenhuttenstadt and it will start in 2014. At the same time a demonstrator with full CCS chain is building at Florange, which will start in 2015 [16].

1.2.2 Non-blast furnace ironmaking technology

In order to achieve an efficient operation from energy, economic and environmental point of view, competitive alternative ironmaking technologies have been extensively investigated since the 1960's [17], which can be classified into two main types. According to the final product of the processes (sponge iron and hot metal), these processes can be grouped as direct reduction process and smelting reduction process [18]. According to the type of fuel used, these processes can also be grouped as gas-based and coal-based processes.

Table 1.2 illustrates the important characteristics and current status of some

selected alternative ironmaking processes. More than the direct reduction process, with solid iron as end product, the SR process can be regarded as a direct competitor of the conventional blast furnace as the product is liquid pig iron or (in some cases) liquid steel. The smelting reduction process has several advantages compared to the conventional blast furnace process as mentioned below, which may lead to the adoption of smelting reduction as the main process for hot metal production in the future.

- Smaller units, allowing a more flexible production;
- Fewer restrictions as to the raw materials used;
- Use of coal as fuel avoiding operation of a coke oven plant;
- Not always a need for an ore agglomeration step avoiding operation of pellet and sinter plants;
- Lower capital costs.

It is also recognized that any alternative ironmaking process ultimately is strongly dependent on local conditions such as availability and cost of natural gas, power and coal, as well as on product requirements. The economics, possibilities and limitations are still largely unknown. Several smelting reduction processes are under further development. The process variants differ in the number of reactors, operating temperature, the ore feed (pellet, lump ore or fines). The variant processes that are relatively well developed are: COREX, DIOS, HIsmelt, CCF, Romelt [17,19] and HIsarna. The most promising direct reduction processes in the worldwide include Hyl III, Midrex, Circored, Circofer, FASTMET and Finmet. Midrex and Hyl III are the only truly established gas based direct reduction processes. The increasing price of the natural gas hampered the development of the gas based direct reduction process. On the other hand, both of them are fed with pellet and lump ore, which results in a high operating cost compared to fines-based processes. However, the sharp drop in gas prices due to the Marcellus shale development has led to resurgence in interest in gas based DRI production. COREX is the first commercially operating alternative to the blast furnace for hot metal production, and HIsmelt is the world's first commercial smelting process for making iron straight from the ore. In addition, HIsmelt is the only hot air based direct smelting process, enabling to recycle a significant proportion of off-gas as fuel for air preheating.

Table 1.2 Characteristics of selected alternative ironmaking processes [17]

Process	Type	Fuel	Ore Type	Product	Status	Start-up year	Inventor
Hyl III	Shaft	Natural gas	Pellet/lump	HBI/DRI	Commercial	1957	Hylsa of Mexico
Midrex	Shaft	Natural gas	Pellet/lump	HBI/DRI	Commercial	1969	Kobe Steel, Ltd. (Japan)
Circored	Fluid bed	Natural gas	Fines	HBI	Commercial	1999	Outotec (Germany)
Finmet	Fluid bed	Natural gas	Fines	HBI	Commercial	1999	VAI
Circofer	Fluid bed	Coal	Fines	HBI/DRI	Pilot	1999	Outotec (Germany)
FASTMET	Rotary Hearth	Coal + gas	Fines	DRI	Pilot	2000	Kobe Steel, Ltd. (Japan)
ULCORED	Shaft	Syngas	Pellet/lump	DRI	Pilot	To be 2013	ULCOS (Europe)
Romelt	Bath	Coal	Fines	Hot Metal	Pilot	1980	MISA (Russian Moscow Institute of Steel and Alloys)
COREX	Shaft/Gasifier	Coal	Lump/pellet	Hot Metal	Commercial	1989	VAI
DIOS	Bath	Coal	Fines	Hot Metal	Pilot	1993	Japan Steel Firms & JISF
HIsmelt	Bath	Coal	Fines	Hot Metal	Commercial	1981	RIO TINTO (Australia)
CCF	Cyclone	Coal	Fines	Hot Metal	Pilot	1989	The UK British Steel and the Dutch Hoogovens
HISARNA	Cyclone/Bath	Coal	Fines	Hot Metal	Pilot	2011	ULCOS (Europe)

Figure 1.5 shows the flow chart for the Midrex direct reduction ironmaking process. The pilot plant was built in Toledo, Ohio in 1967. The first commercial plant, having a production capacity of 150000 t/a, was built in Portland, Oregon, in 1969. In 1978, Kobe Steel began the construction of a plant with a production capacity of 400000 t/a in the State of Qatar. The global production of DRI increased dramatically from 790000 t/a in 1970 to 68.45 Mt/a in 2008. Direct reduction iron made by the Midrex process accounts for about 60 % of global production of DRI. [21]

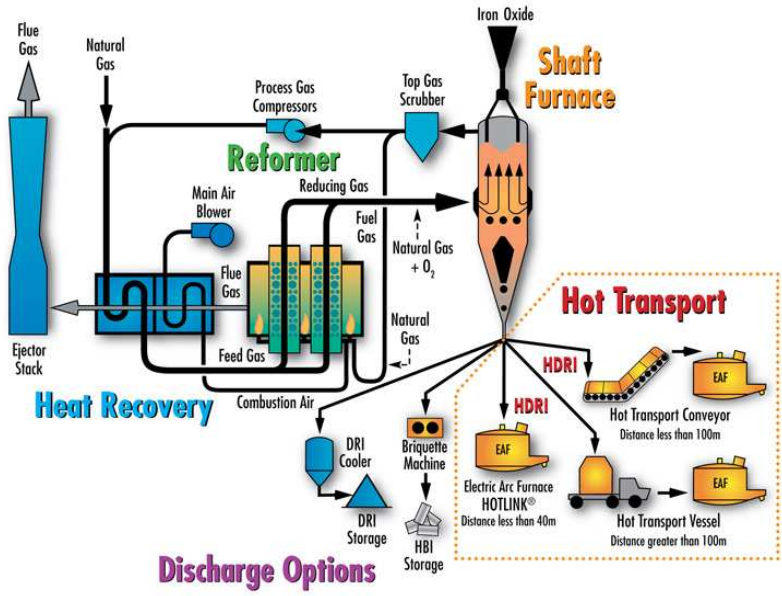

Figure 1.5 Flow sheet of Midrex process [20]

The key components of a Midrex plant are a shaft furnace, a reformer as well as systems for gas cleaning and heat recovery. The goal of the Midrex process is to reduce the iron ore (that is, remove oxygen) which is in the form of oxide compounds. This is done in a countercurrent process using natural gas as the reducing agent. Either lump ore, or pellets prepared for direct reduction ironmaking, are charged as raw material from the top of a shaft furnace. The ore is reduced inside the furnace and the reduced iron is discharged from the bottom of the furnace. Reducing gas blown in from about the middle of the shaft furnace reduces the raw materials above the nozzle level and escapes from the top of the furnace. The cooling gas, which circulates in the lower portion of the furnace, cools the DRI. Both the charging and discharging ports are dynamically sealed by a sealing gas, allowing the continuous charging of raw material and discharging of DRI. The exhaust gas emitted from the top of the shaft furnace is cleaned and cooled by a wet scrubber and recirculated for reuse. The top gas containing CO_2 and H_2O is

pressurized by a compressor, mixed with natural gas, preheated and fed into a reformer furnace. The reformer furnace is provided with several hundreds of reformer tubes filled with nickel catalyst. Passing through these tubes, the mixture of top gas and natural gas is reformed to produce reducing gas consisting of carbon monoxide and hydrogen.

Various improvements have been made to the Midrex process to reduce the specific energy consumption of the process, including downstream steelmaking, and to improve the productivity of the shaft furnace. The diameter of the Midrex shaft furnace was increased from 4.25 m in the 1960's to 7.15 m in 2007. The energy-saving measures not only decrease the operation cost, but also decrease the environmental burden with reduced emissions of CO_2 and other types of exhaust. The Midrex process, which is based on natural gas, emits intrinsically less CO_2 than other processes using coal. Because of this, the Midrex process can also contribute to emission reduction in coal based ironmaking processes. For example, charging HBI produced by a Midrex plant into a blast furnace will decrease the ratio of the reductant used as a heat source and reduces CO_2 emissions as a whole.

ULCORED [4] is a breakthrough direct reduction technology within the ULCOS program designed to minimize emission of greenhouse gases, using CO_2 capture and storage technology and at the same time to minimize the use of energy. It was designed mainly in 2006 by a team led by LKAB, Voestalpine and MEFOS [22].

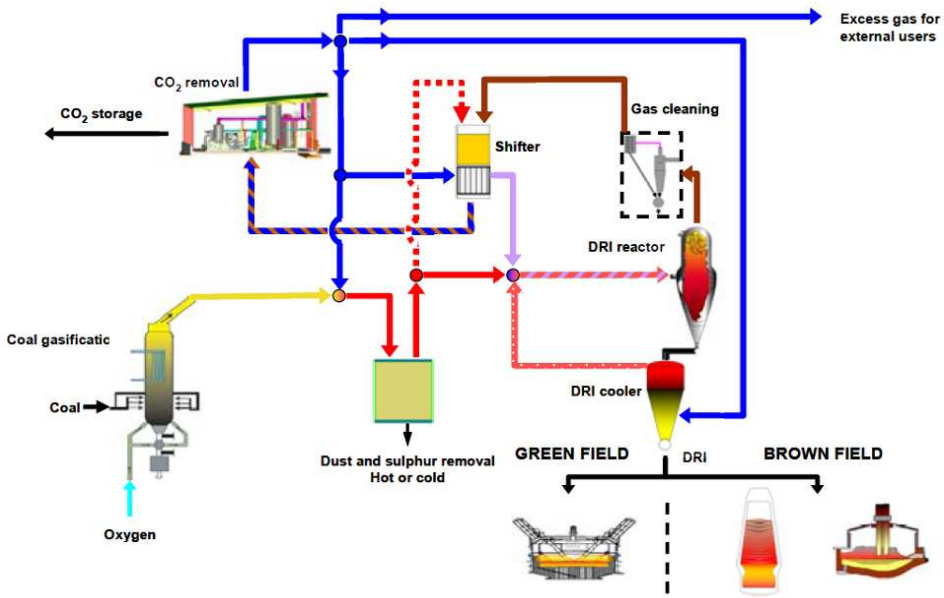

Figure 1.6 ULCORED with syngas from coal [22]

DRI is produced from iron ore in the form of lumps or pellets by reducing gas. The reduced iron is in the solid state and for melting the iron, electric energy is required. This is carried out in an Electric Arc Furnace (EAF). The originality of the concept was the use of natural gas as reducing gas. It was found that large CO_2 emissions arise on site from the use of natural gas in heating ovens and from the use of electricity in EAF melting [22]. However, the other option of syngas from coal gasification is much more efficient. In addition, the production of “excess gas” to be used as fuel gas in various processes will reduce the CO_2 emission for the total site. On the other hand, the price of conventional natural gas will probably be very high compared to coal also in the future. However, according to the current developing status, the shale gas could make natural gas more competitive in the coming years.

The ULCORED direction reduction process can easily be integrated with a coal gasification unit. Figure 1.6 shows the flow sheet of the ULCORED process by using syngas from coal gasification. Coal is supplied to the coal gasifying plant. Sulphur is removed from the syngas by either hot or cold desulphurization. The clean syngas is blended with cleaned H_2-rich recycle gas, preheated in the DRI cooler or from the heat exchanger between the high temperature and low temperature shifter. The direct reduction shaft has a counter current flow of reducing gas injected at the tuyeres and cold iron ore fed from the top. The furnace is operated at a pressure of 6 bars and approximately 900 ^{o}C. The gas pressure from the gasifier is decreased through an expansion turbine to generate electricity (from 30 to 6 bar). The shaft off-gas will mainly contain CO, CO_2, H_2 and H_2O.

Both Midrex and ULCORED employ a shaft furnace to convert iron ore into DRI using natural gas or syngas from coal. The off gas from ULCORED process is also recycled as in the Midrex process, but ULCORED is developed to optimize the application of CCS to DRI and to reduce the natural gas consumption. In addition, ULCORED process takes use of high purity oxygen instead air. The shifter in the ULCORED plant is used to transform CO in the top gas into hydrogen and CO_2, which does not exist in Midrex technology.

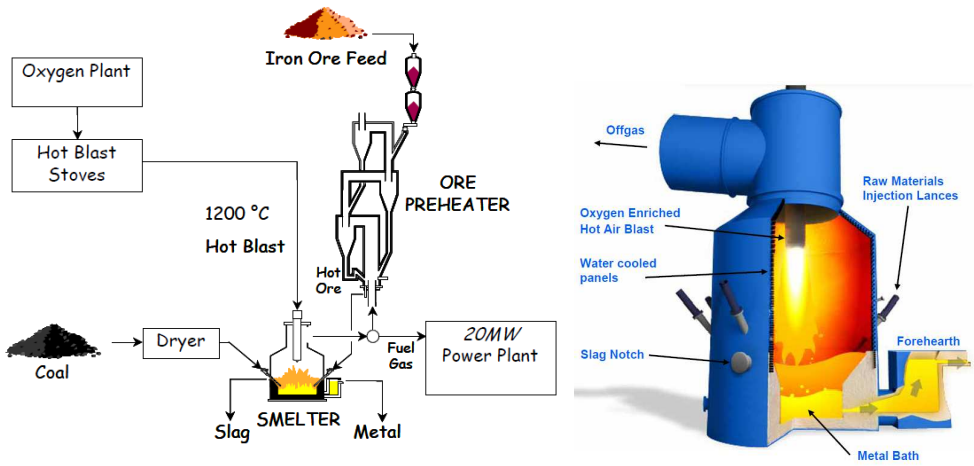

Figure 1.7 Flowsheet of the HIsmelt Kwinana Plant and smelting reduction vessel [23]

The concept of HIsmelt Process can trace back to the early 1980's, which was owned by Rio Tinto Limited. Development of the HIsmelt process commenced with a 60 tonnes K-OBM converter. A small scale pilot plant was constructed and operated at Maxhutte Works in Germany based on the concept. With the experience of the trials in the 60 tonnes converter, the plant design was based on an enclosed horizontal vessel to overcome process containment issues. Following the successful trials the HIsmelt Research and Development Facility (HRDF) was established in Kwinana, Western Australia. The plant had a capacity of 100000 t/a and was a direct scale-up of the small scale pilot plant [24]. The HRDF played an important role in developing the technology which aimed to demonstrate scale-up of the process and provide operating data for commercial evaluation of the technology. The success of the HRDF operation gave the confidence to Rio Tinto Limited to realize the commercialisation of the HIsmelt Process. The first commercial HIsmelt plant has a 6 m inner diameter Smelting Reduction Vessel (SRV) and was located in Kwinana, Western Australia with a design rate of 100 tonnes per hour of hot metal (800000 t/a) [25]. It was owned by a Joint Venture comprising Rio Tinto (60 %), Nucor Corporation (25 %), Mitsubishi Corporation (10 %) and Shougang Corporation (5 %). The construction of the HIsmelt Kwinana plant commenced in January 2003, and was commissioned in April 2005. The plant operated until December 2008 at production rates of more than 80 tonnes per hour using Australian higher phosphorus iron ore. Because of the global financial crisis, the HIsmelt Kwinana operation was shut down. To complete the development of the technology using hematite iron ore, Rio Tinto has signed a Memorandum of Understanding (MoU) with Jindal Steel and Power Limited (JSPL) of India. This MoU reported to move the Kwinana HIsmelt plant equipment from Australia to

JSPL's existing steelmaking facility in Angul, Orissa. The new plant will be fully owned by JSPL, and expected to be started in 2014.

HIsmelt is an air based direct smelting technology which is simple yet innovative. The HIsmelt process is illustrated in Figure 1.7. The core of the HIsmelt technology is the SRV, which replaces the function of a blast furnace. The refractory hearth contains the molten iron bath. A thick slag layer is situated above the metal bath. Iron ore fines, coal and fluxes are injected deep into the bath where iron ore fines are reduced instantly on contact with carbon dissolved in the bath and this reaction produces iron (Fe) and carbon monoxide (CO). Rapid heating of the coal also results in cracking of the coal volatiles releasing hydrogen. A fountain of molten material, consisting largely of slag, erupts into the top space by the rapid expulsion of the carbon monoxide, hydrogen and nitrogen carrier gas from the molten bath. Hot air at 1200 ℃, which is enriched with oxygen, is blasted into the top space through a water-cooled lance. The carbon monoxide and hydrogen is post combusted with oxygen (from the hot air blast), which releases a large amount of energy. The heated metal and slag fall back into the bath providing the energy for direct smelting of the iron ore. The off-gas from the process is partially cooled in a membrane tubed hood. The sensible and chemical energy in the off-gas can then be used to effect some preheating, pre-reduction and/or calcination of the metallic feed and fluxes. Then the off-gas is cleaned in a scrubber and used as fuel for the hot blast stoves or in a co-generation plant.

The Cyclone Converter Furnace (CCF) process originated from the Converted Blast Furnace (CBF) jointly developed by Hoogovens, British Steel and Ilva in the years 1986 to 1989 [17]. In the CBF process, lumpy ore is highly pre-reduced in a shaft with final reduction and melting taking place in an iron bath in which fine coal is gasified. The process can avoid coke making but not ore agglomeration and related environmental problems. To further eliminate ore agglomeration in the process, the Cyclone Converter Furnace (CCF) is developed, in which a melting cyclone is applied for pre-reduction and pre-melting of fine ore. A small CCF pilot plant was built in Taranto, Italy.

A schematic diagram of the CCF process is shown in Figure 1.8. In the CCF process, the pre-reduction and the final smelting reduction stages take place in a single reactor. Fine ores and coal are injected tangentially by carrier gas into the melting cyclone, which is mounted directly on top of a vertical type converter. The pre-reduced molten ore is collected on the water cooled wall of the cyclone and falls into the iron bath for its gravity, where final smelting reduction of the ore and gasification of coal take place. The gases arising from the smelter are further combusted in the melting cyclone in order to generate heat required by melting and pre-reduction. The off-gas of the CCF leaves the process at a temperature of 1800 ^{o}C and the final combustion ratio of the off-gas is about 75 % [26]. As can be seen from the process, the CCF process requires a minimum amount of equipment. Gas conditioning steps such as cooling, de-dusting and reforming are not required.

The gas off-take resembles a closed hood of a BOF gas cleaning system and includes a boiler for the utilization of the sensible heat in the off-gas. The steam generated in the boiler can be used for the production of oxygen and to generate electricity.

Furthermore, the use of a melting cyclone is the unique feature of the CCF process. Due to high pre-reduction and smelting intensity in the melting cyclone, the size of the melting cyclone is much smaller than that of a conventional shaft reduction furnace, and thus a very high volumetric production rate and required pre-reduction degree can be achieved. In addition, as a high degree of pre-reduction and melting occur in the melting cyclone, the final reduction and smelting taking place in the converter bath is relatively moderate, which should result in moderate slag foaming and post combustion requirements. Moderate slag foaming and post combustion are important for the successful operation and maintenance requirements of the converter vessel.

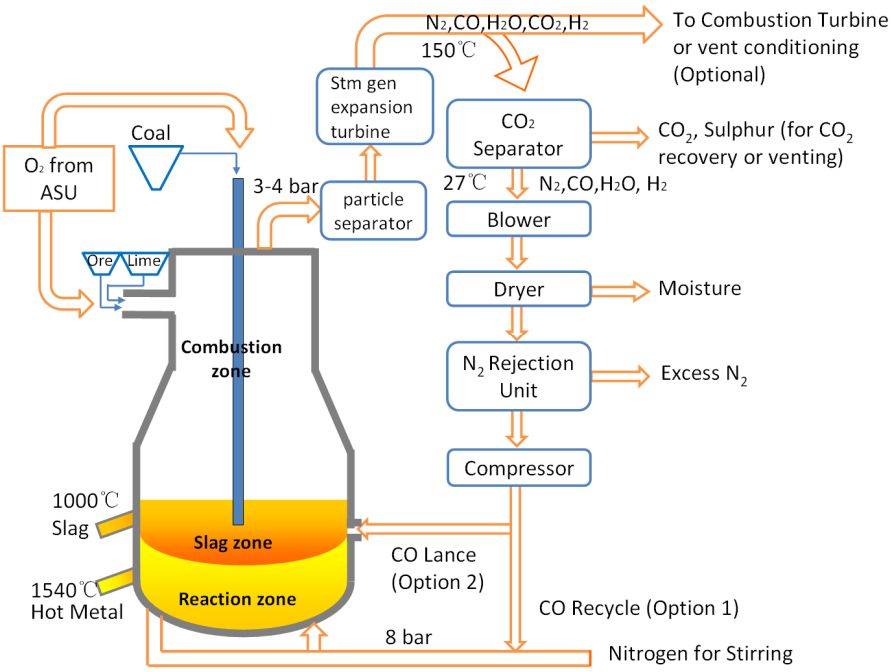

Figure 1.8 The Schematic diagram of CCF process

HIsarna is part of the ULCOS project [4], which aims to cut CO_2 emissions by 50 % per tonne of steel produced. Without CCS technology HIsarna can cut emissions by 20 %, whereas with CCS it can achieve a reduction of up to 80 %. HIsarna represents a new phase in the global smelting reduction development cycle. It is, in

essence, a merger between the smelting cyclone technology of CCF developed by Hoogovens, Corus and Tata Steel and bath smelting technology of HIsmelt developed by Rio Tinto as shown in Figure 1.9. The HIsarna pilot plant which has an annual production capacity of 60,000 tonnes was built and commissioned at Tata Steel's IJmuiden steelworks in the Netherlands. The diameter of the SRV (smelting reduction vessel) bath is 2.5 m. On 18 April 2011 the process, which removes the need for coking and agglomeration, was piloted for the first time. After one failed start three successful attempts followed, and 60 % of capacity was achieved for a short time. After the first campaign several improvement were made to the pilot plant and the operating procedures. The second campaign was carried out on 16 October 2012, which last 6 weeks. The pilot plant achieved the design capacity of 8 t/h. The main process parameters like, metal composition and temperature, the gas utilisation and the heat losses, were within the expected range. The third campaign was planed on the first half of 2013. Industrial scale demonstration will be carried out from 2014-2018. The earliest industrialization of HIsarna, the smelting reduction technology being trialed at the IJmuiden steelworks, will be 2020.

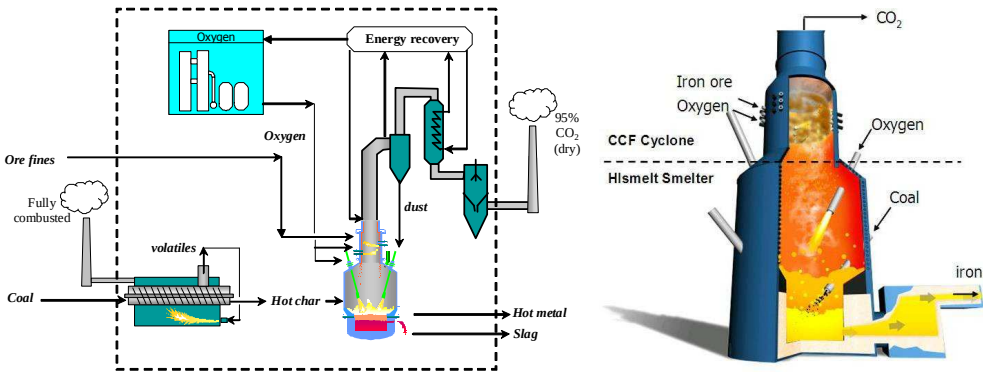

Figure 1.9 Schematic diagram of the HIsarna process [27-28]

As shown in Figure 1.9, the HIsarna process combines coal preheating and partial pyrolysis in a reactor, a melting cyclone for ore melting and a SRV for final ore reduction and iron production. The smelting cyclone and SRV are highly integrated and operated as a single smelting furnace. Fine ore and flux are fed into the smelting cyclone together with oxygen. The high purity oxygen is used to combust the SRV off-gas entering from the bottom of the cyclone. The combustion, which is preferably complete, generates a considerable amount of heat. This heat is used to melt the ore and heat it to the SRV temperature which is around 1723 K. Simultaneously, the ore is pre-reduced to a pre-reduction degree of about 20 % through thermal decomposition and reduction by the SRV gas, while flux is decalcined. After the molten ore droplets hit the wall of the cyclone, they flow down the wall and drip into the SRV. The capture efficiency of the cyclone is maximized

by increasing the rotational velocity through the injection of oxygen and ore. The main reactions in the cyclone are listed as follows,

$$Fe_xO_y(s) = Fe_xO_{y-1}(l) + 1/2\,O_2(g) \quad (1.1)$$

$$Fe_xO_y(s) + CO/H_2(g) = Fe_xO_{y-1}(l) + CO_2/H_2O(g) \quad (1.2)$$

$$CaCO_3(s) = CaO(l) + CO_2(g) \quad (1.3)$$

$$CaMg(CO_3)_2(s) = CaO(l) + MgO(l) + 2CO_2(g) \quad (1.4)$$

$$CO(g)/H_2(g) + 1/2\,O_2(g) = H_2O(g)/CO_2(g) \quad (1.5)$$

Before the coal is injected into the SRV it can be partly pyrolysed and pre-heated. The combustion value of the volatile components that are released during partial pyrolysis can be used to supply the heat for this partial pyrolysis. By pre-heating and partially pyrolysing the coal, the heat requirement of the SRV is reduced, while the attainable post-combustion ratio (PCR) in the SRV is increased.

In the SRV the remainder of the reduction takes place. The molten droplets of iron ore from smelting cyclone drop into the bath where they are reduced by carbon. Oxygen is introduced into the upper part of the reactor via lances, and heat is generated by combustion. The SRV runs at 1673-1723 K. Non-coking coal is supplied to the bath, where it either enters the slag layer or is absorbed in the metal and the dissolved carbon in the metal is around 4 %. [28] There is essentially zero Si present in the metal, and other minor impurities such as manganese are also present at very low levels (compared to blast furnace hot metal). Phosphorous and Titanium partition largely to the slag phase as oxides. The content of FeO in the slag is typically around 5-6 %. The generated gas at the upper part of SRV is around 1673-1773 K and has a post combustion ratio (PCR) around 50 %. The HIsarna process produces liquid hot metal that can be processed in a BOF or EAF plant. The main reactions in the SRV are listed as follows,

$$Fe_2O_3(l) + [C]_{Fe}/C(s) = 2FeO(l) + CO(g) \quad (1.6)$$

$$FeO(l) + [C]_{Fe}/C(s) = Fe(l) + CO(g) \quad (1.7)$$

$$C(s) = [C]_{Fe} \quad (1.8)$$

Above all, the HIsarna ironmaking process has a combination of environmental and economical benefits:

<u>Economic benefits:</u>

- Reduced OPEX (operating expenditure) and CAPEX (capital expenditure) compared to blast furnace route
- Possibility to further reduce costs by application of low grade iron ore (ores

with P, Zn, S, Ti or alkali)
- Use of plant waste oxides (BOF or BF dust) or mining reverts
- Use of coal instead of coke from cokemaking plants

Environmental benefits:
- 20 % lower primary energy consumption and 20 % less CO_2 per ton of hot metal
- Favourable combination with CCS because of N_2 free topgas. 80 % lower CO_2 emission per ton of hot metal when CCS is applied
- Elimination of agglomeration and cokemaking emissions, NO_x, SO_x, dust, CO

Up to now, HIsarna is still in the pilot plant state like a kid in the world of ironmaking and seen as the most promising smelting reduction process to compete with blast furnace technology. To realize this great target, a series of investigations are currently need and in the near future. This project is special focused on the iron ore melting and reduction behaviour in the smelting cyclone.

1.3 Basic reactions and thermodynamics of the gas solid iron oxide reduction

Before the laboratory experimental study, a proper plan was drawn up according to the current well known basic physical and chemical properties of iron oxides at different temperatures and in different gas atmosphere. On other hand, these basic theories could give a good explanation of the phenomena in this study. Iron oxides may exist in three forms, i.e. hematite (Fe_2O_3), magnetite (Fe_3O_4) and wüstite (FeO) depending on temperature and oxygen potential of the system. Although the non-stoichiometric wüstite is usually written as FeO or Fe_xO, the actual oxygen content in wüstite has a wide range from 23.1 to 25.6 wt%. The value of x in Fe_xO is less than unity and close to 0.95 when it co-exists with metallic iron. The iron-oxygen system may be best described in the phase diagram by Darken and Gurry as shown in Figure 1.10. The diagram has been used in a lot of investigations [29-31], which shows that iron oxides with oxygen content from 22.5 % to 27.5 % melt down above 1644 K. Therefore, melting reduction behaviour of iron ore could be achieved, when temperature exceed this value.

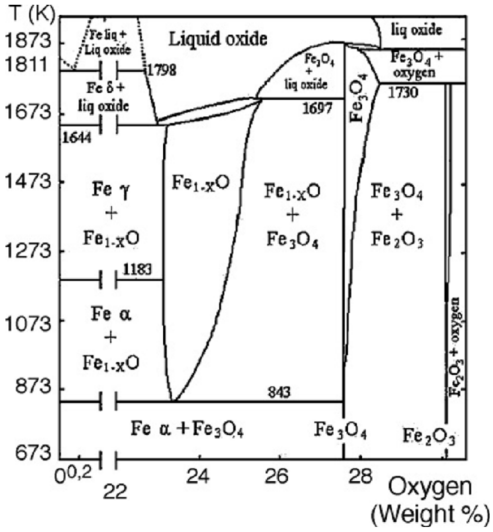

Figure 1.10 Binary system of iron-oxygen [30]

1.3.1 The sequence of reduction of iron oxides with gases

The gas solid reduction of hematite to produce iron takes place step-wise in two or three stages. For temperatures higher than 843 K, hematite (Fe_2O_3) is first transformed into magnetite (Fe_3O_4), then into wüstite (Fe_xO), and finally into metallic iron, whereas at temperatures below 843 K, magnetite is directly transformed into iron since wüstite is not thermodynamically stable. In this study, the temperature is far above 843 K, therefore the reduction should take place in 3 stages.

1.3.2 Equilibrium between iron oxides and reducing gases

Carbon monoxide and hydrogen are the most common reducing agents used in commercial ironmaking processes. Some thermodynamic data are given below. Heats of reaction ΔH^o at 298 K for the stoichiometric equations are given below [32].

$$3Fe_2O_3 + CO = 2Fe_3O_4 + CO_2 \quad \Delta H^o = -52.87 \ kJ/mol \tag{1.9}$$

$$Fe_3O_4 + CO = 3FeO + CO_2 \quad \Delta H^o = 36.25 \ kJ/mol \tag{1.10}$$

$$FeO + CO = Fe + CO_2 \qquad \Delta H^o = \text{-}17.31 \ \ kJ / mol \tag{1.11}$$

At a temperature below 843 K, magnetite is reduced directly to metallic iron,

$$Fe_3O_4 + 4CO = 3Fe + 4CO_2 \quad \Delta H^o = \text{-}15.66 \ \ kJ / mol \tag{1.12}$$

The equilibrium constant, K_e, of reactions listed above can be calculated from the standard free energy change ΔG^o of these reactions as a function of temperature [33]. The results of above reactions are listed in the Eqs.14-17.

$$\ln K_e = \frac{\text{-}\Delta G^o}{R_g T} \tag{1.13}$$

$$K_e = Exp\left(\frac{3968.37}{T} + 3.94\right) \text{ for Eq. (1.9)} \tag{1.14}$$

$$K_e = Exp\left(\frac{-3585.64}{T} + 8.98\right) \text{ for Eq. (1.10)} \tag{1.15}$$

$$K_e = Exp\left(\frac{2744.63}{T} - 2.946\right) \text{ for Eq. (1.11)} \tag{1.16}$$

$$K_e = Exp\left(\frac{2937.21}{T} - 4.25\right) \text{ for Eq.(1.12)} \tag{1.17}$$

K_e can be further calculated. For example, for reaction (1.9), the equilibrium constant is calculated as follows,

$$K_e = \frac{2 \times a_{Fe_3O_4} \times p_{CO_2}}{3 \times a_{Fe_2O_3} \times p_{CO}} \tag{1.18}$$

The hematite and magnetite are assumed to be essentially pure solids, hence, their activities are equal to unity, and then the equilibrium ratio of partial pressure in the wüstite reduction can be calculated from Eq.1.19.

$$K_e = \frac{2}{3} \times \frac{p_{CO_2}}{p_{CO}} \tag{1.19}$$

Where,

R_g – gas constant ($kJ \cdot mol^{-1} \cdot K^{-1}$)
T – temperature (K)
$a_{Fe_2O_3}$ – activity of Fe_2O_3
$a_{Fe_3O_4}$ – activity of Fe_3O_4

p_{CO} – partial pressure of CO
p_{CO2} – partial pressure of CO_2

Similar calculations can be made for the other three reactions. The equilibrium phase diagram is shown in Figure 1.11.

The reduction of iron oxides by hydrogen is endothermic for reactions (1.21) and (1.22). The heats of reactions at 298 K are listed below.

$$3Fe_2O_3 + H_2 = 2Fe_3O_4 + H_2O \qquad \Delta H^o = \text{-}11.72\ kJ/mol \tag{1.20}$$

$$Fe_3O_4 + H_2 = 3FeO + H_2O \qquad \Delta H^o = 77.41\ kJ/mol \tag{1.21}$$

$$FeO + H_2 = Fe + H_2O \qquad \Delta H^o = 23.85\ kJ/mol \tag{1.22}$$

At a temperature below 843 K, magnetite is reduced directly to metallic iron,

$$Fe_3O_4 + 4H_2 = 3Fe + 4H_2O \qquad \Delta H^o = 148.96\ \ kJ/mol \tag{1.23}$$

The equilibrium constant K_e are listed as follows,

$$K_e = Exp\left(\frac{-362.6}{T} + 10.334\right) \text{ for Eq. (1.20)} \tag{1.24}$$

$$K_e = Exp\left(\frac{-7916.6}{T} + 8.46\right) \text{ for Eq. (1.21)} \tag{1.25}$$

$$K_e = Exp\left(\frac{-1586.9}{T} + 0.9317\right) \text{ for Eq. (1.22)} \tag{1.26}$$

$$K_e = Exp\left(\frac{-13657.9}{T} + 10.10\right) \text{ for Eq. (1.23)} \tag{1.27}$$

The phase diagram of the H-O-Fe system is shown in Figure 1.11.

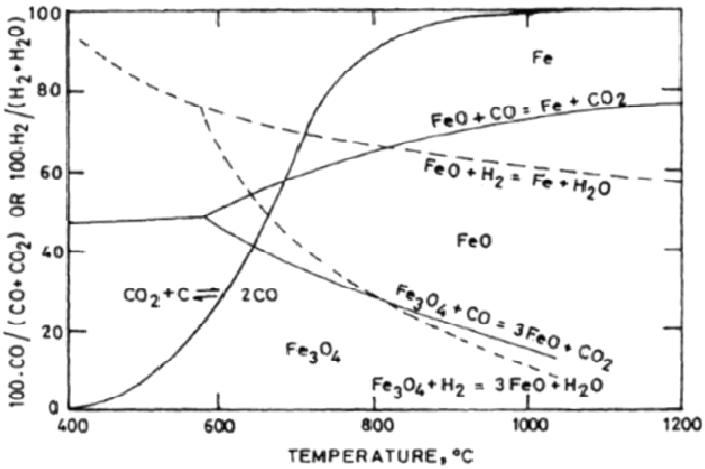

Figure 1.11 Equilibrium iron oxide diagram in a H_2/H_2O and CO/CO_2 atmosphere [34]

The equilibrium phase diagram shows that both curves of reduction of Fe_3O_4 and FeO with CO and H_2 as the reducing agents intersect at 1094 K. It indicates that the reducing ability of H_2 is weaker than CO at the temperature lower than 1094 K, while the reverse happens when the temperature is higher than this value.

1.4 Kinetics of reduction of iron oxides with gases

The main aim of the laboratory study is to determine the kinetic mechanism of the reduction of iron oxides in the HIsarna process. The results can give an insight of the running pilot plant. In addition, the results could be used in the further modelling study. The basic theory and methods for studying the reduction of iron ore is described in this section.

1.4.1 Rate law

In the kinetic study of the reduction of iron oxides by gases, a spherical particle is usually used for mathematical modelling because of its simple geometry and its similarity to commercial products.

Generally, the intrinsic kinetics reaction rate may be represented by the following general equation:

$$\frac{dR}{dt} = k' f_1(C_A) f_2(R) f_3(d) \tag{1.28}$$

Where,

R	– reduction degree;
t	– reaction time (s);
$f_1(C_A)$	– the dependence of the reaction rate on the gaseous reactant concentration;
$f_2(R)$	– the dependence on fraction reacted;
$f_3(d)$	– the dependence on the particle size;
k'	– the reaction rate constant

Eq.1.28 is an ideal comprehensive expression, in which the equations of $f_1(C_A)$, $f_2(R)$, $f_3(d)$ can be determined by experimental study. However, not all influential factors on the reaction rate are possible to be studied at the same time. Usually, under isothermal conditions, gas properties $f_1(C_A)$ and solid particle $f_3(d)$ are fixed, and the following expression is obtained:

$$\frac{dR}{dt} = kf_2(R) \tag{1.29}$$

k is the reaction rate constant accounting for the effect of temperature on the rate, which is described by the Arrhenius equation (1.30).

$$k = A\exp\left(-E_a / R_g T\right) \tag{1.30}$$

Where,

A	– the pre-exponential factor (s^{-1})
E_a	– the activation energy of the process ($kJ \cdot mol^{-1}$),

The function $f_2(R)$ normally depends on the geometric changes occurring in the solid progress of reaction. Various geometric changes have been investigated by previous researchers and defined as different models like unreacted shrinking core model, grain model, nuclei growth model etc. Different kinetic models can be used for various reduction mechanisms.

When Eq.1.29 is integrated under isothermal conditions, the following expression is obtained:

$$G(R) = \int_0^R \frac{dR}{f_2(R)} = \int_0^t k dt = kt = A\exp\left(-E / R_g T\right) t \text{ (Integral form)} \tag{1.31}$$

The function of $G(R)$ has different expressions depending on the kinetic model.

1.4.2 Reaction rate of iron ore reduction

From the literature study the monitoring of reduction kinetics of a single oxide particle is usually carried out by suspending a spherical sample from a balance in a flowing-gas stream of known composition and temperature for continuous measurement of weight loss. In 1958 [35], McKewan has studied magnetite reduction by hydrogen at temperatures below 843 K. In order to analysis the weight-loss data, the experiment was designed for: (a) isothermal conditions; (b) single gas-solid reaction interface; and (c) dense specimens. Finally, he obtained the one interface unreacted shrinking core model of iron ore reduction with the experimental results. Based on this study, the two interfaces unreacted shrinking core model and three interfaces unreacted shrinking core model have been developed. The one interface shrinking core model was employed in this study and was briefly reviewed here.

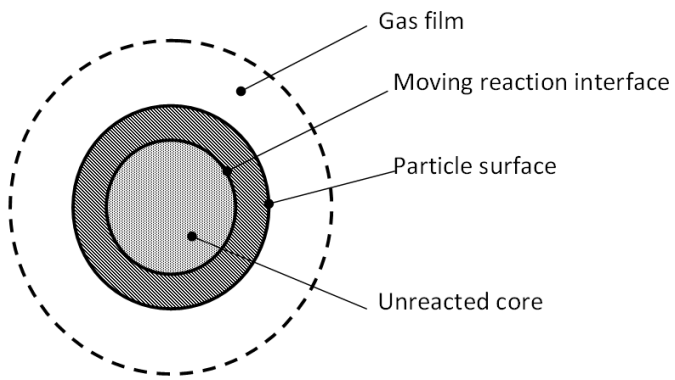

Figure 1.12 Schematic diagram of un-reacted shrinking core model

As shown in Figure 1.12, the system is composed of three phases: the gaseous phase, the product layer and the un-reacted core. The removal of oxygen from the unreacted core takes place at a sharp interface, and results in a weight-loss. The removal of oxygen proceeds through the following steps occurring successively during the reaction:

a) Transport of gaseous reactant (CO/H_2) from bulk gas to exterior surface of the iron ore particle through a gaseous boundary layer.
b) Diffusion of gaseous reactant (CO/H_2) through the product layer to the reaction surface.
c) Chemical reduction reaction of iron oxide with CO and H_2.
d) Diffusion of gaseous product (CO_2/H_2O) outward through the product layer.
e) Transport of the gaseous product (CO_2/H_2O) from the exterior surface of the particle to the bulk gas through the gaseous boundary layer.

Mathematically, according to the unreacted shrinking core model, the rate equations of the above sequential steps can be expressed in three general classifications as follows.

(1) Mass transfer through a gas film (steps (a) and (e)),

When the resistance of the gas film controls the reactions, the concentration profile for the gas-phase reactant is shown in Figure 1.13. The molar flux of CO from the bulk gas phase to the exterior surface of the sphere is given by:

$$n^{m}_{CO} = 4\pi r_0^2 k_{m,CO}(C^{b}_{CO} - C^{0}_{CO}) \tag{1.32}$$

Similarly the molar flux of CO_2 from the exterior surface of the sphere to the bulk gas phase is given by:

$$n^{m}_{CO_2} = 4\pi r_0^2 k_{m,CO_2}(C^{b}_{CO_2} - C^{0}_{CO_2}) \tag{1.33}$$

Where,

r_0 – radius of the original particle, m;

n^{m}_{CO} – molar flow of CO from bulk gas to exterior surface of the iron ore particle, mole/s;

$n^{m}_{CO_2}$ – molar flow of CO_2 from exterior surface of the particle to bulk gas, mole/s;

$k_{m,CO}$, k_{m,CO_2} – mass transfer coefficients for CO and CO_2, m/s;

C^{b}_{CO}, C^{0}_{CO}, $C^{b}_{CO_2}$ and $C^{0}_{CO_2}$ – concentrations of CO and CO_2 at bulk gas phase and the exterior surface of the particle, mole/m^3.

Theoretically, the mass transfer of the boundary-layer gas film is possible to be a controlling step. However, in the plant, it rarely happens. In the laboratory, it can be avoided by increasing the reducing gas velocity. When the gas velocity of reducing gas is high enough, the gas can pass through the gas film easily and the transport resistance of gaseous reluctant in the gas film could be neglected.

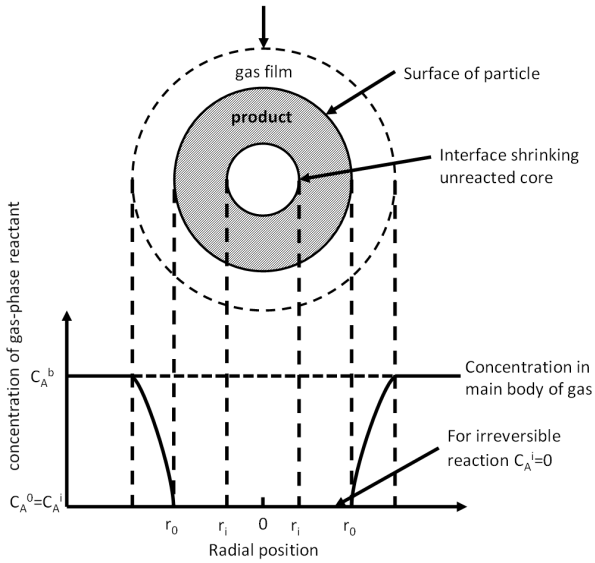

Figure 1.13 Gas-film diffusion is the rate controlling step

(2) Diffusion through product layer (Step (b) and (d))

The molar flow of CO and CO_2 ($n^D{}_{CO}$ and $n^D{}_{CO_2}$) by diffusion through the porous product layer as shown in Figure 1.14 is given by the following equations:

$$n^D{}_{CO} = 4\pi r_i^2 D_{eCO} \frac{\partial C_{CO}}{\partial r} \tag{1.34}$$

$$n^D{}_{CO_2} = 4\pi r_i^2 D_{eCO_2} \frac{\partial C_{CO_2}}{\partial r} \tag{1.35}$$

Where,

D_{eCO} – effective diffusivities for CO, m^2/s;

D_{eCO_2} – effective diffusivities for CO_2, m^2/s;

r_i – radius of the un-reacted core, m.

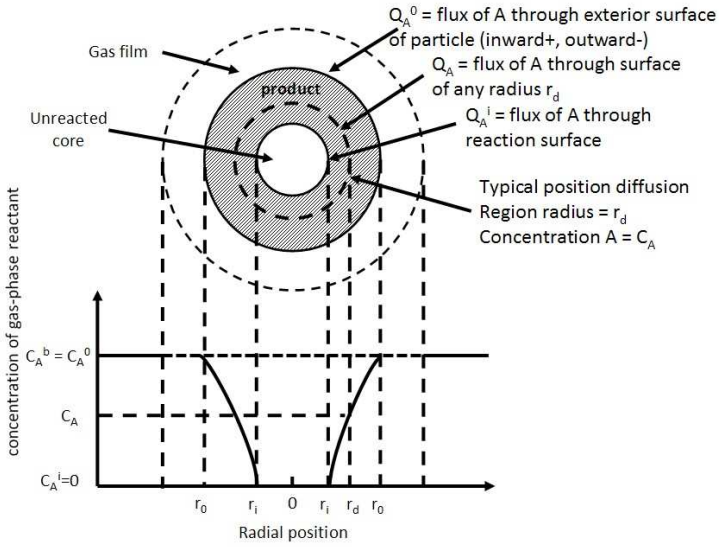

Figure 1.14 Gas diffusion is the rate controlling step

(3) Interfacial chemical reaction (step (c))

The chemical reduction of iron oxides by gases as shown in Figure 1.15 is considered as a first order, reversible reaction with respect to the concentration of a gaseous composition. The rate of interfacial reaction is expressed as follows,

$$r_c = 4\pi r_i^2 \frac{k_f (1 + K_e)}{K_e} \left(C_{CO} - C_{CO}{}^e \right) \tag{1.36}$$

Where,

r_c – the chemical reaction rate, mol/s;

k_f – the forward reaction rate constant, m/s;

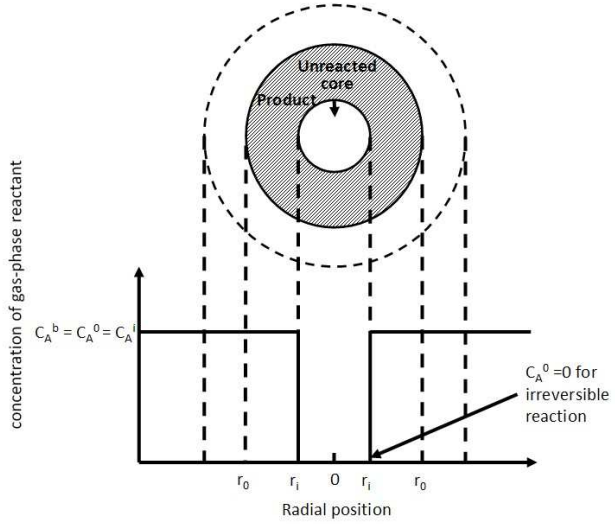

Figure 1.15 Chemical reaction is the rate controlling step

Each step may contribute resistance to the completion of the overall chemical reaction. The slowest step among these five which are connected in series will provide the largest resistance to the overall reaction. If a step is much slower than all others so that resistances attributed by the other steps become relatively insignificant, this step is called the rate-controlling step.

1.5 Determination of rate controlling steps of iron ore reduction

In studies of chemical reactions occurring in more than one step, the determination of the rate controlling step has been a common method to try to identify a particular elementary step as having a very strong influence on the overall rate. The rate controlling step is very important to the optimization and understanding of the reaction process, especially for the reactions occurring at complicated conditions like the fine iron ore in the smelting cyclone. Therefore, it is one of the significant objectives in this study. In the previous study, there are two groups of methods used to analyze either isothermal or non-isothermal kinetic data: model–fitting and model–free methods.

1.5.1 Model–fitting methods

For these methods, different models are fit to the data and the model giving the best statistical fit is chosen as the model of choice from which the rate constant (k) and thus activation energy (E_a), and frequency factor (A) can be calculated [36,37]. For the isothermal model-fitting method, it involves two steps: (1) determine the rate constant (k) of the model that best fits the data according to Eq.1.31; and do this for different temperatures (2) determine specific kinetic parameters such as the activation energy (E_a) and frequency factor (A) using the Arrhenius equation (Eq.1.30). The rate constants at all temperatures from the first step are used in the second step according to the Arrhenius equation. The activation energy (E_a) and frequency factor are obtained from the slope and the intercept, respectively. In Eq.1.31, $G(R)$ depends on the applied kinetic model and rate controlling step.

In 1960, McKewan [38] observed that the rate of weight loss due to the removal of oxygen at the magnetite/iron interface in spherical pellets with a diameter of 0.009 m (9 mm) at a temperature lower than 843 K is proportional to the area of the iron/iron oxide interface. This study has shown that the metallic iron forms a surface layer on the magnetite reactant, and then gradually replaces the magnetite. He proposed a “one interface unreacted shrinking core model”. He assumed that the un-reacted core of magnetite retains the shape of a sphere but shrinks with the increase of reaction time. The rate of reduction was controlled by a gas-solid interfacial reaction. The rate of reduction, in terms of rate of removal of oxygen per unit time, can be expressed as Eq. 1.37.

$$\frac{dw_o}{dt} = 4\pi r_i^2 \rho_o \frac{dr}{dt} \tag{1.37}$$

Where,

dw_o/dt – the rate of removal of oxygen in the solid specimen, mole/s;

ρ_o – the oxygen density of the solid reactant, mole/m^3.

By integrating Eqs.1.36 and 1.37, McKewan obtained the following equation for the calculation of the degree of reduction or the size of the core as a function of the time of reaction.

$$\rho_o r_0 \left(1 - (1 - R)^{\frac{1}{3}}\right) = k_{MK} t \tag{1.38}$$

$$k = \frac{k_{MK}}{\rho_o r_0} = \frac{k_f \left(1 + K_e\right)\left(C_0 - C_e\right)}{\rho_o r_0 K_e} \tag{1.39}$$

R is the reduction degree and it can be expressed as

$$R = 1 - \left(\frac{r_i}{r_0}\right)^3 \tag{1.40}$$

Therefore,

$$G(R) = 1 - (1 - R)^{\frac{1}{3}} \tag{1.41}$$

Based on this breakthrough study by McKewan, in 1962, Kawasaki et al. [39] used larger artificial pellets with a diameter of 0.015 to 0.044 m and conducted the experiments at temperatures of 1143 K to 1473 K. They reported that their data can be explained very well by a model which assumes that the rate of overall reaction is controlled by gaseous diffusion through the porous product layer except at the early period of reduction. Their resulting diffusion mechanism equation is the integrated form of Eqs. 1.34 and 1.37,

$$\frac{w_o r_0}{A_0 \left(C_0 - C_e\right)} \left[\frac{3}{2} \left[1 - \left(1 - R\right)\right]^{\frac{2}{3}} - \frac{r_0 R}{\left(r_0 + y\right)} \right] = D_e t \tag{1.42}$$

Where,

w_o – oxygen molar weight loss of the oxide when fully reduced, mole;
A_0 – outside area of the specimen, m^2;
y – the gas film thickness surrounding specimen, m.

Ginstling and Brownshtein [40] derived the following equation for the kinetics of reactions in spherical particles from an approximate solution of the equation of the diffusion.

$$1 - \frac{2}{3} R - \left(1 - R\right)^{\frac{2}{3}} = \frac{k_{GB}}{r_0^{\,2}} t = kt \tag{1.43}$$

Where k_{GB} is the Ginstling-Brownshtein rate constant, which is proportional to the diffusion coefficient.

$$k_{GB} = 2/\rho_0 \, D_e C_0 \tag{1.44}$$

Therefore,

$$G(R) = 1 - \frac{2}{3}R - (1-R)^{\frac{2}{3}} \tag{1.45}$$

In 1963, Lu [41] recognized that interfacial reaction control and gas diffusion control are two extreme situations in the reduction of an iron oxide. During a reduction reaction, it is possible that rate control may shift gradually from one mechanism to another. He proposed a mixed control model to include interfacial reaction and diffusion in solid layers. In order to eliminate the unknown concentration of gaseous reductant in the interface, Lu proposed a quasi-steady state model to connect steps (b) and (c) and derived a general rate equation in the integrated form as follows,

$$\frac{r_0 D_e k C_0 t}{\rho_O} = D_e r_0 (r_0 - r_i) + (k/6)\left(r_0^3 + 2r_i^3 - 3r_0 r_i^2\right) \tag{1.46}$$

Seth and Ross [29] developed a similar but more convenient Eq.1.47 using reaction fraction instead of *r.*

$$\frac{t}{1-(1-R)^{\frac{1}{3}}} = t_D\left[1+(1-R)^{\frac{1}{3}} - 2(1-R)^{\frac{2}{3}}\right] + t_C \tag{1.47}$$

$$t_{\mathrm{D}} = \frac{\rho_o r_0^2}{6\mathrm{D_e}\left(C_0 - C_e\right)} \tag{1.48}$$

$$t_{\mathrm{C}} = \frac{\rho_o r_0 K_e}{k_f\left(1+K_e\right)\left(C_0 - C_e\right)} \tag{1.49}$$

If the plot of $1 - (1 - R)^{1/3}$ versus t gives a straight line, the rate controlling step is chemical reaction. If the plot of $1 - 2/3R - (1 - R)^{2/3}$ versus t gives a straight line, the rate controlling step is gaseous diffusion. If it is a mixed control, the plot of $t/(1 - (1 - R)^{1/3})$ versus $1 + (1 + R)^{1/3} – 2(1 - R)^{2/3}$ would give a straight line.

Prakash and Shanker studied the reduction kinetics of iron ore under fluctuating temperature conditions [42]. The material in this study was sieved into two size

fractions namely (-10~+6) and (-6~+3) mm. The reducing gas was composed of CO and N_2 (30:70) and the gas mixture was produced in the laboratory by gasification of graphite/coke by CO_2. In the furnace, an iron ore sample (~500 g, bed height ~75 mm) enclosed in a stainless steel cage was suspended with a platinum wire connected to a balance. The sample was heated to 1073 K, 1173 K and 1273 K, respectively. The results fitted the Eq.1.43 very well. Therefore, the unreacted shrinking core model was successfully used in this study and the conclusion can be obtained that the reduction of the iron ore sample was controlled by gas diffusion in the product layer.

Itaya and his co-workers studied the circulation and reduction behaviour of iron ore in a circulating fluidized bed [43]. The experiment was carried at the temperature between 973 K and 1073 K with the very fine iron ore particles (30 µm, 141 µm and 162 µm). The un-reacted shrinking core model has adopted as the mathematical kinetic model. The results showed that the rate controlling step in the reduction of very fine ore was the chemical reaction. On the other hand, the reduction of larger size ore was affected by both chemical reaction and diffusion in the particles. However, the experimental temperatures were far below the melting point of the iron ore, for that the fluidized bed reactor was used.

In 2007, Takeuchi and his co-workers reported the results of kinetic analysis of spherical wüstite reduction transported with CH_4 gas [44]. In this work, the mechanism and the kinetics of the reduction by CH_4 gas were accurately investigated with spherical wüstite fine particles. Reduction temperature was varied from 1373 K to 1573 K. As a result, reduction degree of spherical wüstite by CH_4 gas reached over 80 % at 1573 K within 1 second. From the cross section observation of the particle after reduction, it was found that the periphery of the wüstite particle was metalized by the reduction reaction and un-reacted wüstite core remained inside. Therefore, it indicated that the reduction progressed topochemically under this experimental condition. From the kinetic analysis, it was concluded that the reduction rate controlling step was the chemical reaction on the Fe-FeO interface.

In the investigation of Habermann et al. [45], fine iron ore was reduced in a wide range of fluidized bed conditions. The temperature was changed from 773 K to 1173 K. The reducing gas contains H_2, CO, CO_2, CH_4, H_2O and N_2. Through analysis of the experimental data and the microscope photos of the partial reduced particles obtained by scanning electron micrographs, the rate controlling step was determined based on the one interface unreacted core model. The results showed that during the first phase of reduction (a reduction degree of 0 to 0.15), the reduction rate was controlled by the transport of the reduction gas from the bubble phase of the fluidized bed to the iron ore particle and the transport of product gas from the particle to the bubble phase. During the second phase of reduction, the reduction rate seemed to be controlled by interface reaction control or by pore diffusion. From the curves obtained from Eq.1.38 and Eq.1.43, it was hard to tell

which one is the rate controlling step.

1.5.2 Model–free methods

Model-free methods [36,37] calculate the reaction activation energy (E_a) without modelling assumptions, which is usually done by grouping terms such as the frequency factor (A) into the intercept of a linear equation and using the slope of that equation to calculate the activation energy (E_a). The frequency factor (A) can be calculated from the intercept of the linear equation but requires modelling assumptions for such a determination. Therefore, model-free methods usually report only activation energies. For the isothermal study, the two most popular methods can be used to determine the activation energy (E_a): the standard method and Friedman's method.

1.5.2.1 Standard method

This method is based on the logarithm of the isothermal rate law (Eq.1.31):

$$\ln G(R) = \ln(A) - \frac{E_a}{R_g T} + \ln(t) \tag{1.50}$$

This can be rearranged to,

$$-\ln(t) = \ln\left(\frac{A}{G(R)}\right) - \frac{E_a}{R_g T} \tag{1.51}$$

A plot of ln(t) versus $1/T$ gives E_a from the slope for that R regardless of the model according to,

$$-\ln(t_R) = \ln\left(\frac{A}{G(R)}\right)_R - \frac{E_{aR}}{R_g T_R} \tag{1.52}$$

1.5.2.2 Friedman's method

This method is a differential method. The logarithm of the isothermal rate law gives

$$\ln\frac{dR}{dt} = \ln\left(Af\left(R\right)\right) - \frac{E_a}{R_g T} \tag{1.53}$$

A plot of ln(*dR/dt*) versus *1/T* at each *R* gives E_a from the slope for that *R* regardless of the model according to,

$$\ln\left(\frac{dR}{dt}\right)_R = \ln\left(Af\left(R\right)\right)_R - \frac{E_{aR}}{R_g T_R} \tag{1.54}$$

Model-fitting methods were the first and most popular methods to be used in evaluating solid state kinetics for that they have the ability to directly determine the kinetic triplet (*A*, E_a, and model). However, these methods have several problems, among which is their inability to uniquely determine the reaction model. The use of model-free methods has increased recently [46-48] due to the ability of these methods to calculate Ea values without modelling assumptions.

1.6 Objectives and layout of the thesis

The HIsarna process is a new ironmaking process developed on the basis of the CCF and the HIsmelt process. The experiences and experimental data from the two processes are not sufficient to understand and describe the HIsarna process because it has a lot of new features. The pilot plant engineering for this project is currently underway and several trials have been done from 2010 to 2012. The laboratory study is also necessary to start in parallel with the pilot plant tests. In the HIsarna process, the smelting cyclone is one of the most complicated parts as the iron ore inside it has a lot of intensive physical and chemical transformations. Its efficient and smooth running is very important for the following processes. This project focused on the iron ore in-flight melting and reduction behaviour of small iron ore particles in the smelting cyclone. The reduction mechanism of individual iron ore particles in the reducing gas at high temperatures has been investigated with the high temperature drop tube furnace in this project. The laboratory study aims to provide significant information for in-depth understanding the process insights and will be useful for scaling up the pilot plant.

The thesis is composed of six chapters. For easy reading and understanding, they are introduced and listed as follows.

Chapter 1 Introduction

The research work started with the literature study as shown in this Chapter. The HIsarna process is very young in the ironmaking world. A brief introduction on the

background and current status is given in this chapter. Besides, the theoretical and experimental investigations by previous researchers on kinetics of the iron ore reduction are illustrated in this chapter.

Chapter 2 Experimental Apparatus and Analysis Methods

The experimental study started with the selection and the design of the laboratory experimental set-up which is described in detail here. The materials, sizes and functions of each facility are presented. In addition, the analysis methods for analyzing the reduced samples are also given in this chapter.

Chapter 3 Experimental Study on the Thermal Decomposition Behaviour of Iron Ore Particles

For the special condition in the cyclone reactor, the weight loss of oxygen from an iron ore sample is caused by both thermal decomposition and reduction. Chapter 3 analyzes the thermal decomposition behaviour of iron ore from theoretical evaluation and experimental study.

Chapter 4 Reduction Behaviour of Individual Iron Ore Particles in the High Temperature Drop Tube Furnace

This chapter shows the experimental investigation of reduction behaviour of individual iron ore particle in the high temperature drop tube furnace. The experimental study was focused on the effects of temperature, gas composition, particle size, and residence time on the iron ore reduction.

Chapter 5 Kinetic Modelling of Pre-reduction of Iron Ore Particles

This chapter presents the kinetic analysis of iron ore reduction at high temperature on the basis of the experimental results of Chapter 4. The kinetic model has been determined by the model-fitting method and model-free method. The kinetic data has been calculated for quantitative analysis of the iron ore reduction mechanism.

Chapter 6 Conclusions and Outlook

The most important conclusions derived from the present work in this thesis are summarized. Recommendations are given based on the work in the previous chapters.

References

[1] Orth, A., Anastasijevic, N., and Eichberger, H.: Low CO_2 emission technologies for iron and steelmaking as well as titania slag production, Minerals Engineering, 20(2007) 854-861.

[2] www.worldsteel.org

[3] Birat, O. J. P.: Addressing the climate change challenge: ULCOS Breakthrough program, CAMP-ISIJ 14(2001).

[4] www.ulcos.org

[5] Gupta, S. and Sahajwalla, V.: The scope for fuel rate reduction in ironmaking, The University of New South Wales, editor: John Burgess, 2005.

[6] Birat, J.P., Hanort, F., and Danloy, G.: CO_2 mitigation technologies in the steel industry: A benchmarking study based on process calculations, Proceedings of the 3rd International Conference on Science and Technology of Ironmaking (ICSTI), Dusseldorf, 16-20 June, 2003, 588-592.

[7] Ge, A. X.: A neural network approach to the modelling of blast furnace, Master thesis, Department of Electrical Engineering and Computer Science, 1999.

[8] Lundkvist, P.: Experiments and capability analysis in process industry, Thesis, Lulea University of Technology, 2012.

[9] Saheb, V.: Studies on blast furnace slag flow characteristics, Master thesis submitted to National Institute of Technology, Rourkela, 2012.

[10] http://webs.purduecal.edu/civs/research/educationtraining/virtual-blast-furnace/

[11] Birat, J. P.: Alternative ways of making steel: Retrospective and prospective, La Revue de Metallurgie-CIT, 11(2004) 937-955.

[12] Best available techniques (BAT) reference document for iron and steel production, Report by Joint Research Centre of the European Commission, 2011, 521-536.

[13] Afanga, K., Mirgaux, O., and Patisson, F.: Assessment of top gas recycling blast furnace: A technology to reduce CO_2 emissions in steelmaking industry, Carbon Management Technology Conference, Orlando, Florida, USA, 7-9 February 2012.

[14] Zuo, G. and Hirsch, A.: The trial of the top gas recycling blast furnace at LKAB'S EEBF and scale-up, Proceedings of the 4th Ulcos seminar, 1-2 October 2008.

[15] Danloy, G., Berthelemot, and A., Grant, M.: ULCOS-Pilot testing of the low-CO2 blast furnace process at the experimental BF in Lulea, La Revue de Metallurgie – CIT, 1(2009) 1-8.

[16] Birat, J. P.: ULCOS II has been shaping up, Presentation, Brussels, 5 March 2009.

[17] Wingrove, G., Keenan, B., Satchell, D., and Aswegen, C. V.: Developments in ironmaking and opportunities for power generation,

Gasification technologies conference, San Francisco, California, 17-20 October 1999.
[18] Gojic, M. and Kozuh, S.: Development of Direct Reduction Process and Smelting Reduction Processes for the Steel Production. Kem. Ind., 55(2006) 1-10.
[19] Lockwood Greene: Ironmaking process alternatives screening study, Volume I: Summary report, 2000.
[20] http://www.midrex.com/handler.cfm/cat_id/166/section/global
[21] Atsushi, M., Uemura, H., and Sakagushi, T.: MIDREX Processes, Kobelco technology review, 29(2010) 50-57.
[22] Bergman, L. and Larsson, M.: HSC simulations of coal based DR in ULCORED, Proceedings of the 4th Ulcos seminar, Lulea, Sweden, 1-2 October 2008.
[23] Burke, P. and Gull, S.: HIsmelt – The Alternative Ironmaking technology, Smelting reduction for ironmaking, Bhubaneswar, 18-19 December, 2002.
[24] Fruehan, R.J.: Future Ironmaking process, Doe Final Report, 2004.
[25] Joseph, J.P.: Future trends in ironmaking, Prepared for McMaster Blast Furnace Ironmaking Course, 2012.
[26] Meijer, H.K.A., Flieman, G.A., Teerhuis, C.P., Bernard, J.G., and Boom, R.: The Cyclone Converter Furnace (CCF) - A Hot Metal Route Avoiding the Cod Carborization and Ore Agglomeration Stages, Ironmaking 2000 - 18th Advanced Technology Symposium, TMS, October, 1994, 56-61.
[27] Link, J.: " IRMA – Flowsheet Model Examples of Application", La Revue de Metallurgie, 2009, 398-403.
[28] Meijer, K.,Guenther, C., Dry, R.J.: "HIsarna pilot plant project", METEC conference. Dusseldorf, Germany, July 2011.
[29] Wagner, D., Devisme, O., Patisson, F., and Ablitzer, D.: A laboratory study of the reduction of iron oxides by hydrogen. TMS, 2(2006) 111-120.
[30] McKewan, W.M., Kinetics of iron oxide reduction, Trans. Met. Soc. AIME, 218 (1962) 2-6.
[31] Grigore, M., Sakurovs, R., and French, D.: Mineral reactions during coke gasification with carbon dioxide, International Journal of Coal Geology, 75(2008) 213-224.
[32] Strezov, V., Liu, G. S., Lucas, J. A., and Wibberley, L.J.: Computational calorimetric study of the iron ore reduction reactions in mixtures with coal, Ind. Eng, Chem, Res, 44(2005) 621-626.
[33] Valipour, M. S.: Mathematical modeling of a non-catalytic gas-solid reaction: Hematite pellet reduction with syngas, Transactions C, 16(2009) 108-124.
[34] Biswas A. K.: Principles of blast furnace ironmaking, 1981.
[35] Sun, S.S.: A Study of Kinetics and Mechanisms of Iron Ore Reduction in Ore/Coal Composites, PhD thesis, McMaster University, 1997.
[36] Khawam, A, and Flanagan, D. R.: Basics and applications of solid-state kinetics: A pharmaceutical perspective, Journal of pharmaceutical sciences, 95(2006) 472-498.

[37] Khawam, A. and Flanagan, D. R.: Solid-state kinetic models: Basics and mathematical fundamentals, J. Phys. Chem. B, 110(2006), 17315-17328.
[38] McKewan, W.M., Kinetics of Iron Oxide Reduction. Trans. Met. Soc. AIME, 218(1960) 2-6.
[39] Kawasaki, E., Sanscrainte, J., and Walsh, T.J., Kinetics of reduction of iron oxide with carbon monoxide and hydrogen. A.I.Ch.E. Journal, 8(1962) 48-52.
[40] Ginstling, A. M. and Brounshtein, B. I., Concerning the Diffusion Kinetics of Reactions in Spherical Particles, J. Appl. Chent. USSR (English Translation) 23(1950) 1327-1338.
[41] Lu, W. K.: The general rate equation for gas-solid reaction in metallurgical process, Trans. Met. Soc. AIME, 227(1963) 203-206.
[42] Prakash, S. and Shanker, H.: Reduction and sintering of fluxed iron ore pellets – a comprehensive review, The Journal of the South African Institute of Mining and Metallurgy 1996, 3-16.
[43] Itaya, H., Seiji, M. S.: Circulation and reduction behaviour of iron ore in a circulating fluidized bed, ISIJ International, 34(1994) 393-400.
[44] Takeuchi, N., Nomura, Y., Ohno, K., Maeda, T., Nishioka, K., and Shimizu, M.: Kinetic analysis of spherical wüstite reduction transported with CH_4 gas, ISIJ International, 47(2007) 386-391.
[45] Habermaan, A., Winter, F., Hofbauer, H., Zirngast, J., and Schenk, J. L.: An experimental study on the kinetics of fluidized bed iron ore reduction, ISIJ International, 40(2000) 935-942.
[46] Vyazovkin, S., and Dranca, I.: Physical stability and relaxation of amorphous indomethacin, J. Phys, Chem. B, 109 (2005), 18637-18644.
[47] Yu, Y. F., Wang, M. H., Gan, W. J., Tao, Q. S., and Li, S. J: Polymerization-induced viscoelastic phase separation in polyethersulfone-modified epoxy systems, J. Phys. Chem. B, 108(2004), 6208-6215.
[48] Bendall, J.S., Ilie, A., Welland, M. E., Sloan, J., and Green, M. L. H: Thermal stability and reactivity of metal halide filled single-walled carbon nanotubes, J. Phys. Chem. B, 11(2006) 6569-6573.

Chapter 2 Experimental Apparatus and Analysis Methods

2.1 Introduction

For the HIsarna process, the smelting cyclone is the most complicated and important part, in which a series of chemical reactions and physical transitions take place accompanied by intensive heat and mass transfer. Therefore, the in-depth understanding of the thermal dynamics and kinetic behaviour of the very fine iron ore particles during the in-flight melting and reduction process in the cyclone reactor is highly relevant for understanding the overall process. With this scientific aim, the laboratory scale experiments were carried out with different laboratory set-ups to obtain a comprehensive investigation. Main focus is on the stage where the injected iron ore particles are in free flight and the conditions studied are within the window of gas composition, gas temperature, particles size, and particle residence time experienced in the smelting cyclone. To satisfy all these requirements, the selection of an appropriate laboratory reactor is the first and important mission for the overall research.

Through literature study, it can be concluded that most laboratory experiments of kinetic reduction of iron oxide like pellet reduction were carried out with the thermogravimetry method in a high temperature chamber or were carried out in a crucible. For the very fine iron ore sample, the laboratory kinetic experiments were carried out in batch using a fluidized bed reactor. However, in this study, on one hand, the main purpose is to investigate the reduction behaviour of an iron ore particle at high temperatures. (The temperature above the melting point of iron ore is also studied.) On the other hand, the particle size of the iron ore is very fine, less than 100 µm. Furthermore, the prospective reduction degree of the product is around 20 % which needs a very short residence time of less than 2 s. Tsukihashi et al. [1] have reported that the fractional reduction of fine wüstite using a CO-CO_2 mixture gas reached 70 % at 1873 K in 1.3 s. In the case of using a H_2-N_2 mixture gas, Hayashi and Iguchi [2] have reported the fractional reduction reached about 80 % at 1823 K in 0.5 s.

In the thermogravimetry method, the sample is loaded on a balance on a thin metal wire. The chemical reactions take place in the slow reaction rate zone where reaction barely progresses within several minutes [3]. In other words, the experiments run at low temperature and in low reduction potential gas composed of carbon monoxide, hydrogen or syngas. A crucible allows a wide temperature range operation even above the melting point [4], but the chemical reaction is non-

uniform, as it usually takes place only intensively at the interface between reactant and reducing gas. This method also suffers from the danger of contaminations from the crucible especially at very high temperature as well as from heat-transfer limitations within the sample batch. The reduction in laboratory fluidized bed can avoid agglomeration, and have uniform and wide range temperature in the reactor and excellent heat and mass transport. Therefore, it is often used to investigate the reduction kinetics of iron ore fines under conditions similar to industrial scale [3, 5, 6] units like FINMET process and FINEX process [7]. However, the temperature can't be higher than the melting point of the iron ore sample.

Drop tube furnaces have been used extensively in the laboratory study of flash smelting processs [8, 9] and in the studies of coal and carbonaceous materials combustion which occur at high temperature, e.g. Barranco et al. [10]. In the drop tube furnace, temperature, residence times, and gas-phase composition are closely controlled. It can well simulate the flash condition of individual reacting particles flying through the flash smelting furnace as well as the burnout performance of coal. The laboratory studies using the drop tube furnace provided useful insights of individual particle behaviour in the industrial reactor. Huffman et al. [11] took advantage of the drop tube furnace to investigate the transformation of pyrite removal from coal. Gas temperature was in the range from 1311 K to 1727 K and residence time was in the range from 0.07 s to 1.2 s. Particle size was less than 75 µm.

In the smelting cyclone of the HIsarna process the injected very fine iron ore experiences heating up, reduction and melting in a short time, which is similar to what happens in the flash smelting process. From the above analysis, the drop tube furnace is adopted as the laboratory experimental set-up for simulating the cyclone reactor. This system has the following advantages [2, 9].

- It is effective in measuring a fast reaction rate at a high temperature even above the melting point of iron ore without particle sticking or fusion problems;
- High mass and heat transfer from gas film to particles can be expected for this system, hence it is applicable to monitor a rapid reaction rate reduction;
- There is no contamination from external parts, because no crucible is used;
- Individual particle behaviour can be studied in a short residence time at high temperature.

Above all, from the three critical standpoints of this study: high temperature, individual particle behaviour, and flash reaction, the drop tube furnace is the most suitable choice as a laboratory experimental apparatus. A detailed description of the improved equipment used in this study is given here and is published

elsewhere [12, 13]. In addition to the drop tube furnace, thermal decomposition experiments of hematite and hematite ore were conducted in a TGA-DSC analyser and a horizontal furnace to obtain more details of the reaction mechanism.

2.2 High temperature drop tube furnace

The drop tube furnace is a type of laminar flow reactor and its performance is characterized by temperature profiles, velocity profiles, and expected particles residence times to study reaction mechanisms under very well controlled conditions. The design parameters of the furnace include pressure (kPa), maximum temperature (K), particle residence time (s), particle feed rate (g/h), reaction tube size (D × L mm), the number of heat zones, variable or fixed reaction length, and location of optical access. Ouyang Shan [13] has summarized the general characteristics of drop tube furnaces as shown in Table 2.1. As mentioned above, the drop tube furnace is popular in the study of coal combustion for that it can better reflect the pulverized fuel combustion environment. The atmospheric pressure drop tube furnaces have been wildly using and in recent years the pressured drop-tube furnaces have been built for measurement of reaction kinetics of coals at high pressures and temperatures. The design and operation of drop tube furnace used for coal combustion were used as a source of reference for this study, and the atmospheric pressure drop tube furnace is already good enough for the current experimental investigation.

The design and manufacture of a drop tube furnace was carried out at the first stage of the experimental study. Comparing the design parameters in the literatures (Table 2.1), the atmospheric pressure drop tube furnace was adopted. The maximum temperature of this design is 1873 K and the particle feed rate is around 1 g/h. It has one heat zone. The optical access is not available for the reaction zone, but there is an optical access on the wall of sample collector. As it was specially designed for running at high temperature in this study, it is called “High Temperature Drop Tube Furnace” or HDTF in the flowing description. The concept of experimental set-up of HDTF is shown in Figure 2.1. The laboratory set-up can be divided into four parts:

(1) The gas line system
(2) The particle feeding system,
(3) The reactor system
(4) The particle collection system

The gas line system includes four digital mass flow controllers, four gas flow meters, a gas mixer and a gas pre-heater. The particle feeding system includes a multi-speed syringe pump connected to a water cooled injection probe and a

ceramic honeycomb gas flow straightener. The reactor system consists of an electrically heated vertical tube furnace, a laminar flow reactor of an Alsint tube, a pair of top water cooled flanges and a pair of bottom water-cooled flanges. The particle collection system includes a sampling probe, a sample collector and a jack. A B-type thermocouple was used for detecting the temperature in the hot zone. A K-type thermocouple was used for detecting the temperature in the gas pre-heater and the other K-type thermocouple is used for detecting the temperature in the particle collector. Details of the main parts in the apparatus are given in the following sections.

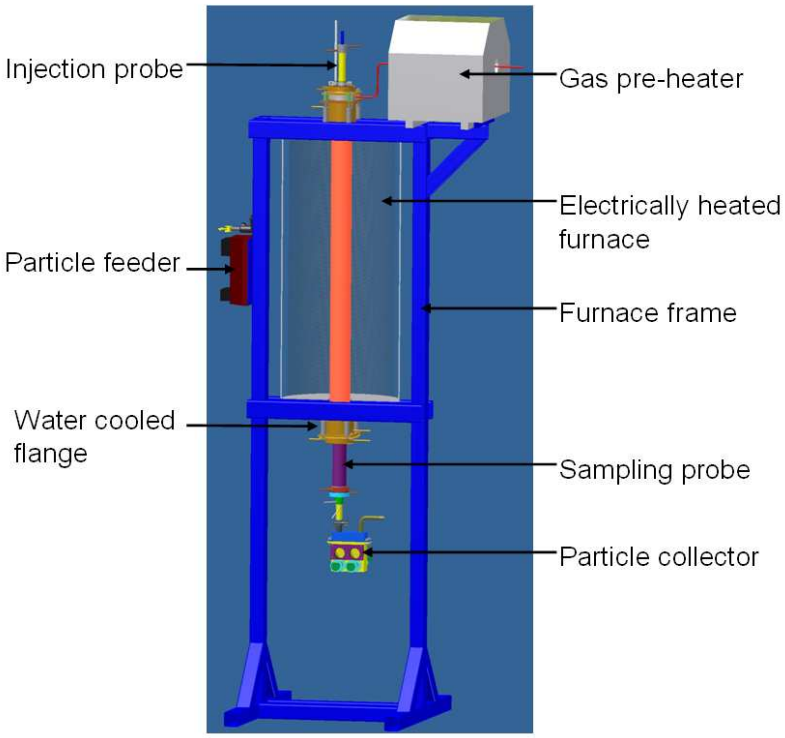

Figure 2.1 3-D illustration of the structure of HDTF

Table 2.1 General characteristics of some drop-tube furnaces [13]

Pressure (kPa)	Maximum T (K)	Particle residence time (s)	Particle feed rate (g/min)	Reaction tube D×L (mm)	Multiple heat zone	Variable reaction length	Optical access
100	1237	0.03-0.11	0.25-0.5	50×950	N	N	N
100	1250	0.025-0.27	~0.01	50×600	N	Y	Y
100	1700	----------	----------	63×2000	Y	----------	----------
100	2100	0.005-0.2	0.12-0.18	51×460	N	Y	Y
100	1923	0.01-0.7	2.0-3.0	51×750	N	Y	Y
600-7000	1373	0.06-1.7	0.2-0.5	40×550	N	Y	N
100-1600	1700	0.03-1.0	0.5-1.5	51×1200	Y	Y	Y
100-8000	1773	----------	----------	70×2000	Y	Y	Y
100-2500	1873	----------	0.2-0.5	50×1000	Y	----------	Y
100-2500	2073	2.0-8.0	----------	50×2050	Y	Y	N
100-1600	1673	0.02-10.0	0.3-1.5	75×1500	Y	Y	Y

2.2.1 The furnace

The furnace is 880 mm high and the outside diameter is 410 mm, heated with six SiC heating elements. The furnace is capable of reaching a temperature up to 1873 K. An Alsint tube (99.7 % Al_2O_3) is used as reactor, which can stand the temperature as high as 2073 K. The outer diameter (OD) of the tube is 70 mm, the inner diameter (ID) is 60 mm and the length is 1100 mm.

In order to make the temperature gradient in the hot zone as small as possible, the middle part of the Alsint reactor tube is externally surrounded by a SiC tube which has an ID of 72 mm and length of 400 mm. The thermal conductivity coefficient of Alsint tube is only 5 W/m·K at the temperature of 1773 K. The thermal conductivity coefficient of silicon carbide tube is 40 W/m·K at the same temperature. It is 8 times higher than the Alsint tube. It is supported by an alumina tube with the same diameter. Two pairs of large water-cooled brass flanges attached on the furnace frame seal off the top and bottom of the reaction tube. The upper part of the top flange is used to centre the injection probe. In addition, the other hole was made on the upper part of the flange allows the thermocouple to pass. The Alsint tube and SiC tube are supported by the upper part of the bottom flange. The ring-shape of the lower part of the bottom flange having two X-rings allows the sampling probe to be inserted into the furnace and to move freely to adjust the length of the hot zone.

2.2.2 The syringe pump feeder

In order to obtain the individual particle behaviour during the reaction, it is essential to have a feeder that could provide a small quantity of iron ore steadily and continually. The syringe pump feeder is such an apparatus which is designed for feeding very fine particles at a very low feed rate. The schematic diagram of the feeder is shown in Figure 2.2. It consists of a syringe pump, a transparent glass tube, two capillary tubes and two vibrators. A number of particles are held in a transparent glass tube which is supported by the piston of a syringe pump moving at a pre-set, slow and constant speed. The carrier gas flows into the transparent tube and exits through a capillary discharge tube carrying a small amount of the powder continually.

The syringe pump (No. NE1000) is employed as the driver of the particle feeder. Actually, it is used in medical or pharmaceutical or biomedical field. It is a small infusion pump for delivering accurate and precise amounts of fluids slowly (with or without medication) to an object. However, it has been successfully applied to the feeding system of the drop tube furnace like the use in Prof. Sohn's group at the university of Utah. This study makes use of the slow moving rate of the syringe pump to control the particle feed rate. The maximum speed of the piston is

306.03 cm/h and the minimum speed is 0.004205 cm/h. Taking into account of the cross-sectional area of the glass tube and the bulk density of the sample, the feed rate in grams per hour is calculated. The length of the glass tube is 15 cm. Its OD and ID are 7 mm and 9 mm, respectively. It is capable of holding approximately 10 grams of fine iron ore. As shown in the schematic diagram, the open end of the culture glass tube is inserted into a holder which is made of a vacuum fitting and a series of different size of fitting tubes. The capillary tube is made of stainless steel with the ID of 1.2 mm and OD of 2.2 mm. Its length is 1000 mm. One end of the tube is grounded to a high angle to achieve a larger entrance for the fine particle. This end is inserted into the glass tube through the holder, and adjusted such that the tip is just on the top of the fine particles surface. The whole feeder is vibrated by two electric vibrators to keep the feed rate constant and to prevent clogging. The fine particle feed rate is mainly determined by the speed of the syringe pump. From the experience, the flow rate of carrier gas also has some influence. However, the small error of charging rate from the gas flow could be neglected in this study because the particle feed rate just needs to make sure that there is no agglomeration among particles.

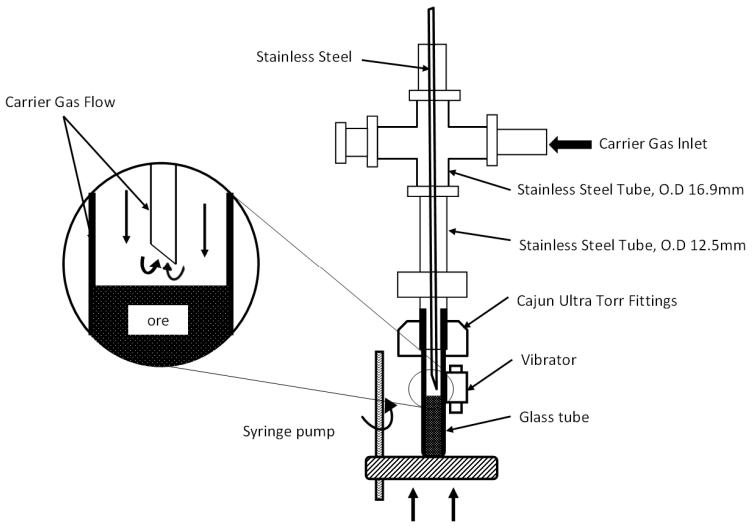

Figure 2.2 Schematic diagram of the simplified syringe pump particle feeder

2.2.3 Injection probe

For the kinetics study, it is important to keep identical treatment times for all particles in the drop tube furnace, which, in turn, demands that dispersion of the central stream of fine material is kept to a minimum. The velocity can be varied

strongly with the radius of the central jet. Aimed at this question, two types of injection probes were compared in the study of Flaxman and Hallett [14] as shown in Figure 2.3: 1. An injection probe incorporates a thick water cooling jacket around the central tube; 2. The cooling jacket at the lower part of the injection probe was eliminated and a honeycomb flow straightener was attached. Results are presented in terms of ratio U_p/U_s ratio of the average velocities of the primary (carrier gas) and secondary (main gas) flows and the Reynolds number of the secondary flow Re_s, where

$$U_p = \frac{m_p}{\rho_g \pi R_i^2} \tag{2.1}$$

$$U_s = \frac{m_s}{\rho_g \pi \left(R_o^2 - R_s^2\right)} \tag{2.2}$$

$$\mathrm{Re}_s = \frac{2\rho_g U_s \left(R_o - R_s\right)}{\mu} \tag{2.3}$$

Where, ρ_g - gas density, kg/m^3;

μ - gas viscosity, kg/m·s.

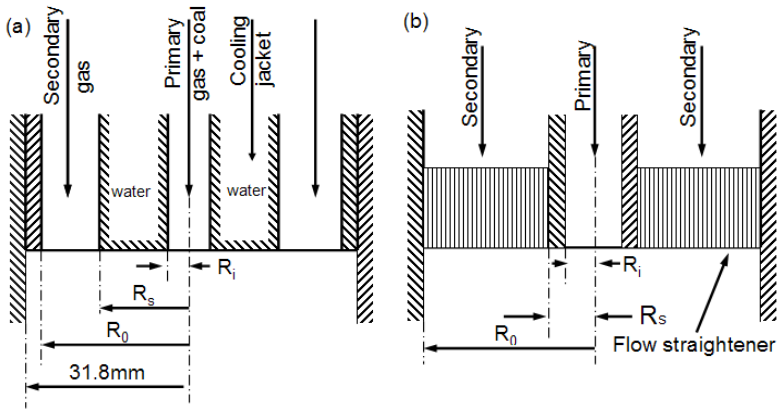

Figure 2.3 Burner head: (a) with cooling jacket, R_o=28.6 mm, R_s = 19.0 mm, R_i = 3.2 mm; (b) with flow straightener, R_o= 31.8 mm, R_s = 6.4mm, R_i = 3.2 mm [14]

Test result shows that for injection probe with a cooling jacket (a), a thorough mixing and dispersion of the jet prevailed over the entire range of Reynolds number and velocity ratio of practical interest (Re_s up to 2000, U_p/U_s from 1 to 8). Only at Re_s well below 100 the flow became more ordered. In contrast, injection probe with flow straightener (b) produced a stable laminar flow with negligible dispersion over a wide range of conditions. Only at high Reynolds number the central jet began to break up, first in unsteady laminar fashion, and then becoming fully turbulent as the flow increased as shown in Figure 2.4. A comparison by cold experiment as shown in Figure 2.5 presents the superiority of injection probe with flow straightener (b) clearly. That is because the flow straightener generates a sufficient pressure loss and produces a nearly uniform flow. Any wall between the straightener and the primary flow should be as thin as possible. Therefore, the burner head with flow straightener (b) was adopted in this study.

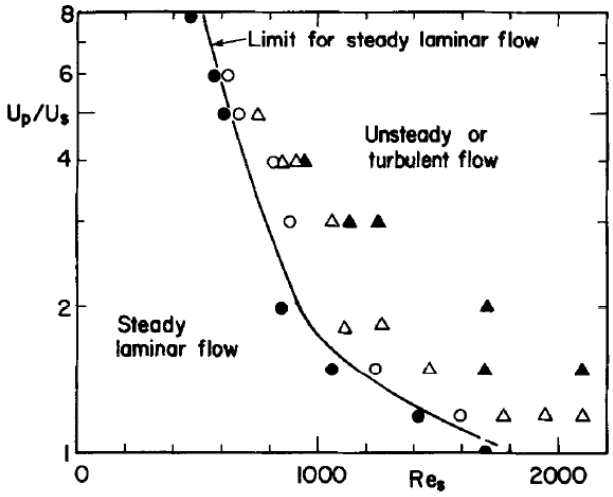

Figure 2.4 Flow regimes in reactor model with burner b (as shown in Figure 2.3). Key: ●, steady laminar; ○, nearly steady laminar; □, unsteady laminar; ▲, fully turbulent [14]

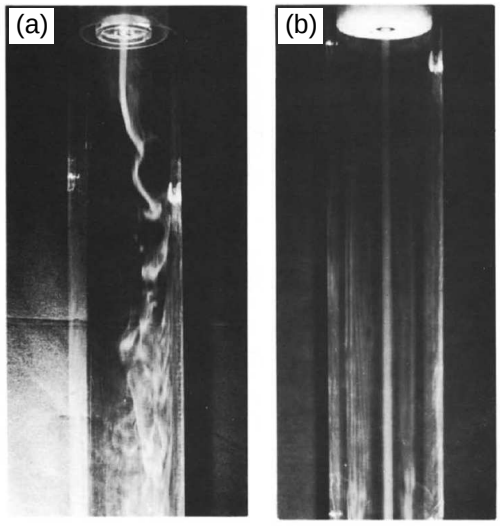

Figure 2.5 Cold experiment (a) with burner a; (b) with burner b, burner a and b are shown in Figure 2.3 [14]

The injection probe is used to transfer the particles from the syringe pump feeder to the hot zone in the reactor tube. Therefore, a cooling jacket (except the part of the flow straightener) is necessary for the injection probe to work in the high temperature reactor and prevent unexpected reactions between carrier gas and iron ore. Normally, there are two basic types of the structure for the water cooling jacket as shown in Figure 2.6, which are concentric annulus and segmented annulus. The concentric annulus probe consists of three concentric tubes. Water flows down to the probe tip through one annulus and comes back through the other. The intermediate tube (partition wall) acts as a baffle, forcing all of the water to pass through the tip region. For the segmented annulus design, there is only one annulus. The intermediate tube is replaced by a series of tubes, evenly spaced in the annulus. Water flows to the probe tip through these tubes and returns through the spaces between the tubes, or vice versa. It was reported that the water flow rate for probes with a segmented annulus is 30 % higher than for probes with a concentric annulus [15].

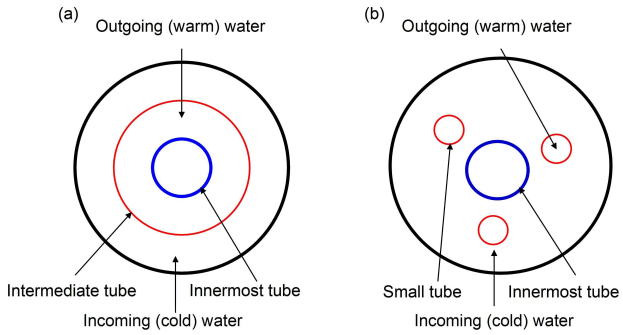

Figure 2.6 Schematic diagram of cross-sectional view of the water cooling injection probe (a) concentric annulus; (b) segmented annulus

Thus the segmented annulus is adopted in this study. As shown in Figure 2.7, the water cooled injection probe is made of stainless steel. The length of the injection probe is 700 mm. The inner diameter of the injection probe is 3 mm and outer diameter is 22 mm and 8 small tubes are designed for the cooling purpose. A small flange which is used for supporting the flow straightener is attached at the end of the injection probe through a thread connection.

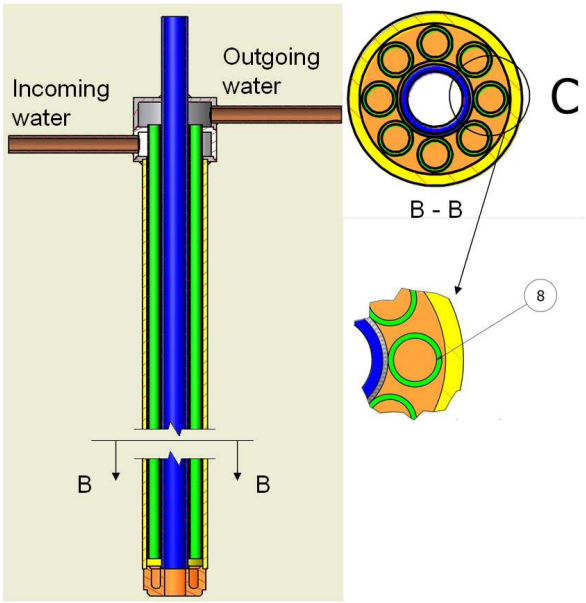

Figure 2.7 Skeleton drawing of injection probe

2.2.4 Sampling probe

The sampling probe is used to collect the partially reduced particles and reducing gas from the hot zone. The schematic diagram of the sampling probe is shown in Figure 2.8. The length of the probe is 780 mm. The OD of the probe is 47 mm and the ID is 12.7 mm. The inner most tube is made of sintered stainless steel. The rest parts are made of stainless steel. The cooling system combines the water cooling and gas cooling. The design of the water cooled jacket (segmented annulus) is the same with that of injection probe. Rapid quenching for the products is provided by nitrogen injected radially through sintered stainless steel tube at the top 30 mm of the probe. The key point is that the rapid quenching nitrogen could dilute the reducing gas immediately to stop the further reaction. In addition, the sintered tubing distributes along the entire length of the probe and the average diameter of the porosity is 5 µm. Additional nitrogen is injected at a small flow rate along the remaining length of the sintered tube to eliminate deposits of powder on the walls. A separate cap (Figure 2.8 (b)) is made of stainless steel to help collecting particles, which has an angle of 75 degrees from horizontal.

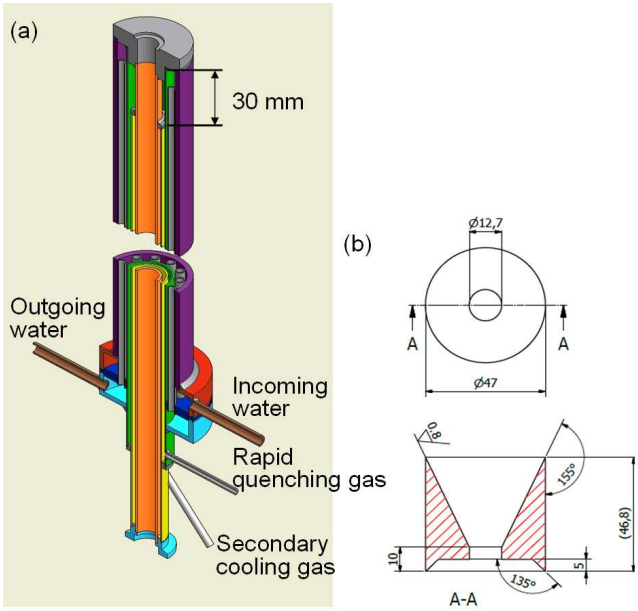

Figure 2.8 3-D drawing of sampling probe (a) and schematic diagram top cap (b)

2.2.5 Sample collector

The sample collector is another important part of the HDTF, which is shown in Figure 2.9. It is the other factor to determine the capture efficiency of the reacted particles. The end of the sampling probe connects to a sample collector by a clamp. The sample collector is made of stainless steel. It has two collection chambers divided by a baffle. For each chamber, there is a visual window on one side of the wall of the collector. There is a cylindrical collector at the bottom of each chamber. The partially reduced particles and off-gas flow into the chamber from a narrow space to a wide space, therefore the gas velocity drops sharply. Finally, particles fall into the bottom collectors for their own gravity. The bottom collectors have cylindrical shape with smooth and shining surface to reduce the friction force. The using channels during the experiment can be replaced by pushing the spare channel into the collector. Therefore, the sample can be collected at any time during the experiment. Preliminary tests indicate that the capture efficiency of powder is around 70 % to 80 %.

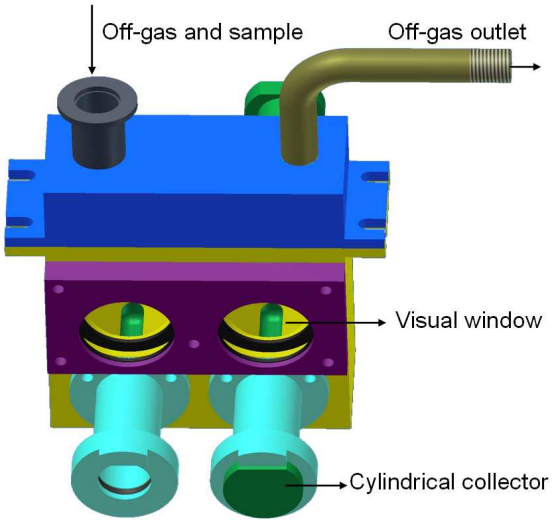

Figure 2.9 3-D drawing of the sample collector

2.2.6 Pre-tests before the experiment

2.2.6.1 Syringe pump particle feeder

The construction of the syringe pump particle feeder is based on the theory of pneumatic conveying. To have a smooth running, the tip of the capillary tube should be kept just above the top surface of the materials bed. A stable feeding rate is determined by three factors: movement rate of the piston, gas flow rate and particle size. In other words, the movement rate of the piston determines the sample feeding rate in grams per hour and an appropriate flow rate of carrier gas should be chosen to match the particle size and the feeding rate for a stable feeding.

Table 2.2 gives the map of the minimum gas flow rate (F) for different particle sizes at different syringe pump feed rates (m). The interested particle feed rates are assumed to be 1 g/h, 2 g/h and 2.5 g/h. The minimum gas flow rate means a gas flow rate can keep the tip of the capillary tube just above the bed of iron ore. If the gas flow rate is lower, the tip of the tube would be submerged by the iron ore bed. From the table it can be found that the minimum carrier gas flow rate goes up with the increase of particle size and feed rate. As the experimental study focuses on the individual particle fast reduction and melting behaviour at high temperatures, the number of particles in the reactor should be as low as possible to avoid agglomeration at high temperatures. From the high temperature preliminary tests, there is no agglomeration phenomena found of the collected samples of all the three feed rates, and no significant difference on the reduction degree observed among the three feed rates. However, considering the heat transfer in the reactor, a low feed rate could achieve a better experimental condition than a high feed rate. Therefore, the feeding rate of 1 g/h is used in the following study.

Table 2.2 Particle feed rate and its required carrier gas flow rate, l/min

m, g/h	Particle size (μm) with its corresponding carrier gas flow rate							
	<38	38-45	45-53	53-75	75-95	95-125	125-250	250-500
1	≥ 0.055	≥0.055	≥0.055	≥0.055	≥0.087	≥0.087	≥0.095	≥0.20
2	≥0.055	≥0.055	≥0.072	≥0.072	≥0.087	≥0.087	≥0.095	≥0.22
2.5	≥0.055	≥0.055	≥0.072	≥0.083	≥0.087	≥0.087	≥0.110	≥0.24

2.2.6.2 Temperature profile and cooling effect in the reactor

A B-type thermocouple was used to measure the temperature in the reactor. Firstly, it was calibrated by the standard B-type thermocouple. The program temperature of the high temperature furnace (without cooling system) was set to 1473 K, 1673 K and 1873 K, respectively. The temperature of the isothermal zone was

measured by the two thermocouples. The results are shown in Table 2.3. The measured values with the thermocouple used in this study are only 2-3 K lower or higher than the measured values with the standard B-type thermocouple. It indicates that the B-type thermocouple used in this study is reliable.

Table 2.3 Calibration of the B-type thermocouple used in this study, T (K)

Set furnace T	Standard thermocouple	Thermocouple used in this study
1473	1476	1479
1673	1674	1675
1873	1873	1871

The program temperature of the electrically heated furnace is set to 1603 K, 1653 K, 1703 K, 1753 K and 1803 K. The temperature profiles of the 41 cm hot zone of the reactor were measured by the B-type thermocouple at the five temperatures with a typical gas flow rate of 4 l/min, which are given in Figure 2.10. In the HDTF, the water-cooled injection probe and the water-cooled and gas-quenched sampling probe are inserted into the furnace. It was found to be a very influential factor on the temperature profile in the reactor. The highest temperatures in the furnace are lower than the program temperatures. The hot zone is the length between the tip of the injection probe and the top of the sampling probe.

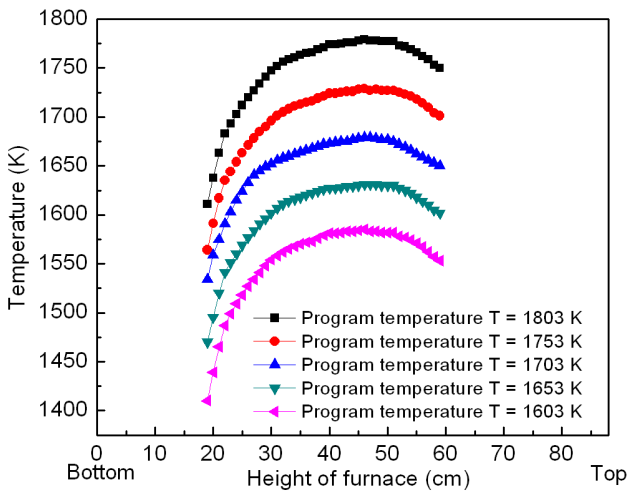

Figure 2.10 Temperature profiles in the hot zone at 5 temperatures

The average temperature in the hot zone is calculated by the weighted average method by assuming that the temperature over 1 cm is the same. The program temperatures, highest temperatures, average temperatures, and calibrated average temperatures are given in Table 2.4. The five average temperatures are

calibrated to 1550 K, 1600 K, 1650 K, 1700 K and 1750 K, and these five values are used in the following text to represent the average temperatures in the furnace. It is reasonable due to that the thermocouple has a small deviation (± 2-3 K) from the values measured by the standard thermocouple.

Table 2.4 Average temperatures in the furnace

Program T	Highest T	Average T	Nominal T
1603	1585	1553.3	1550
1653	1631	1601.2	1600
1703	1679	1652.3	1650
1753	1729	1698.3	1700
1803	1778	1747.7	1750

The temperature in the sampling probe is also measured to make sure that the cooling rate is high enough as shown in Figure 2.11. The average temperature of the hot zone was 1750 K. The flow rate of the quenching gas was 4 l/min and the flow rate of the secondary cooling gas is 300 ml/min. The temperature was measured from top to bottom with 1 cm descending height of each measurement. The temperature at the junction between hot zone and sampling probe is the highest temperature. However, due to the use of quenching gas at the top 30 mm, it decreases quickly to around 673 K. Then the temperature decreases slowly along the sampling probe until the collector, in which the temperature is around 330 K.

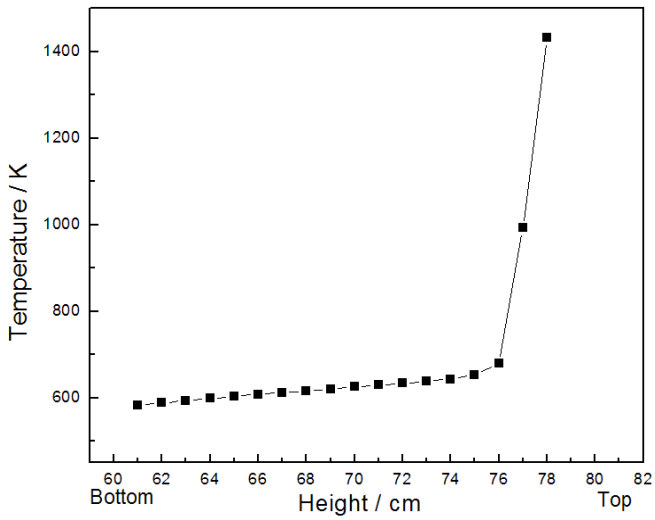

Figure 2.11 Temperature profile in the sampling probe, T = 1750 K; rapid quenching gas: 4 l/min; secondary cooling gas: 0.3 l/min

2.3 TGA – DSC

Thermo Gravimetric Analysis (TGA) and Differential Scanning Calorimetry (DSC) were extensively used in the laboratory study. According to the requirement of this study, TGA and DSC (NETZSCH Thermal Analysis STA 409) were used jointly to evaluate the reaction occurring during the heating of iron ore particles in the smelting cyclone. The maximum temperature of the STA 409 DSC equipment is 1723 K.

The whole equipment consists of a measuring part, power unit, controller system and a computer software system [16]. The basic controller system of the equipment contains the power-pack, the temperature programmer, the temperature controller and the temperature preamplifier. NETZSCH has developed special software to control the measurement, data acquisition and evaluation. The software can be used by different compatible computer systems.

The cross-sectional view of the working/measuring part of the equipment is shown in Figure 2.12. It consists of a furnace in which two balance beams are placed. Each beam is connected to a detector and on each beam a platinum crucible is placed. A small amount of samples was charged into the sample crucible. The other one worked as the reference crucible and was left empty. The small scale of the experiments ensures controlling and safe surroundings, while small changes in mass and temperature of the sample can be easily detected because of the comparison with the reference material. Both the sample and the balance should be protected with purge gas which is introduced into the furnace at the cross head. Nitrogen is used to protect the balance in this equipment with a maximum flow rate of 100 ml/min. The type of gas used in the protective tube depends on the sample. In this research argon was led through the furnace with a flow rate of 30 ml/min to protect the samples. To keep the accuracy of the measurement, the temperature controller system of the DSC equipment has to be calibrated frequently against the melting temperature of pure metals.

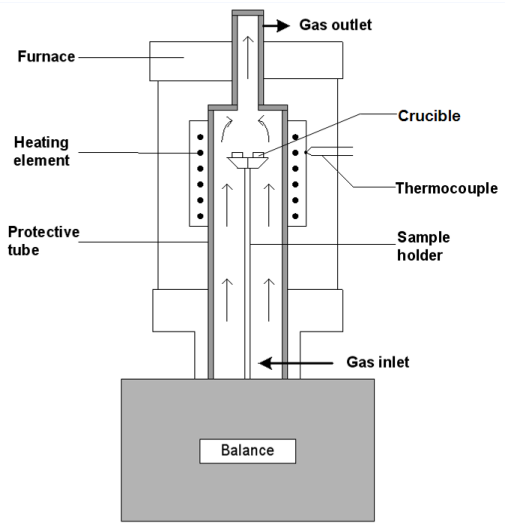

Figure 2.12 Cross-section of the measuring part of the STA 409

The results are exported as two curves: TG signal and DSC signal. TGA measures the percentage mass change as a function of increasing temperature. It can provide an in-situ measurement of what happens in a sample during heating, combined with DSC. In the furnace, there are two crucibles on the sample holder. One is used to for sample and the other one is empty and used as reference. The heat flow in the samples is measured by comparing the temperature change between the empty reference crucible and the crucible containing the sample, expressed as a potential in μV. This indicates an endothermic or exothermic reaction occurring at a specific temperature during the heating and is indicative of phase changes in the solid state, melting points and the losses by evaporation or decomposition. A positive signal indicates an exothermic reaction and a negative signal indicates an endothermic reaction.

2.4 Electrically heated horizontal furnace

The study of the thermal decomposition of hematite was scaled up in a horizontal furnace for further investigation. The schematic diagram of the furnace is shown in Figure 2.13. The furnace body is electrically heated by six SiC heating elements to obtain the highest temperature of 1873 K. The length of the furnace body is 880 mm and its outside diameter is 410 mm. The furnace tube is made of an Alsint with 99.7 % Al_2O_3. The inner diameter of the Alsint tube is 40 mm and the outer diameter is 50 mm. It is capable to work at the maximum temperature of 2073 K. The temperature of the furnace is controlled by a digital controller, with which a

program containing heating stages, dwell stages and cooling stages can be pre-set. In order to determine the exact position of the highest temperature zone, an S-type thermocouple is inserted into the reactor tube from one side to monitor the temperature. The crucible with a number of samples (about 10 grams) was pushed into the reactor tube slowly from the other side until that it touches the tip of the thermocouple. Then it is at the right position (isothermal zone). The inert gas flows in from one side and flows out from the other side of the furnace.

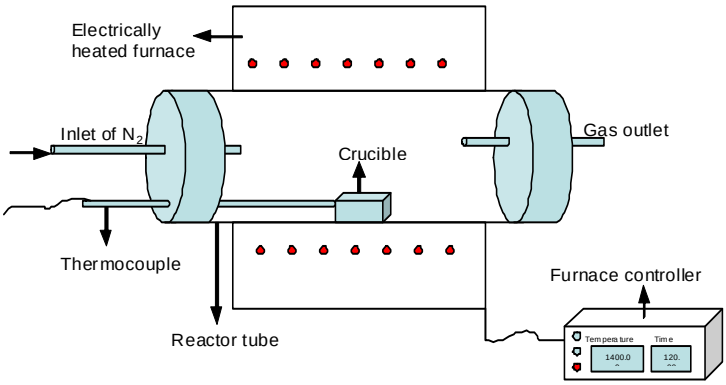

Figure 2.13 Schematic diagram of the experiment in the horizontal furnace

2.5 Analysis methods

The Fe^{2+} and total Fe in the partially reduced sample was analyzed by the method of redox titration to calculate the reduction degree. The method of redox titration can provide an accurate measurement with a small amount of samples than other methods. In this study, potassium dichromate was employed as the standard solution (known concentration solution) instead of potassium permanganate for its several advantages over permanganate. Unlike potassium permanganate, potassium dichromate is available in high purity and is highly stable up to its melting point. Its aqueous solutions are not attacked by oxidisable impurities like rubber or any other organic matter and thus composition of aqueous solution does not change on storage. The aqueous solutions do not change under the influence of light either. It is thus an excellent primary standard. The contents of Fe^{2+} and total Fe in the iron ore sample were determined according to the reaction 2.4.

$$Cr_2O_7^{2-} + 6Fe^{2+} + 14H^+ = 2Cr^{3+} + 6Fe^{3+} + 7H_2O \qquad (2.4)$$

Chemical titration was first carried out with a certified reference material JK 29 consisting of 28.35 % wüstite and 28.35 % hematite, the components of which has

been analyzed and sold by BAS (Bureau of Analyzed Samples). Thereafter the samples in this study were analysed, thus the results of chemical titration are much more reliable.

Optical microscopy is used to study the morphology change of the fine iron ore particles. The existing phases in the iron ore are investigated by X-ray Diffraction (XRD). XRD also provides the semi - quantitative determination of iron oxides by comparing the integrated intensities of the diffraction peaks from each of the known phases, their weight fraction can be identified. In addition, complex mixtures containing more than two phases also can be quantified. Even if one phase is amorphous, diffraction can still yield the relative amount of each phase. In some situations though, it is necessary to prepare calibration standards to obtain the highest accuracy. Therefore, it provides comparisons among the samples in one group. In some experimental conditions, the morphology change of some samples cannot be detected directly by the optical microscope. These samples are analysed by Scanning Electron Microscopy (SEM) – Energy dispersive spectrometry (EDS) methods which provides more details of the iron ore particles, because the SEM can produce very high-resolution images of a sample surface, revealing details less than 1 nm in size.

References

[1] Tsukihashi, F., Kato, K. and Soma, T.: Reduction of Molten Iron Oxide in CO Gas Conveyed System, ISIJ International 22 (1982) 688-695.

[2] Hayashi, S. and Iguchi, Y.: Hydrogen Reduction of Liquid Iron Oxide Fines in Gas-conveyed Systems, ISIJ International 34 (1994) 555-561.

[3] Ghosh, S.K.D.A.: Kinetics of Gaseous Reduction of Iron Ore Fines, ISIJ International 33 (1993) 1168-1173.

[4] Gilles, H.L. and Clump, C.W.: Reduction of Iron Ore with Hydrogen in a Direct Current Plasma Jet., Industrial & Engineering Chemistry Process Design and Development 9 (1970) 194-207.

[5] Ariyama, T., Isozaki, S., Matsubara, S., Kawata, H. and Kobayshi, I.: Fluidization and Degradation Characteristics of Iron Ore Fines in Prereduction Fluidized Bed, ISIJ International 33 (1993) 1220-1227.

[6] Habermann, A., Winter, F., Hofbauer, H., Zirngast, J., and Schenk, J.L.: An Experimental Study on the Kinetics of Fluidized Bed Iron Ore Reduction. ISIJ International 40 (2000) 935-942.

[7] Pawlik, C., Schuster, S., Eder, N., Winter, F., Mali, H., Fischer, H., and Schenk, J.L.: Reduction of Iron Ore Fines with CO-rich Gases under Pressurized Fluidized Bed Conditions, ISIJ International 47 (2007), 217-225.

[8] Morgan, G.J. and Brimacombe, J.K.: Kinetics of the Flash Converting of MK (Chalcocite) Concentrate, Metallurgical and Materials Transactions B 27 (1996) 163-175.

[9] Jorgensen, F.R.A. and Koh, P.T.L.: Combustion in Flash Smelting Furnaces, Combustion in Pyrometallurgy 53 (2001) 16-20.

[10] Barranco, R., Cloke, M., and Lester, E.: Prediction of the burnout performance of some South American coals using a drop-tube furnace, Fuel 82 (2003) 1893-1899.

[11] Huffman, G.P., Frank, E., Huggins, E. and Levasseur, A.A.: Investigation of the Transformations of Pyrite in a Drop-tube Furnace, Fuel 68 (1989) 485-490.

[12] Card, J. B. A. and Jones, A. R.: A Drop Tube Furnace Study of Coal Combustion and Unburned Carbon Content Using Optical Techniques, Combustion and Flame 101 (1995) 539-547.

[13] Ouyang, S., Yeasmin, H. and Mathews, J.: A Pressurized Drop-tube Furnace for Coal Reactivity Studies, Review of scientific instruments 69 (1998) 3036-3041.

[14] Barranco, R., Cloke, M. and Lester, E.: Prediction of the Burnout Performance of Some South American Coals Using a Drop-tube Furnace, Fuel 82 (2003), 1893-1899.

[15] Zeng, T.: Transformation of iron and trace elements during coal combustion, PhD thesis, Massachusetts institute of technology, 1998.

[16] NETZSCH STA 409 Manual book. Germany, (2006).

Chapter 3 Experimental Study on the Thermal Decomposition Behaviour of Iron Ore Particles

3.1 Introduction

The function of the smelting cyclone (shown in Figure 3.1) in the HIsarna process is to partially pre-reduce the iron ore with around 20 % pre-reduction degree and melt solid particles (iron ore, limestone and dolomite) completely heated by a high temperature reducing gas. The environment inside the smelting cyclone is complicated. The thermal decomposition, reduction and melting processes of iron ore there are extremely fast and the details are not studied and well understood. At high temperatures both thermal decomposition and gas reduction could take place, contributing to the expected pre-reduction degree. From thermodynamics point of view, the products of the thermal decomposition and reduction are the same because both of the processes remove oxygen from the high oxygen concentration iron oxides and generate the low oxygen concentration iron oxides. However, from kinetics point of view, the required reaction conditions and reaction rates are different. In order to obtain a comprehensive and clear understanding of the iron ore behaviour in the smelting cyclone, the laboratory experiments of thermal decomposition and reduction mechanisms of iron ore particles were investigated. This chapter focuses on the thermal decomposition of iron ore in inert gas at different conditions. The experimental results of iron ore reduction are presented in chapter 4.

Up to now, most of the previous studies [1-3] focused on the mechanisms of the gas-hematite reaction at low temperature and the gas-wüstite reduction at high temperature for the blast furnace process, with agglomerated ore of sinter or pellets. Thermal decomposition of hematite is normally neglected because of the requirement of the higher decomposition temperature than gas-hematite reduction. However, the smelting cyclone can provide a suitable condition for the thermal decomposition of hematite ore. The thermal decomposition degree of iron ore in the smelting cyclone is determined by the following parameters: gas atmosphere, temperature profile, particle trajectory, particle size, and residence time.

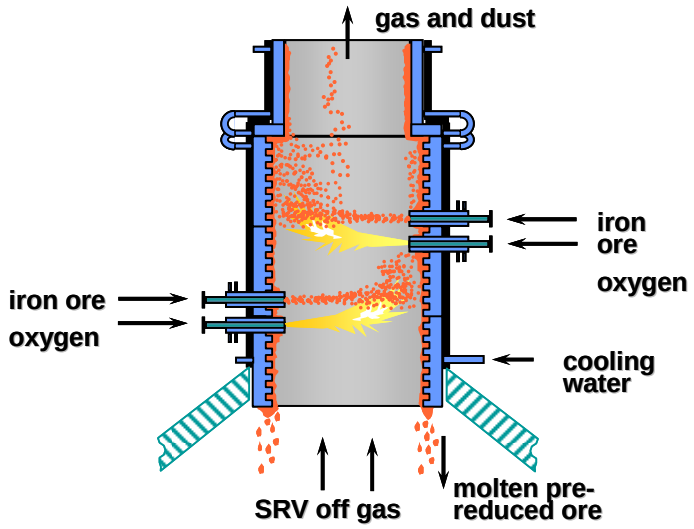

Figure 3.1 Schematic diagram of the cyclone reactor [4]

I. Gas composition and temperature profile: Fine particles of ore and flux are fed into the smelting cyclone together with oxygen. Oxygen reacts with the off-gas from the SRV entering at the bottom of the cyclone. The combustion within the smelting cyclone, which is preferably complete, largely reduces the amount of carbon monoxide and hydrogen in the reducing gas especially at the top part of the cyclone [5]. On the other hand, the combustion generates a considerable amount of heat which could keep the whole reactor at required high temperature. The temperature of the off-gas from the SRV (smelting reduction vessel) is around 1723 K and the highest gas temperature in the cyclone is estimated in the range of 1973-2073 K which is much higher than the starting decomposition temperature of hematite.

II. Particle trajectory: The characteristics of the smelting cyclone cause an intense swirling flow inside the reactor. The fine iron ore is injected in the middle level of the cyclone together with oxygen. On the one hand, the swirling flow extends the path of iron ore particles in the reactor. On the other hand, most of the small particles could be carried to the upper part of the reactor by the ascending gas. During the flying time of particles from the bottom to top, thermal decomposition could take place at its best suitable conditions.

III. Particle size and residence time: Particle residence time will vary with particle size as well as gas flow rate. The average residence time of iron ore particles in the cyclone reactor before hitting the cyclone wall is estimated between 0.16 and 0.20 s [6]. The particle size of fine ore ranges from 30 µm

to 500 µm. The short residence time is the main reason for the low pre-reduction degree of iron ore. Small particle size would accelerate the thermal decomposition rate.

Above all, the smelting cyclone is a complicated high temperature reactor. The combustion of high purity oxygen with SRV off-gas generates a considerable amount of heat to raise the temperature of the particles to the very high temperature of the SRV off-gas. Therefore, thermal decomposition of hematite ore in the cyclone would also contribute to the pre-reduction degree of iron ore.

3.2 Theoretical evaluation

There are three main forms of iron oxides: hematite (Fe_2O_3), magnetite (Fe_3O_4) and wüstite (FeO), and the melting points are 1838 K, 1870 K and 1650 K, respectively. From the literature survey, the thermal decomposition of hematite ore has been investigated in many laboratory experiments that were carried out at high temperatures. Gilles [7] stated that the highest oxide form is unstable above 1810 K and decomposes into gaseous oxygen and an oxide containing 71.6 % iron which is close to the composition of magnetite. This reaction was also mentioned in the study of Nakamura et al. [8] in 1981. A laboratory-scale test made in which iron oxide contained in a water-cooled crucible was melted and reduced by using 10-15 % H_2-Ar transferred arc plasma. It was stated that at high temperatures, the oxygen removed by thermal decomposition before the start of the reduction corresponds to a degree of reduction of about 18 %. The equation for calculating the thermal decomposition degree (equivalent reduction degree) [9] and thermal decomposition reactions of iron oxides are as follows.

$$R = \frac{\Delta m_{oxygen}}{m_{tot\text{-}oxygen}} \tag{3.1}$$

$Fe_2O_3 \rightarrow Fe_3O_4$ $\quad m_{loss}$ = 3.3 %; R = 11.11 %

$Fe_3O_4 \rightarrow FeO$ $\quad m_{loss}$ = 10 %; R = 33.33 %

$FeO \rightarrow Fe$ $\quad m_{loss}$ = 30 %; R = 100.00 % (3.2)

The thermal decomposition degree R of iron ore is defined as the ratio of weight loss of oxygen Δm_{oxygen} to the total initial weight of oxygen that bounds with iron in the iron ore $m_{tot\text{-}oxygen}$ shown in Eq. 3.1. According to this definition, when the weight loss of iron ore m_{loss} equals 3.3 %, the thermal decomposition degree is 11.11 % and Fe_2O_3 transfers to Fe_3O_4 completely. When the weight loss is 10 %,

the thermal decomposition degree is 33.33 % and Fe_2O_3 transfers to FeO completely. Finally, when the weight loss is 30 %, the thermal decomposition degree is 100 % (as shown in Eq. 3.2) and it means that Fe_2O_3 transfers to Fe completely. The reversible reactions and their standard Gibbs free energy values (J/mol·K) are shown in Eqs. 3.3-3.5.

$$6Fe_2O_3(s) \rightleftharpoons 4Fe_3O_4(s) + O_2(g) \quad \Delta G^o = 500600 - 280.7T \tag{3.3}$$

$$2Fe_3O_4(s) \rightleftharpoons 6FeO(l) + O_2(g) \quad \Delta G^o = 858200 - 392.6T \tag{3.4}$$

$$FeO(l) \rightleftharpoons Fe(l) + O_2(g) \quad \Delta G^o = 256061 - 53.681T \tag{3.5}$$

$$\Delta G = \Delta G^o + R_g T \ln \frac{p_{o_2}}{p^o} \tag{3.6}$$

At a given temperature, the direction of a reaction can be judged by calculating the Gibbs free energy ΔG (J/mol·K) as shown in Eq. 3.6. For the above three reactions, if $\Delta G < 0$, the thermal decomposition reactions (the forward reactions) could take place. If $\Delta G > 0$, the oxidation reactions (the reverse reactions) could take place. If $\Delta G = 0$, the reactions achieve an equilibrium state. The equilibrium state at each temperature has an equilibrium oxygen partial pressure. In other words, the start temperature of thermal decomposition is dependent on the partial pressure of oxygen in the reaction system, or vice versa. The equilibrium partial pressure of oxygen of the three iron oxides as a function of temperature can be calculated from Eq. 3.7 which is derived by substituting Eq. 3.3 or 3.4 or 3.5 into Eq. 3.6.

$$\ln \frac{p_{o_2}}{p^o} = \frac{-\Delta G^o}{R_g T} \tag{3.7}$$

Where,

ΔG^o – the standard Gibbs free energy (J/mol·K)

p^o – the total pressure of gas (Pa)

p_{o_2} – the partial pressure of oxygen (Pa)

R_g – the gas constant (J/mol·K)

Figure 3.2 shows that the equilibrium partial pressure of oxygen as a function of temperature for hematite, magnetite and wüstite increases with the increase of temperature. If the partial pressure of oxygen in the reaction system is less than the equilibrium value at a given temperature, the reaction could take place forward. The calculation results of the decomposition of hematite show that when the partial

pressure of oxygen is 0 Pa, the reaction would take place at room temperature. Above around 1473 K, the equilibrium partial pressure of oxygen increases rapidly with the increase of temperature, which can be seen in the figure. If the partial pressure of oxygen in the reaction system is controlled close to 0 Pa, the thermal decomposition of hematite is possible to speed up above 1473 K. At 1473 K, the thermal decomposition of iron ore can take place when the partial pressure of oxygen is less than 82.39 Pa which is about 0.08 % of 1 atm. When the partial pressure of oxygen is less than 1107.84 Pa which is about 1.1 % of 1 atm, the reaction would take place at 1573 K. It can also be calculated that if the temperature is 1783 K, the equilibrium partial pressure of oxygen will reach 1 atm (also called boiling temperature). The thermodynamic outcome confirms the experimental result of Gilles [7]. The thermal decomposition of magnetite is much more difficult than that of hematite. Although the thermal decomposition of magnetite can also take place when the partial pressure of oxygen is 0 Pa according to the thermodynamic calculation, the equilibrium partial pressure of oxygen only has an obvious increase above 1673 K. If the partial pressures of oxygen are less than 0.052 Pa and 1.70 Pa, the decomposition would take place at the temperatures of 1673 K and 1773 K, respectively. If the temperature is 2186 K, the equilibrium partial pressure of oxygen could reach 1 atm. The decomposition of wüstite is the most difficult process as shown in the black profile in Figure 3.2. Below the temperature of 2200 K, the equilibrium partial pressures are always almost kept at the value of zero. If the temperature is 4770 K, the equilibrium partial pressure of oxygen can reach 1 atm.

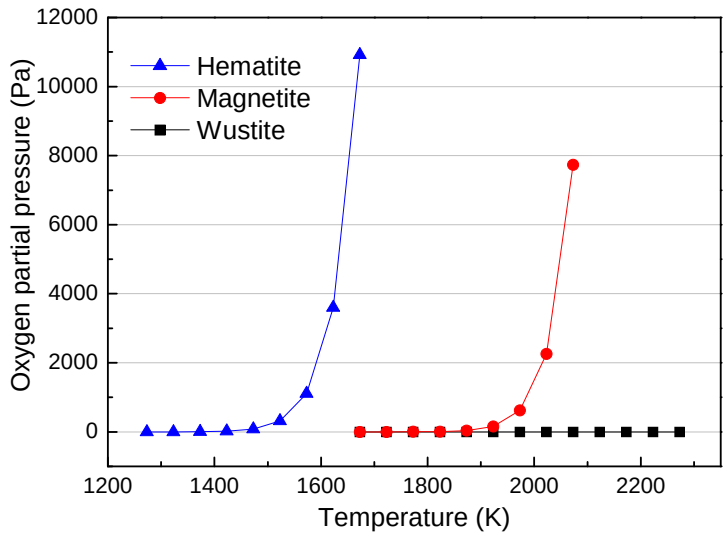

Figure 3.2 Oxygen partial pressure as a function of initial decomposition temperature of hematite, magnetite and wüstite

Above all, if the oxygen partial pressure is kept low enough in the reaction system, hematite could decompose to magnetite completely, and then magnetite could decompose to wüstite completely at high temperatures. The temperature in the cyclone reactor is high enough for the decomposition of iron oxides at least for the hematite. Therefore, both thermal decomposition and gas reduction would take place. From the theoretical evaluation based on thermodynamics, if hematite decomposes to wüstite completely, the equivalent reduction degree of 33.33 % is beyond the required reduction degree of 20 % of the cyclone reactor. Even though hematite doesn't decompose to wüstite completely, the equivalent reduction degree resulting from decomposition would be also possible to account for a part of the total reduction degree. It is thus highly important to study the hematite decomposition behaviour at high temperatures. On the other hand, the raw material is the other important consideration. In the practical situation, the raw material for ironmaking is hematite ore which is composed of Fe_2O_3 and balanced gangue. The particle behaviour at high temperatures would be somewhat different from pure Fe_2O_3. The high temperature experimental investigation is aimed to study the thermal decomposition of hematite ore at different conditions from thermodynamic and kinetic aspects. The thermodynamic study gives the essential thermal composition behaviour of hematite in a long reaction time to supply sufficient time for the exchange heat between iron ore particles and gas. For that the reaction time of iron ore is quite short in the smelting cyclone, the kinetic study is necessary.

3.3 Experimental

3.3.1 Experimental strategy

The actual thermal decomposition degree of hematite ore in the cyclone furnace is difficult to estimate because of the complicated environment, because the reduction takes place simultaneously. The laboratory experimental study of the thermal decomposition of hematite and hematite ore has been conducted in three methods (I to III) with three different reactors, and 4 influential factors (temperature, gas composition, particle size, and residence time) were investigated.

I. Thermal decomposition of pure Fe_2O_3 and hematite ore with a TGA-DSC analyser (small sample size: 80 mg; 293-1750 K; p_{o2} = 0 Pa)

II. Thermal decomposition of pure Fe_2O_3 and hematite ore at different temperatures with an electrically heated horizontal furnace (larger sample size: 10 grams; 1673 K, 1773 K, 1873 K; p_{o2} = 0 Pa)

III. Thermal decomposition of hematite ore in different inert gas compositions, with different particle sizes, and residence times in a HDTF (individual particles: total sample size of 3 grams; 1550 K, 1600 K, 1650 K, 1700 K, 1750 K; p_{o2} = 0 Pa)

Flowing inert gas was used in all the three methods to keep the partial pressure of oxygen close to zero during the reaction time. With the TGA-DSC analyser, the thermal decomposition behaviour of 80 mg of pure hematite and hematite ore has been measured at elevated temperature. The highest temperature that the TGA-DSC analyser can provide is 1773 K and 1753 K was used as the highest experiment temperature in this part. The experiment in the second part has been conducted with an electrically heated furnace with larger sample size of 10 grams. The accurate thermal decomposition degree could be tested with the larger sample size by chemical titration. The highest temperature of the horizontal furnace is 1873 K which was also adopted as the highest temperature in this part of experiment. The kinetic mechanism of thermal decomposition of hematite has been studied in the HDTF at different conditions. The highest temperature that the HDTF can provide is 1873 K, but for the safety and furnace maintenance reason, 1750 K was used as the highest temperature. The study specially focused on the effect of particle size, residence time and gas composition on thermal decomposition.

3.3.2 Materials

The raw material of the iron ore used in the experiment was provided by Tata Steel in IJmuiden, the Netherlands, as shown in Table 3.1. The hematite content is as high as 94.9 %. The raw material was prepared by sieving to get different size groups (38-45 μm, 45-53 μm, 53-75 μm; 75-90 μm; 90-125 μm, 125-250 μm) of particles and then dried in a dry furnace at 423 K for 2 h to remove the water. The other type of sample is pure Fe_2O_3, of which the content of Fe_2O_3 is above 99 %. The average size of the particles is about 5 μm.

Table 3.1 Iron ore composition

Composition	Weight %	Composition	Weight %
Al_2O_3	0.845	MnO	0.147
CaO	0.015	SiO_2	2.800
Fe_2O_3	94.935	Rest	1.228
MgO	0.030	—	—

3.3.3 Experimental conditions

3.3.3.1 Thermal decomposition of iron ore in the TGA-DSC

The first part of the experiments has been carried out by using a thermogravimetric analyser TGA-DSC. This study focused on obtaining the start thermal decomposition temperatures of hematite and hematite ore. Simultaneously, the TGA-DSC experiment provides an in-situ measurement of the approximate weight loss and the temperature of phase changes. The experimental conditions are shown in Table 3.2.

The weight of the empty crucible and the weight of sample were measured with the electronic balance with the precision of 0.1 mg. And then the sample was put on the holder in the TGA-DSC analyser carefully. The gas flow rate of Ar was set to 30 ml/min for the protection of the heating element and the gas flow rate of N_2 was set to 50 ml/min for the protection of the sample. Before starting the experiment, the balance in the TGA-DSC analyser was adjusted to obtain a stable state. The program interface provides convenient operation for setting different heating rates and holding times in a run. The temperature in the furnace was firstly raised up at a certain heating rate to the highest temperature, and then the highest temperature was hold for some time which is called holding time in this study. The temperature changes, weight loss and heat release (or heat absorption) are recorded every minute.

Table 3.2 Experimental condition in the TGA-DSC analysis

Experimental condition	Operating parameters
Sample	Hematite: Fe_2O_3 99 %+ Hematite ore: Fe_2O_3 94.9 %
Holding time	4 h
Heating rate	10 K/min, 20 K/min
Particle size	Hematite: 5 μm ; Hematite ore :45-53 μm, 125-250 μm
Temperature	293-1753 K

3.3.3.2 Thermal decomposition of iron ore in the horizontal furnace

The sample size in the TGA-DSC analyser is too small (~80 mg) to do chemical analysis or other tests. The experiments were further carried out in the horizontal tube furnace to obtain an accurate thermal decomposition degree with a larger sample size. The experimental conditions are listed in Table 3.3.

The experimental temperature was set to different value with the digital controller of the horizontal furnace. The holding times of one hour, two hours and three hours have been tested to find out a sufficient reaction time for the thermal decomposition of hematite ore. Only the small particle size of hematite ore was used in the experiment. When the holding time is long enough, the particle size doesn't play an important role in the final thermal decomposition degree.

The rough weight loss of the sample was recorded by measuring with an electronic balance with 0.1 mg precision. The sample size in this part of experiment is around 10 g. The crucible with the sample was pushed into the isothermal zone from one side of the horizontal furnace as quick as possible, when temperature of the furnace reached the designated value. Before putting the sample, 1 l/min N_2 was introduced into the furnace for at least 10 minutes to blow away air in the furnace, and after putting the sample, the N_2 flow rate to 100 ml/min to prevent air getting into the furnace. For the flowing N_2 and the weight of the iron ore sample is quite small, the partial pressure of oxygen could be kept close to zero. From the theoretical analysis, the decomposition of magnetite is much more difficult than hematite at high temperature (1473-1873 K). In the horizontal furnace 1 h, 2 h and 3 h holding times were tested respectively to study how much of the thermal decomposition degree could be contributed by the thermal decomposition of magnetite in different holding time. After the experiment, the sample was ground into powder for the further analysis by chemical titration. Before the chemical titration, the samples were kept in an evacuated glove box which has a circulation system with argon gas all the time. The content of O_2 and H_2O are always kept below 1 ppm.

Table 3.3 Experimental condition in the horizontal furnace

Experimental condition	Operating parameters
Sample	Hematite: Fe_2O_3 99 %+ Hematite ore: Fe_2O_3 94.9 %
Holding time	1 h, 2 h, 3 h
Heating rate	10 K/min
Particle size	Hematite: 5 μm ; Hematite ore :45-53 μm
Temperature	1673 K, 1773 K, 1873 K

3.3.3.3 Thermal decomposition of iron ore in the HDTF

The kinetics study of the thermal decomposition of the hematite ore has been carried out in the HDTF. The details of the experimental set-up are described in Chapter 2. A gas flow of N_2 or CO_2 or Ar from the gas cylinder was regulated

digitally by the mass flow controllers. A small part of the gas was separated as carrier gas which was measured by a mass flow meter. The carrier gas was led into the glass tube of the particle feeder and took several particles with it at a time, and then flowed into the water cooled injection probe. The other part of the gas was heated to 773 K in a pre-heat furnace before entering into the furnace. The thermal decomposition took place in the hot zone of the furnace. The reacted particles and gas were received by the water cooled and gas quenched sampling probe. Finally, the particles were collected in the sample collector. The highest temperatures were measured by B-type thermocouple in all the experiments and compared with the highest temperatures in the preliminary tests as shown in Chapter 2. The deviation is ±3 K. The effects of gas, temperature, residence time, and particle size on the thermal decomposition of iron ore have been studied in the HTDF. The experimental conditions are shown in Table 3.4.

Table 3.4 Experimental condition in the HTDF

Experimental condition	Operating parameters
Sample	Hematite ore: Fe_2O_3 94.9 %
Particle feed rate (g/h)	1
Gas composition	100 % N_2; 100 % Ar; 100 % CO_2
Particle size (μm)	38-45, 45-53, 53-75, 75-90, 90-125, 125-250
Residence time (ms)	210, 970, 2020
Temperature (K)	1550, 1600, 1650, 1700, 1750, 1800

During the stages of heating up and cooling down of the furnace, 1 l/min N_2 gas was used to prevent the sampling probe and injection probe from oxidizing by the oxygen in the air. When the temperature of the furnace reached the designated temperature, the N_2 gas was switched to the experimental gas. The gas flow rate of the total gas and carrier gas was set according to the particle feed rate and residence time. For each experiment, a part of the collected sample was ground to very fine powder for the chemical titration and put into the glove box. The other part of the sample was also put into the glove box for the study of morphology. The heating rate of the furnace was set very low to prevent the thermal shock in the furnace and extend the life of the reactor tube and heating elements. It is much more important for the HTDF because of the cooling system of the sampling probe and injection probe inside the hot reactor tube. In most cases the heating rate was set to 3 K/min and the cooling rate was set to 2 K/min.

A low feeding rate minimizes the interaction between particles to ensure single particle flow and reaction behaviour. The residence time of the particles in the hot zone was calculated by applying Newton's second law and Stokes law to the

motion of the particles through fluids. Three forces act on a single particle as shown in Figure 3.3: a gravity force, buoyancy force and a drag force. The equations used in the calculation are listed below assuming that the gas velocity keeps constant in each time step Δt of 0.02 s.

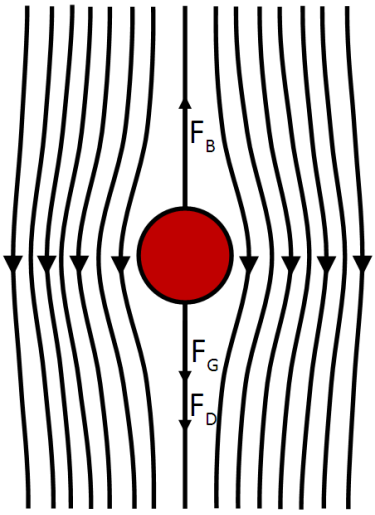

Figure 3.3 Force balance on a single particle in the gas fluid

- Net external accelerating force

$$m_P \frac{du_P}{dt} = F_D + F_G - F_B \tag{3.8}$$

- Drag force

$$F_D = 1/2 C_D A_p \rho_g \left(u_g - u_p\right)^2 \tag{3.9}$$

- Difference of gravity and buoyant force

$$F_G - F_B = u_g g \left(\rho_p - \rho_g\right) \tag{3.10}$$

- Drag coefficient

$$C_D = 24/\mathrm{Re} \tag{3.11}$$

- Reynolds number of the particle

$$\mathrm{Re} = \frac{\rho_g d_p \left(u_g - u_p\right)}{u_g} \tag{3.12}$$

- Particle velocity (P_1: first step; P_2: second step)

$$u_{P_2} = u_{p_1} + a\Delta t \tag{3.13}$$

- Residence time

$$t = n\Delta t \tag{3.14}$$

Where,

ρ_g, ρ_p – Gas density and the particle density, kg·m^{-3}

m_p – Mass of the iron ore the particle, kg

A_p – Cross sectional area of the particle, m^2

a – Accelerating rate of the particle, m/s^2

d_p – Diameter of the particle, m

F_B – Buoyancy force, N

F_G – Particle gravity, N

F_D – Drag force, N

The length of the hot zone was measured before the experiment by a B-type thermocouple. The calculation of the velocity of particle in the hot zone was performed step by step. Finally, the residence time of a particle in the hot zone was obtained. Local gas properties such as density and viscosity were calculated as a function of temperature. The gas properties used in the study of Acevedo [10] were adopted in this study to calculate the residence time of the particle.

3.4. Results and discussion

3.4.1 Experimental results with TGA-DSC

3.4.1.1 Thermal decomposition of hematite ore

Firstly, a series of experiments have been carried out with hematite ore with different particle sizes and heating rates. Figure 3.4 shows the TGA and DSC profiles of one test. The weight of the sample was 80.2 mg and the particle size was in the range of 45-53 µm. The highest temperature achieved was 1750 K and the heating rate was set at 10 K /min. In Figure 3.4 (a), the temperature history in the furnace is presented by the red line. It was linearly increased to the maximum temperature and then held for 4 hours. There are three steps on the TG curve and two troughs on the DSC curve before the holding time. The total weight loss of the sample is about 4.43 %. A slight weight loss appears at the first stage of the heating time due to the dissociation of carbonates such as $CaCO_3$ and $MgCO_3$ in the hematite ore. Both the decomposition of calcium carbonate and magnesium carbonate are endothermic reactions. It is the reason why the DSC curve goes down below zero. The thermal decomposition of magnesium carbonate starts at about 773 K and should be completed at a temperature below 1173 K [11]. The decomposition of calcium carbonate starts at 1023 K and full decomposition occurs at 1123 K [12].

The slight weight loss at the beginning of the heating time (30-120 min.) is followed by the sharp weight loss (at about 130 min.). The total weight loss at the end of the stage of sharp weight loss is around 3.55 %. It indicates that hematite is not stable with the increase of temperature in the inert gas, which is in agreement with the theoretical evaluation perfectly. Hematite started to decompose slowly with the increase of temperature in the first stage (heating time: 0-120 min. and temperature: 293-1473 K), while the decomposition rate was accelerated when temperature was raised above 1473 K and the sharp weight loss was obtained. The stage of sharp weight loss is corresponding to the first big trough on the DSC curve which means that the mass loss was caused by an endothermic reaction of the thermal decomposition of hematite. The reaction heat of thermal decomposition of 1 mol Fe_2O_3 is about 78.24 kJ/mol (ΔH_{298}) at 298 K and it increases to 78.71 kJ/mol (ΔH_{1473}) at 1473 K. The reaction heat only has a small increase with the increase of temperature. Therefore, the big trough on the DSC curve at the sharp weight loss stage is caused by the high decomposition rate. As mentioned above, the weight loss resulting from the decomposition of Fe_2O_3 to Fe_3O_4 is about 3.3 %. It means that the hematite was probably completely transferred to magnetite at the end of the sharp weight loss. The weight loss of 0.25 % (3.55 % - 3.3 %) is probably caused by the thermal decomposition of magnetite. The second trough shows that the heat absorption during this period is less than for the first trough. The weight loss during the second trough is also not obvious. By the end of the second trough, the weight loss is about 3.74 % (3.55 % + 0.19 %). The weight loss of the sample is larger than 3.3 %, therefore the second trough would be caused by the decomposition of magnetite. The total weight loss during the rest time is only 0.69 % (4.43 % - 3.55 % - 0.19 %), although it includes a 4 hours holding time. Actually, the result shows that the weight loss decreases slowly after 200 minutes. The holding time at this moment is 52 minutes.

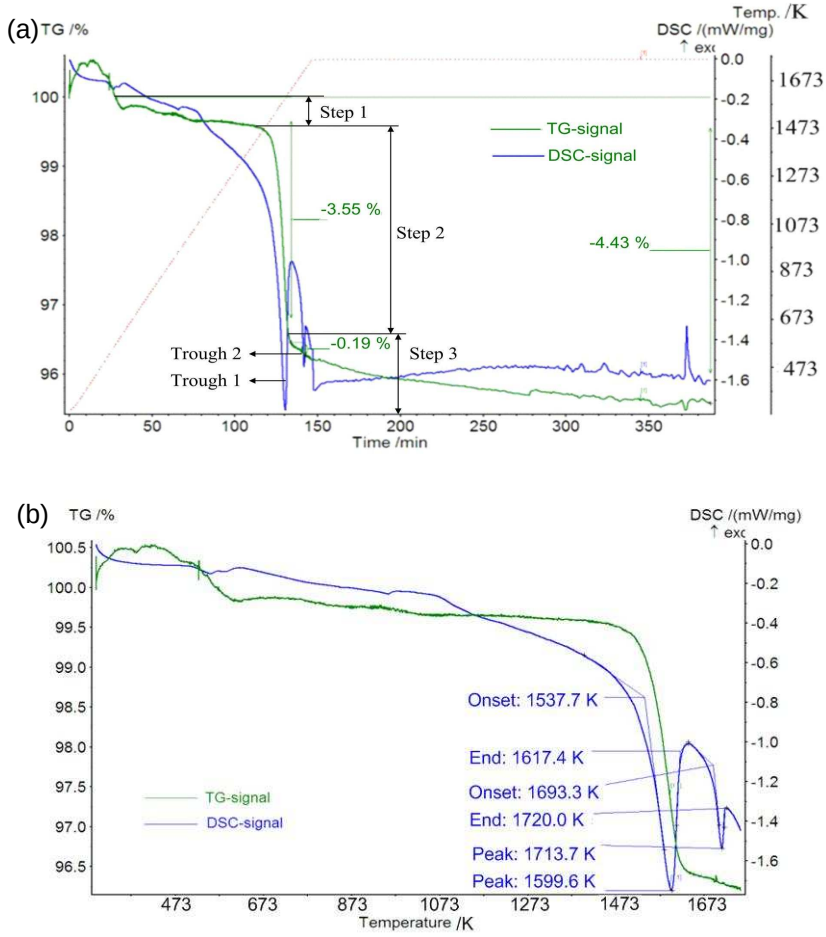

Figure 3.4 TG-DSC analysis of hematite ore (heating rate: 10 K/min) in N_2, (a) as a function of time, (b) as a function of temperature

If it is assumed that all the weight loss is caused by thermal decomposition of iron oxides, the thermal decomposition degree of hematite ore can be roughly estimated to be 14.8 %. According to the theoretical calculation, all the hematite was decomposed to magnetite and about 16.7 % of the generated magnetite was decomposed to wüstite. Only a small amount of weight was lost during the 4 hours holding time. From Figure 3.4 (b), it can be clearly seen that the sharp weight loss stage is exactly marked by the big trough on the DSC curve. According to the analysis of the DSC curve, the onset and end temperatures of the first trough are 1537 K and 1617 K, respectively. The point of 1537 K can be seen as the start temperature of thermal decomposition of the hematite ore at the sharp weight loss stage. In other words, the thermal decomposition rate of hematite is accelerated

above 1537 K. The onset and end temperatures of the second trough are 1693 K and 1720 K. It indicates that the thermal decomposition of magnetite has a small fluctuation at 1693 K, but it is much weaker as compared to the sharp weight loss stage of hematite. The start temperatures of thermal decomposition of both hematite and magnetite obtained from experiments are in agreement with the range of the theoretical evaluation. The same conclusion can be obtained that thermal decomposition of magnetite is much more difficult than the hematite.

The second test has been carried out at the same condition but with a different heating rate of 20 K/min. The results are shown in Figure 3.5. The total weight loss during the process is 4.34 %. The weight loss of the sharp dropping stage is 3.13 %. The start temperature of thermal decomposition of hematite at its sharp mass loss stage is about 1563 K and the start temperature of thermal decomposition of magnetite at its small fluctuation stage is about 1700 K. Both of them are slightly higher than the results in Figure 3.4 (b), but they are still in the range of theoretical evaluation. This is logical because the iron ore particles in the material bed cannot follow the heating rate of the system. However, it doesn't have much effect on the finally results.

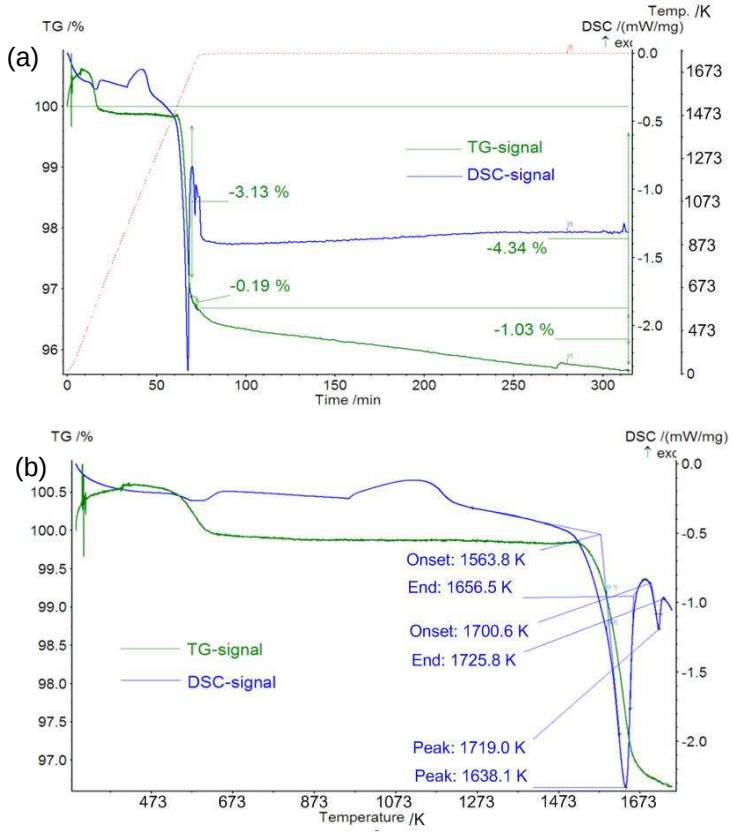

Figure 3.5 TGA-DSC analysis of hematite ore (heating rate: 20 K/min) in N_2, (a) as a function of time, (b) as a function of temperature

The big particle size was also tested with the TGA-DSC analyser as shown in Figure 3.6. The particle size is the group of 125-250 µm. The heating rate is 10 K/min. The sharp weight loss is about 3.4 % and the total weight loss is about 4.6 % in the 4 h holding time. In Figure 3.6 (b), the start temperature of the sharp weight loss stage of hematite is about 1556 K and the start temperature of the thermal decomposition of magnetite at its small fluctuation stage is about 1698 K. The two temperatures are higher than the results in Figure 3.4 (b), but lower than the results in Figure 3.5 (b).

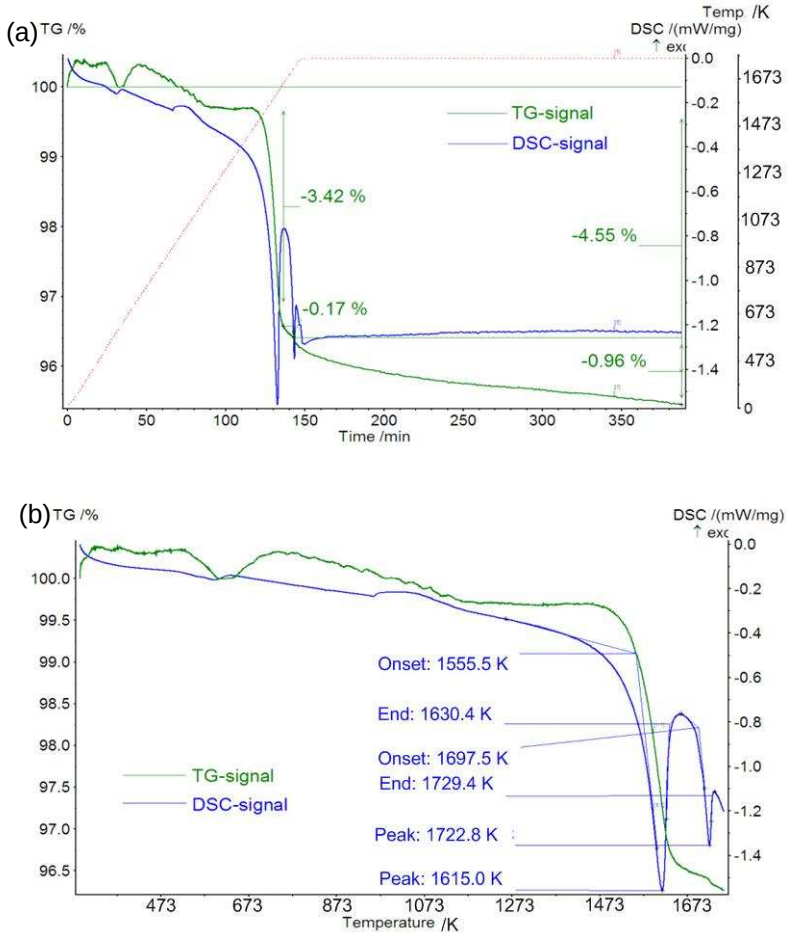

Figure 3.6 TGA-DSC analysis of hematite ore (particle size: 125-250 µm) in N_2, (a) as a function of time, (b) as a function of temperature

3.4.1.2 Thermal decomposition of hematite

The thermal decomposition of hematite has been tested by the TGA-DSC analyser to compare the results with hematite ore. The weight of the sample is 31.5 mg. The highest temperature is 1753 K with the heating rate of 10 K/min. According to the result of thermal decomposition of hematite ore, 2 hours holding time is enough for that after 2 h holding time, the weight loss is quite small. There is also a sharp weight loss on the TG curve and it corresponds to a big trough on the DSC curve. The weight loss by the end of the sharp weight loss is 3.1 % which results from Fe_2O_3 thermal decomposition as Figure 3.7 shows. But the second small trough as shown during the thermal decomposition of hematite ore doesn't appear on the

DSC curve. The total weight loss is 4.37 % which is also higher than 3.3 %. There is still about 1 % weight loss produced by the decomposition of magnetite, although the thermal decomposition of magnetite is not strong enough to generate a trough on the DSC curve. The total equivalent reduction degree of Fe_2O_3 is 14.6 %. Figure 3.7 (b) shows that the start temperature of the small fluctuation of the thermal decomposition of Fe_2O_3 is around 1493 K which is lower than that of hematite ore at the same conditions.

The comparison of the three TGA-DSC tests for the two materials (hematite ore and hematite) with different particle size and heating rate is given in Table 3.5. A sharp weight loss stage was found during the thermal decomposition process of hematite and a small fluctuation stage was found during the thermal decomposition process of magnetite. The start temperatures of the two stages of each test were obtained from the DSC curves. These two temperatures were also estimated from the theoretical calculation (in Figure 3.2) and the comparison of the experimental results and calculation results are shown in Table 3.5. It shows that all the experimental results are in the range of theoretical calculation. The results of thermal decomposition degree of iron ore show that the thermal decomposition behaviour of pure hematite has almost no difference compared to the thermal decomposition behaviour of hematite ore. The particle size also has a small influence on the thermal decomposition of hematite ore. The equivalent reduction degree of big particle size (125-250 μm) is slight higher than that of small particle size (45-53 μm). It is probably because that the porosity of the sample bed of big particle size is larger than that of the sample bed of small particle size and the big porosity makes it easy for the release of oxygen. It slightly accelerates the thermal decomposition rate. According to the theoretical evaluation, if the decomposition of hematite to magnetite takes place completely in the inert gas, the weight loss is 3.3 %. If the decomposition of hematite to wüstite takes place completely in the inert gas, the maximum weight loss is 10 %. In this study the highest temperature is 1753 K and the total weight loss of hematite ore is around 4.4 % which is between 3.3 % and 10 %. Therefore the product is a mixture of wüstite and magnetite. The rough thermal decomposition degree of hematite ore is estimated to be 14.8 % based on the assumption that the system error caused by the set-up and the weight loss caused by the other carbonates in the hematite ore at high temperature are ignored.

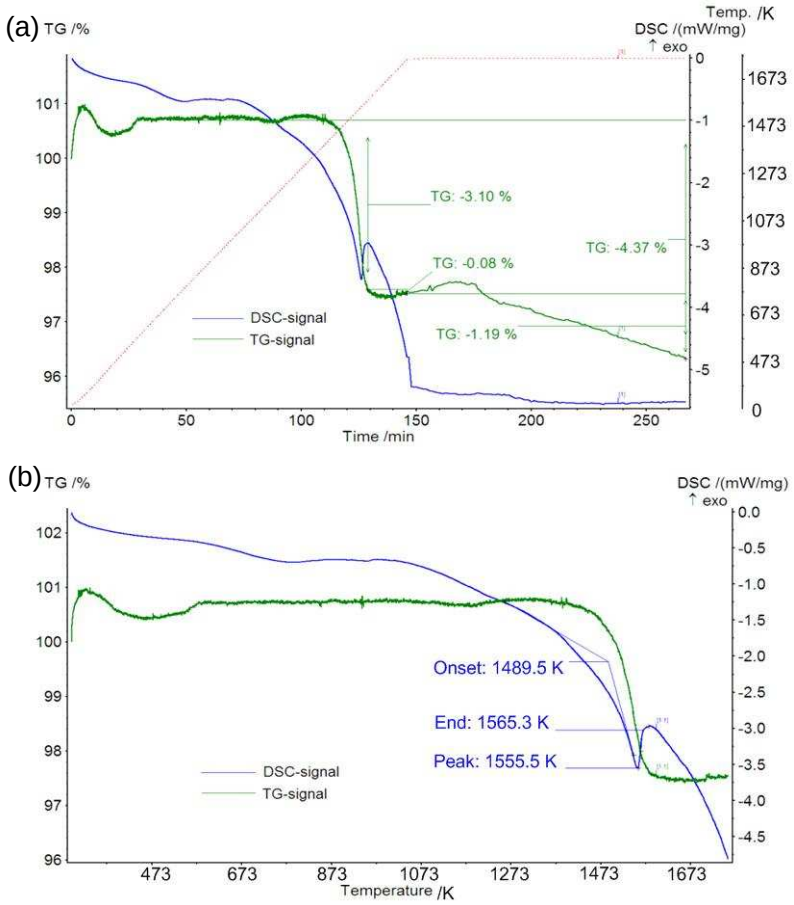

Figure 3.7 TGA-DSC analysis of pure Fe_2O_3 in N_2, (a) as a function of time, (b) as a function of temperature

Table 3.5 Comparison of the three TGA-DSC tests for the two materials with different particle size and heating rate, atmosphere: N_2

Sample	Particle size (μm)	Heating rate (K/min)	Weight loss (%)	R (%)	$T_{E\text{-}H}$ (K)	$T_{E\text{-}M}$ (K)	$T_{T\text{-}H}$ (K)	$T_{T\text{-}M}$ (K)
Hematite ore	45-53	10	4.43	14.8	1538	1693	1473~1573	1673~1773
Hematite ore	45-53	20	4.34	14.5	1564	1701		
Hematite ore	125-250	10	4.55	15.2	1556	1698		
Hematite	45-53	10	4.37	14.6	1490	------		

$T_{E\text{-}H}$: Start temperature of the sharp weight loss stage of the thermal decomposition of hematite from TGA-DSC test
$T_{E\text{-}M}$: Start temperature of the small fluctuation stage of the thermal decomposition of magnetite from TGA-DSC test
$T_{T\text{-}H}$: Start temperature of the sharp weight loss stage of the thermal decomposition of hematite estimated from theoretical calculation
$T_{T\text{-}M}$: Start temperature of the small fluctuation stage of the thermal decomposition of magnetite estimated from theoretical calculation

3.4.2 Experimental results in the horizontal furnace

3.4.2.1 Effect of holding time

The experiments in the horizontal furnace differ from the TGA-DSC analysis by the amount of the sample and the way of heating (temperature profile). The small sample size used in the TGA-DSC analyser would cause a low accuracy of the result of the weight loss. In addition, the weight loss from decomposition of carbonates in the hematite ore could not be eliminated. Therefore, the larger sample size has been tested in the horizontal furnace and the sample after the experiment could be analysed by chemical analysis to obtain a more accurate result. More importantly the thermal decomposition experiments in the horizontal tube furnace were conducted at a constant temperature, and the time to reach the reaction temperature is very short. The temperature of the sample before pushing to the hot zone of the reactor tube is room temperature. TGA-DSC tests have a constant heating rate of 10 K/min.

Both hematite ore and hematite samples were used and positioned at the isothermal zone of the horizontal furnace. According to the thermodynamic theory, the thermal decomposition reactions would not stop as long as the samples are kept in the flowing inert gas at the high temperature and the released O_2 is constantly removed and maintain the real partial pressure of oxygen lower than the equilibrium value at that temperature (open system). However, according to the

results of TGA-DSC analysis, the reaction rate becomes very low after two hours holding time. The heating time and the holding time of 2 hours already contain the stage of sharp weight loss observed in the TGA-DSC tests. Different holding times of 1 hour, 2 hours and 3 hours at 1673 K in the horizontal furnace were also tested to make sure that the total experimental time is long enough to cover the sharp weight loss stage. The results shown in Figure 3.8 indicate clearly that the sharp weight loss already takes place in the experiment with 1 hour holding time, and the thermal decomposition degree of hematite ore after 2 hours holding time increases slowly. Finally, the holding time was fixed to 2 hours for the other experiments.

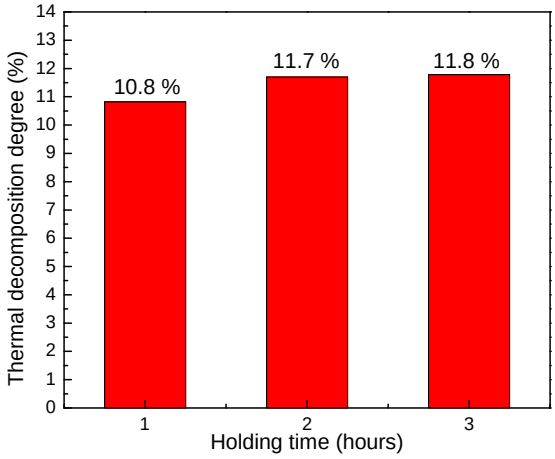

Figure 3.8 Thermal decomposition degree of iron ore in different holding time, T = 1650 K, atmosphere: N_2

3.4.2.2 Effect of temperature

The effect of temperature on the thermal decomposition degree is shown in Table 3.6. Both pure hematite and hematite ore have been tested. In Table 3.6, T_{Fe}% denotes weight percentage of total iron in the sample, Fe^{2+}%, and Fe^{3+}% are the weight percentages of Fe^{2+} and Fe^{3+} in the sample, respectively. R denotes the thermal decomposition degree which is also called equivalent reduction degree. According to the composition of the raw material, the elemental Fe is completely in the form of Fe_2O_3 in the raw material. Therefore the original oxygen percentage in the sample can be calculated with the weight percentage of the total iron in the sample. On the other hand, the oxygen weight loss by decomposition can be calculated with the weight percentage of Fe^{2+} in the sample. Finally, the reduction degree can be evaluated by Eq. 3.1. The rough product composition is calculated by assuming that Fe_2O_3 firstly decomposes to Fe_3O_4 completely and then Fe_3O_4 decomposes to FeO. In other words, FeO is generated until the transformation from Fe_2O_3 to Fe_3O_4 is completed. According to the assumption and theoretical

evaluation, if the decomposition degree is below 11.11 %, the final product is composed of Fe_2O_3 and Fe_3O_4. If the thermal decomposition degree is between 11.11 % and 33.33 %, the final product is composed of Fe_3O_4 and FeO. If the thermal decomposition degree is above 33.33 %, there should be a mixture of FeO and metallic iron (though it is very difficult to reach, as is indicated by thermodynamic evaluation).

Table 3.6 Thermal decomposition degree in horizontal furnace (atmosphere: N_2)

T /K	t /h	Chemical titration result (wt%)						R %	Weight loss %	Physical state
		T_{Fe}	Fe^{2+}	Fe^{3+}	Fe_2O_3	Fe_3O_4	FeO			
Hematite Fe_2O_3 (99%+)										
1673	2	71.8	23.7	48.0	1.6	98.4	0.0	11.0	3.3	Solid
1773	2	72.1	23.7	48.4	1.6	98.4	0.0	10.9	3.3	Solid
1873	2	73.6	35.6	37.9	0.0	78.6	21.4	16.1	4.9	Liquid
Hematite ore (94.9 % Fe_2O_3)										
1673	2	69.1	24.3	44.9	0.0	93.0	2.3	11.7	3.5	Solid
1773	2	68.9	26.0	42.9	0.0	88.9	5.8	12.6	3.8	Solid
1873	2	69.5	34.3	35.2	0.0	73.1	21.4	16.4	4.9	Liquid

The comparison of the experimental results for the two materials is clearly shown in the Figure 3.9. The thermal decomposition degree increases with the increase of temperature for both hematite ore and pure hematite. The difference between the thermal decomposition degree at 1673 K and 1773 K is small. For pure hematite, the result at 1673 K is almost the same as that at 1773 K. For hematite ore, the result at 1773 K is slightly higher than that at 1673 K by 0.87 %. However, the thermal decomposition degree increases strongly from the temperature of 1773 K to 1873 K. At 1873 K, the decomposition reaction of pure Fe_2O_3 takes place intensively resulting in 16.1 % thermal decomposition degree and hematite ore has the thermal decomposition degree of 16.4 %. It indicates that the thermal decomposition of magnetite becomes faster at 1873 K. Both hematite and hematite ore at 1873 K were melted down completely, while the samples were still in solid state at 1673 K and 1773 K. At the same condition, the result of thermal decomposition degree of hematite ore is slight higher than of pure hematite. The analysis of sample composition shows that the product of hematite ore is mainly

composed of magnetite and wüstite and the percentage of wüstite goes up with increasing temperature.

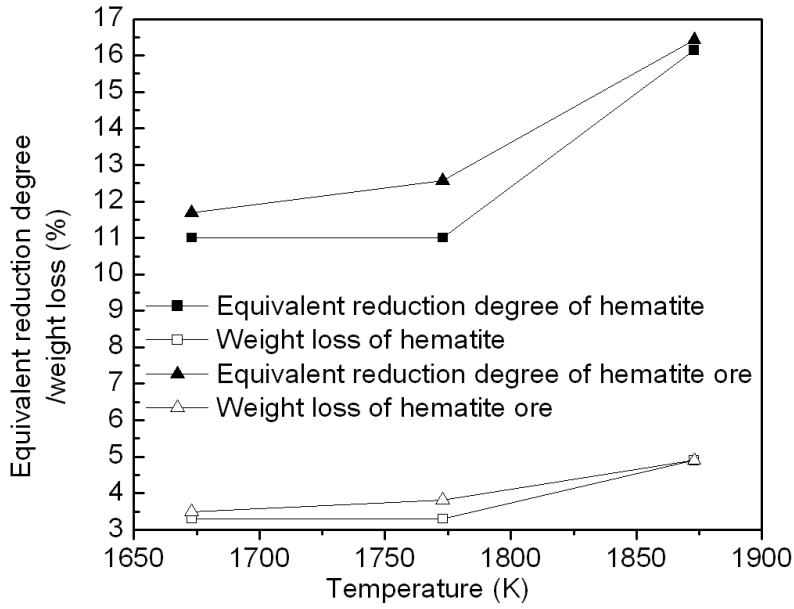

Figure 3.9 Comparison of the experimental results for the two materials

3.4.3 Experimental results in the HDTF

The approximate thermal decomposition degree of hematite at 1750 K and the thermal decomposition behaviour of hematite at elevating temperature have been studied with the TGA-DSC analyser, and the accurate thermal decomposition degree of hematite at different temperatures has been studied with the horizontal furnace. The results show that a sharp weight loss stage exists during the heating time of the sample. The residence time of the iron ore particles in the cyclone reactor is much shorter than the time investigated in the TGA-DSC and horizontal tube furnace. Whether the sharp weight loss stage will be present in the smelting cyclone and how fast the thermal decomposition will proceed during the sharp weight loss stage are not known and cannot be deduced from the above results. Therefore, the thermal decomposition behaviour of individual particle was further studied with the HDTF. The composition of the iron ore is shown in Table 3.1. The collected samples were analysed by chemical titration to obtain the accurate thermal decomposition degree.

3.4.3.1 Effect of temperature and gas

The reducing gas in the cyclone reactor consists mainly of CO, CO_2, H_2, H_2O and N_2. According to the analysis of the composition of off-gas from the cyclone reactor, it was found that CO_2 is around 70 % and N_2 is around 5-10 % [6]. In the HDTF, both CO_2 and N_2 were used as the inert gas to study the hematite thermal decomposition behaviour during the particle flying time.

Figure 3.10 shows the effect of temperature and the type of gas on the thermal decomposition of iron ore particles. The experiments of thermal decomposition of hematite ore in CO_2 gas were carried out at 1550 K, 1600 K, 1650 K, 1750 K and 1800 K. The particle size was in the range of 45-53 µm. The particle residence time in the hot zone was maintained at 2020 ms (limited by the length of the hot zone), which was calculated by Eqs.3.8-3.14. In order to study the influence of different inert gas on the thermal decomposition degree of iron ore, the experiments also have been carried at three selected temperature: 1650 K, 1750 K and 1800 K in N_2 gas and Ar gas. The results show that the thermal decomposition degree of hematite ore increases with the increase of temperature for all inert gases used. But the difference of thermal decomposition between the temperature of 1750 K and 1800 K is quite small. At the three selected temperatures, the thermal decomposition degrees of hematite ore particles in CO_2 gas (solid circle) are much higher than that in N_2 gas (solid triangle). The difference of the thermal decomposition degrees in the two gases (CO_2 and N_2) is about 3-4 %. By estimation of the composition of the iron ore sample, it shows that the remaining hematite content in the sample with N_2 gas is much higher than that in the sample with CO_2 gas. For example, at 1750 K, the Fe_2O_3 in the product which wad decomposed in N_2 gas is about 31.2 %, but the Fe_2O_3 in the product which was decomposed in CO_2 gas is only about 2.3 %. The experimental results in Ar gas (solid square) as shown in the figure are almost the same with the results in N_2 gas. It is because CO_2 is an asymmetric diatomic molecule, while N_2 is a symmetric molecule and Ar is a monatomic molecule. The structure of molecules is important for molecular radiation - emission and absorption which occurs only when an atom makes a transition from one state with a certain amount of energy to a state with lower and higher energy, respectively. Homonuclear diatomic molecules like N_2 and O_2 and monatomic molecules like Ar don't have radiative capability for its symmetrical distribution of charges. Compared to N_2 and Ar, CO_2 has strong thermal radiation capacity. That is also why CO_2 gas is the most important greenhouse gas. Therefore a fine particle is heated up more quickly in CO_2 gas than in N_2 and Ar.

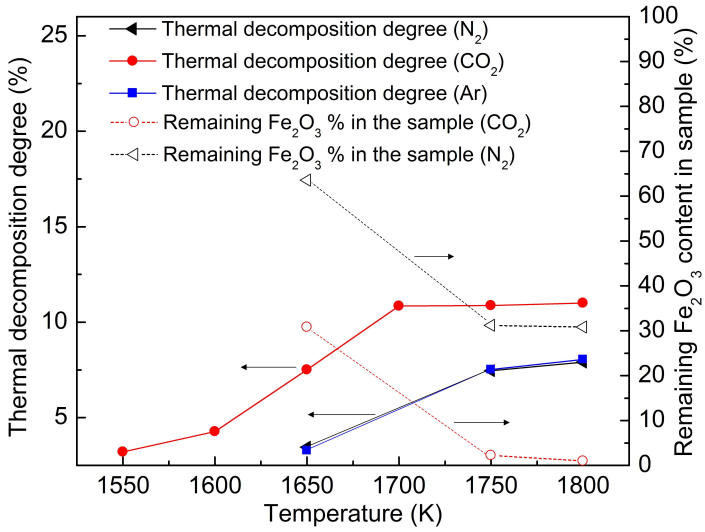

Figure 3.10 Thermal decomposition of hematite ore in Ar, CO_2 and N_2 at different temperatures

The experiments carried out at 1673 K, 1773 K and 1873 K in the horizontal furnace are selected to compare the experiments carried out at 1650 K, 1700K, 1750 K and 1800 K in the HTDF as shown in Figure 3.11. It's found that the sharp weight loss stage still exists in the HTDF during the particle flying time through the hot zone. However, the sharp weight loss stage was not completed at 1650 K. The thermal decomposition degree of iron ore in CO_2 gas is 7.5 % and in N_2 gas is 3.5 % which are far below the result of 11.7 % in the horizontal furnace. At 1700 K, 1750 K and 1800 K, the thermal decomposition degrees of 10.8 %, 10.9 % and 11.0 % of iron ore in the HTDF with CO_2 are quite close to the result of 12.6 % at 1773 K in the horizontal furnace. It indicates that almost the whole sharp weight loss stage observed in TGA-DSC tests is achieved at the temperature from 1700 K to 1800 K in the HTDF, although the residence time of iron ore particles are much shorter than the holding time in the horizontal furnace. This is cased by two reasons. Firstly, the particles in HTDF is moving individual particles, having much better and more favorite kinetic conditions than in the horizontal furnace where they are packed and steady and perhaps with lower relative moving velocity from the gas. Secondly, the thermal decomposition rate of iron ore at the sharp weight loss stage is extremely fast. How fast of thermal decomposition rate of iron are at its sharp weight loss stage could not be estimated from the results with TGA-DSC analyzer and the horizontal furnace. Although TGA-DSC analyzer supplies the online report of weight loss as a function of time, the heating rate (10 K/min.) in the TGA-DSC analyzer is different from the heating in the smelting cyclone. Therefore, further experiments were carried out in the HTDF with different residence time as described in the following section.

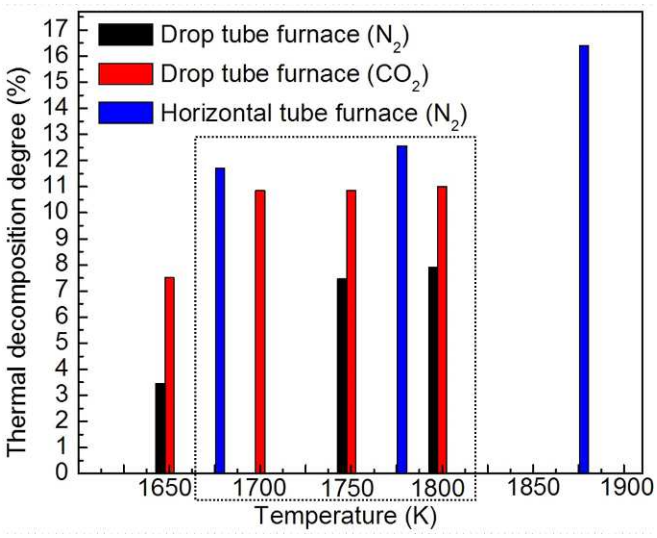

Figure 3.11 Comparison of thermal decomposition of hematite ore in the horizontal furnace and the HDTF, residence time in HDTF is 2020 ms, residence time in horizontal tube furnace is 2 hours.

3.4.3.2 Effect of residence time

The effect of residence time on the iron ore thermal decomposition degree in the HTDF has been studied. The results of chemical analysis of the sample are shown in Table 3.7 and the comparison of the results in different gas and residence time is given in Figure 3.12. Both N_2 gas and CO_2 gas were used. The residence time of the flying iron ore particle was adjusted by varying the gas flow rate. In the first part, the temperature in the hot zone was set to 1650 K and 1800 K with the inert gas of N_2. The particle size was in the range of 45-53 µm. Two residence times of 2020 ms and 970 ms were tested. The results show that the thermal decomposition degree increases with the increase of temperature for both the experiments carried out in 2020 ms and the experiments carried out in 970 ms. In addition, it is found that the decomposition degree of hematite ore in the N_2 gas goes up with the increase of residence time. The thermal decomposition degree in 2020 ms is about 1-1.5 % higher than that in 970 ms in N_2 gas. In the smelting cyclone the bulk gas is mainly composed of CO_2 gas which has a strong thermal radiation capacity. Therefore, more experiments have been carried out in CO_2 gas. It was found that the thermal decomposition degree of iron ore increases with the increase of temperature (Figure 3.10). However, it was not changed by changing the residence time. For example, at 1750 K, the influence of residence time of iron ore particles was verified from 210 ms to 2020 ms, but the thermal decomposition degree of iron ore was all around 10.8 % which is very close to 11 %. The difference between the results can be neglected. The compositions of the products were estimated by

assuming that wüstite could not be generated before the complete consumption of hematite. The iron ore particles decomposed in CO_2 at 1750 K consisted mainly of generated magnetite and a small amount of unreacted hematite. The content of magnetite is above 80 % and the content of hematite is less than 10 %.

Table 3.7 Hematite ore thermal decomposition with different residence times (size: 45-53 µm)

Gas	T (K)	t (ms)	Chemical titration result (wt%)			R (%)	Calculation composition (wt%)		t_{du} (h)	m_{sample} (g)
			T_{Fe}	Fe^{2+}	Fe^{3+}		Fe_2O_3	Fe_3O_4		
N_2	1650	2020	64.4	9.7	54.7	5.0	50.5	40.1	~ 5	3 - 4
		970	64.6	6.7	57.9	3.5	63.6	27.7	~ 5	3 - 4
	1800	2020	65.9	17.4	48.5	8.8	19.5	72.2	~ 5	3 - 4
		970	65.5	15.5	49.9	7.9	30.8	62.1	~ 5	3 - 4
CO_2	1750	2020	66.0	21.3	44.7	10.8	3.0	88.2	~ 5	3 - 4
	1750	970	67.2	21.9	45.3	10.9	2.4	90.6	~ 5	3 - 4
	1750	210	66.8	21.2	45.6	10.6	10.0	82.5	~ 5	3 - 4

*m_{sample} is weight of collected samples; t_{du} means duration of each experiment.

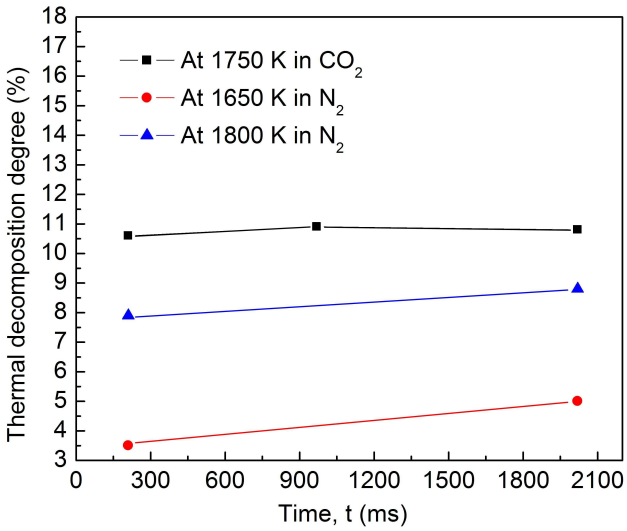

Figure 3.13 Effect of residence time and gases on thermal decomposition in the HTDF

The residence time has influence on the thermal decomposition degree of iron ore with N_2 in the HTDF, but has no influence on the thermal decomposition degree of iron ore with CO_2 in the HTDF. It is mainly caused by the gas radiation properties,

which makes the so effective for heat transfer. In other words, the particle heating rate in N_2 gas would be the rate controlling step of the iron ore thermal decomposition. In the CO_2 gas, the studied range of residence time does not affect the thermal decomposition degree of iron ore. That does not mean that a residence time longer than 2020 ms also has no effect on the thermal decomposition degree of iron ore. However, the sharp weight loss stage could be partly achieved in 210 ms when the inert gas is CO_2 in the drop tube furnace and no further change of thermal decomposition degree can be detected during the residence time between 210 ms to 2020 ms.

3.4.3.3 Effect of particle size

The experiments have been conducted with different particle sizes in CO_2 gas. The average temperature of the hot zone was set to 1750 K. The experiments were divided into two groups: small particle and large particle. The residence time of the smaller particles was 970 ms and that of the larger particles was 210 ms. The particle sizes in the first group were in the range of 38-45 µm and 75-90 µm and in the second group were in the range of 90-125 µm and 125-250 µm. The results are listed in Table 3.8. It can be seen that in all the studied particle sizes of 38-250 µm, the thermal decomposition degree of iron ore is in the range of 10.3-11.3 %. The small deviation can be neglected. Therefore, the particle size below 250 µm does not have significant influence on the thermal decomposition degree of the hematite ore in the HDTF when the inert gas is CO_2. On the other hand, the residence time of the larger particles is shorter than the smaller particles. The results proved again that residence time is not a significant factor for the thermal decomposition behaviour of fine iron ore particles with the CO_2 gas in the HTDF.

Table 3.8 Thermal decomposition of hematite ore in different particle size

Gas	d_p (µm)	t (ms)	Chemical titration result (wt%)			R (%)	Calculation composition (wt%)			t_{du} (h)	m_{sample} (g)
			T_{Fe}	Fe^{2+}	Fe^{3+}		Fe_2O_3	Fe_3O_4	FeO		
CO_2	38-45	970	66.6	21.8	44.8	10.9	1.7	90,4	0.0	~ 5	3 - 4
	75-90		66.0	21.0	45.0	10.6	4.7	87.0	0.0	~ 5	3 - 4
	90-125	210	66.9	22.6	44.3	11.3	0.0	91.7	0.6	~ 7	5 - 6
	125-250		64.9	20.1	44.8	10.3	6.7	83.1	0.0	~ 5	3 - 4

*m_{sample} is weight of collected samples; t_{du} means duration of each experiment.

The sample of 90-125 µm in Table 3.8 was analysed by XRD method to identify the product forms as shown in Figure 3.14. In the figures the measured XRD patterns are shown in black. The colour sticks give the peak positions and intensities of the identified phases. This confirms fully the analytical results of chemical titration. The main phase in the reacted iron ore sample is magnetite and the phases of hematite and wüstite are either not present (hematite) too small to be detected (wüstite).

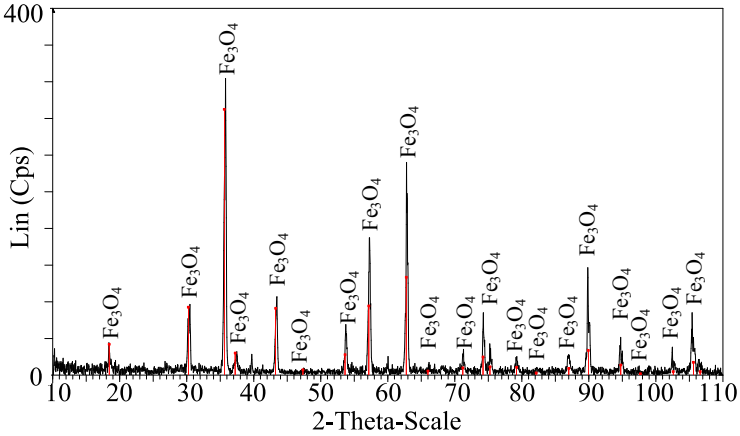

Figure 3.14 XRD pattern of reacted iron ore sample at 1750 K in CO_2

3.4.4 Reproducibility tests

A series of repeated tests have been conducted to check the reproducibility of the high temperature experiment in both horizontal furnace and HTDF. In order to test the reproducibility of the experiment in the horizontal furnace, the thermal decomposition of hematite ore at each studied temperature has been conducted three times. The results are shown in Figure 3.15. The experimental conditions were the same as the experiments shown in Table 3.6 (the part of hematite ore). The three points at each temperature are quite close to each other and they just have a slight deviation as shown the figure. Therefore the experiments in the horizontal furnace can be considered to be very well reproducible.

The experimental results of hematite ore in HDTF showed that the particle size and residence time do not have influence on the thermal decomposition degree of iron ore. This outcome was unanticipated before conducting the experiment and suspected a lot. Therefore, the reproducibility of the experiment in the HDTF has been proved with a lot of repeated experiments. An example is shown in Figure 3.16. The particle size is 45-53 µm. The gas of CO_2 was used as the inert gas. The error bar in the figure is ± 3 %. The two results of the experiments carried out at the same condition show a good agreement. All the deviations of the results are within 3 %.

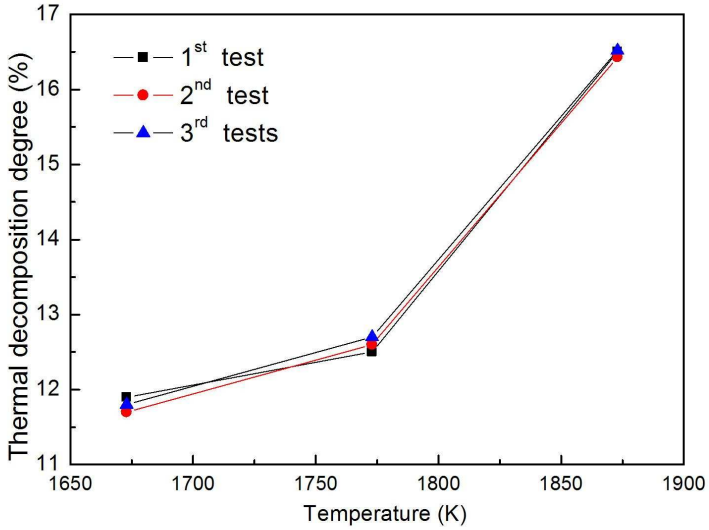

Figure 3.15 Reproducibility of the experiments in horizontal furnace

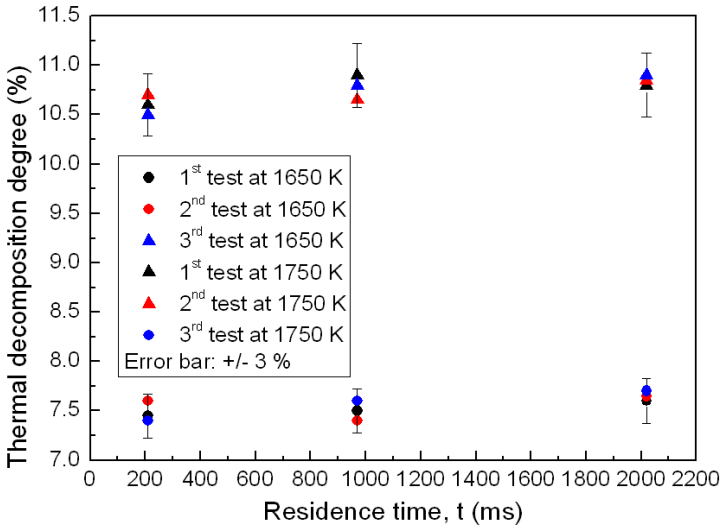

Figure 3.16 Reproducibility of the experiments in HDTF

3.4.5 Summary of the main results

The thermal decomposition behaviour of hematite has been studied through theoretical and experimental methods. The most important results of each method and the cooperation between the methods are drawn and given in Figure 3.17. Theoretical evaluation based on thermodynamics is necessary besides the experimental investigation and supplies the thermodynamic reference for the experimental results. TGA-DSC tests make it visible of the process of thermal decomposition, which cannot be realized by either horizontal furnace method or HDTF method.

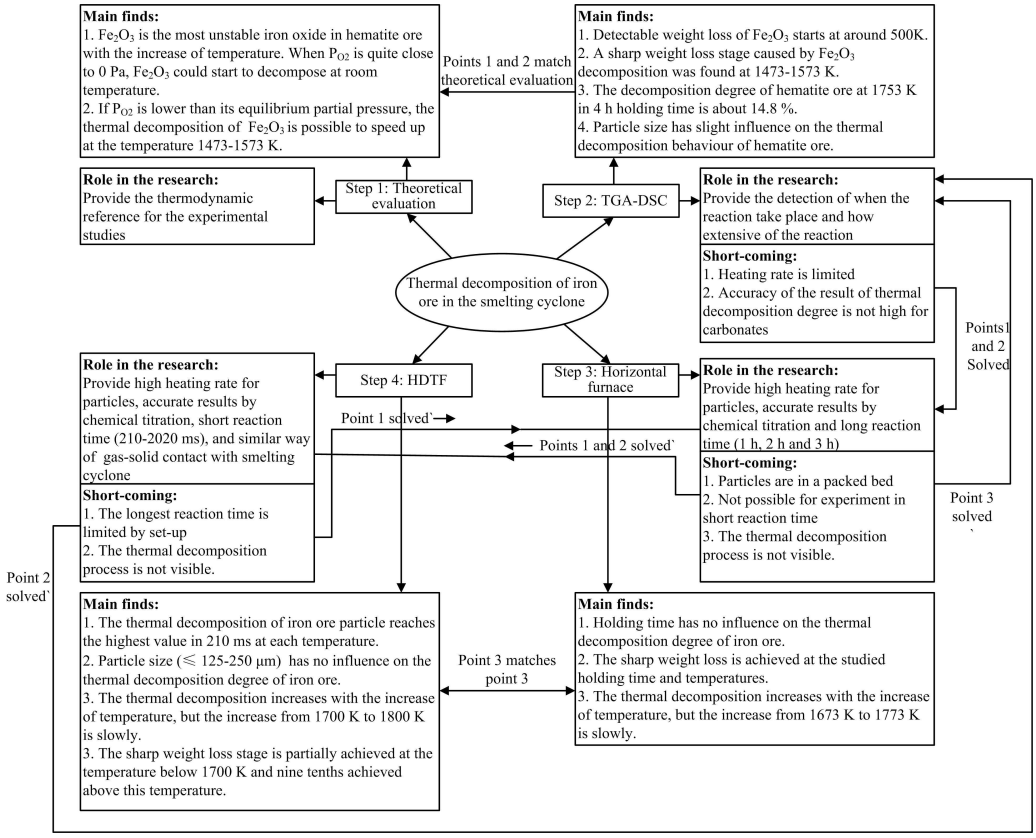

Figure 3.17 Summary of the important results of the thermal decomposition of hematite ore from theoretical evaluation, TGA-DSC analysis, horizontal furnace and HTDF, and the contribution and short-comings of each method

The start temperature of thermal decomposition, the stages of intensive reactions and weight loss as a function of time and temperature can be obtained through the

TGA-DSC method. The particles can be heated up slowly in the TGA-DSC furnace. However, in the lab the heating rate of TGA-DSC is normally limited below 20 K/min for the reason of maintenance. The heating rate of iron ore particle is far below that in the smelting cyclone. The accuracy of the result of thermal decomposition degree is not very high for the carbonates in the sample and the accuracy of the TGA-DSC is highly depend on the high accuracy of calibration which is conducted before the experiment. Therefore, the results from TGA-DSC are confirmed by the experiments with horizontal tube furnace. The heating rate of sample is increased by pushing the sample into the furnace, when the temperature of the furnace reaches the designated value. The large sample size (~10 g) allows the analysis by chemical titration which gives the high accuracy results of thermal decomposition of iron ore. The holding time of the experiments in horizontal furnace was varied from 1 h to 2 h and then to 3 h. For both TGA-DSC method and horizontal furnace method, the particles were put in a crucible and form a packed bed. However, in the smelting cyclone, the individual particle contacts with reducing gas during the flying time in the cyclone reactor. The high simulation and kinetic study were performed with the HTDF. Although the longest residence time of particle is limited by the set-up (Now, it is 2020 ms.), the thermal decomposition degree of iron ore in long residence time (> 2020 ms) could be deduced from the result with horizontal furnace.

3.5 Conclusions

With the experimental and theoretical study, the following conclusions are obtained,

- From the theoretical calculation, in the inert gas environment, the start temperature of Fe_2O_3 thermal decomposition could be room temperature when p_{O2} is 0 Pa. If p_{O2} is lower than the equilibrium pressure of oxygen (82 Pa) at 1473 K, the intensive thermal decomposition is possible to take place above 1473 K. The lowest start temperature of thermal decomposition of Fe_3O_4 is also room temperature when p_{O2} is 0 Pa. If p_{O2} is lower than the equilibrium pressure of oxygen (1.7 Pa) at 1773 K, the thermal decomposition of Fe_3O_4 is possible to speed up above 1773 K. Fe_2O_3 is the most unstable iron oxide among the three iron oxides, while FeO is the most stable one.

- From TGA-DSC analysis, it is found a sharp weight loss stage appeared on the TG curve in the range of temperature of 1473-1573 K. A big trough was presented by the DSC curve at the same time. It caused by the intensive decomposition of hematite. The result is highly in accordance with the theoretical estimation.

- From the experimental results in the horizontal furnace, the accurate thermal decomposition degree of hematite at a given temperature and holding time was obtained. The holding times (1 h, 2 h, 3 h) almost has no influence on the thermal decomposition degree of iron ore. Generally, the thermal decomposition degree of hematite increases with the increase of temperature. No significant difference was observed between the results at 1673 K and 1773 K. The thermal decomposition degree of hematite at 1873 K is much higher than that at 1773 K. It was found that the thermal decomposition of magnetite could be accelerated at 1873 K which is in the range of the theoretical estimation. The sharp weight loss stage observed in TGA-DSC test is achieved in all the studied temperatures and holding time.

- In the HDTF, the effects of particle size, residence time, temperature, and gas composition on the thermal decomposition degree have been investigated. It was found that the sharp weight loss stage which was observed in the TGA-DSC experiments could be partly achieved in the HTDF especially in the CO_2 gas. The fine iron ore particles could be heated up faster in CO_2 gas than in N_2 gas due to the strong radiation properties (emission and absorption) of CO_2 gas. For this reason, in the HDTF, the thermal decomposition degree of fine iron ore particles in N_2 gas increases with the increase of temperature and particle residence time. As CO_2 is the main gas in the smelting cyclone, more experiments have been conducted in CO_2 gas. It is found that the thermal decomposition degree in CO_2 gas increases also with the increase of temperature and the increase between 1700 K and 1800 K is every slow. However, there is no significant influence of particle size and residence time on the observed thermal decomposition degree, when the particle diameter is smaller than 250 µm. At the temperature of 1750 K in CO_2 gas, the thermal decomposition degree of iron ore in the HTDF is around 10.9 % which is slightly lower than the value of 12.6 % obtained in the horizontal tube furnace (holding time 2 hours). The thermal decomposition degree of iron ore achieved a high value in such a short time in the HTDF is because that the particles in HTDF is moving individual particles, having much better and more favorite kinetic conditions than in the horizontal furnace where they are packed and steady and perhaps with lower relative moving velocity from the gas.

References

[1] Voitkovsky, Y.B.: On Kinetics of High-temperature Air Reduction of Hematite, Physics of the solid earth 21 (1995) 349-351.

[2] Piotrowski, K.; Mondalb, K.; Wiltowski, T.; Dydod, P.; Rizeg, G.: Topochemical Approach of Kinetics of the Reduction of Hematite to Wüstite, Chemical Engineering Journal 137 (2007) 73-82.

[3] Takeuchi, N., Nomura, Y., Ohno, K., Maeda, T., Nishioka, K. and Shimizu, M.: Kinetic Analysis of Spherical Wüstite Reduction Transported with CH_4 Gas, ISIJ International 47(2007) 386-391.

[4] Boggelen, J. V.: HIsarna, a Low CO_2 Ironmaking Process, Presentation, January 10 2012.

[5] Link, J.: " IRMA – Flowsheet Model Examples of Application", La Revue de Metallurgie Volume number (2009) 398-403.

[6] Private information from Tata Steel.

[7] Gilles, H.L.; Clump, C.W.: Reduction of Iron Ore with Hydrogen in a Direct Current Plasma Jet, Industrial & Engineering Chemistry Process Design and Development 9 (1970) 194-207.

[8] Nakamura, Y., Michihisa, I., Hideki, I.: Reduction and Dephosphorization of Molten Iron Oxide with Hydrogen-Argon Plasma, Plasma Chemistry and Plasma Processing 1 (1981) 149-160.

[9] Habermann, A.; Hofbauer, F.W.H.: A Experimental Study on the Kinetic of Fluidized Bed Iron Ore Reduction; ISIJ International 40 (2000) 935-472.

[10] Acevedo, C. M. U.: Mathematical Modeling and Control of the Blast Process, PhD thesis, Purdue University, 1981.

[11] Bron, A. V., Savchenko, Y. I., Shchetnlkova, I.L.: Decomposition of Magnetite During Heating, East Institute of Refractories 3 (1973) 49-52.

[12] Ruiz, A. E., Rodriguez, N.C., Luque, A.: A TME and 2D-XRD Study of the Thermal Decomposition of Calcite, Revista de la sociedad española de mineralogía 9 (2008) 223-224.

Chapter 4 Reduction Behaviour of Individual Iron Ore Particles in the High Temperature Drop Tube Furnace

4.1 Introduction

The reduction kinetics of individual particles of the very fine iron ore in the smelting cyclone has been studied in the HDTF. The partially reduced particles were firstly analysed by chemical titration. The morphology study was conducted with an optical microscope and SEM–EDS methods. XRD analysis was used to detect the different iron oxide phases contained in the partially reduced iron ore sample and to provide the semi–quantitative analysis of their composition. XRF was also used to verify the results from chemical titration and determine the contents of the other compounds in the iron ore.

4.2 Experimental procedures

The details of the experimental set-up are described in Chapter 2. In order to give a clear introduction of the HTDF and the experimental procedures, the cross-sectional drawing of the electrically heated vertical tube furnace and the particle feeder are shown in Figure 4.1. The four gas flows of CO, H_2, CO_2 and N_2 from the gas cylinders were regulated by the four mass flow controllers which have been especially calibrated for the four gases separately. A small part of the gas was separated as carrier gas for the particles which was measured by a mass flow meter. The carrier gas flowed into the glass tube of the particle feeder and brought several particles together with it, and then flowed into the water cooled injection probe. The other part of the gas flowed into the furnace directly from the top of the furnace. The reactions took place in the hot zone of the furnace (marked with the red colour) which starts from the tip of the injection probe and ends at the top of the sampling probe. The reacted particles and gas were received by the water cooled and gas quenched sampling probe. Finally, the particles were collected in the sample collector.

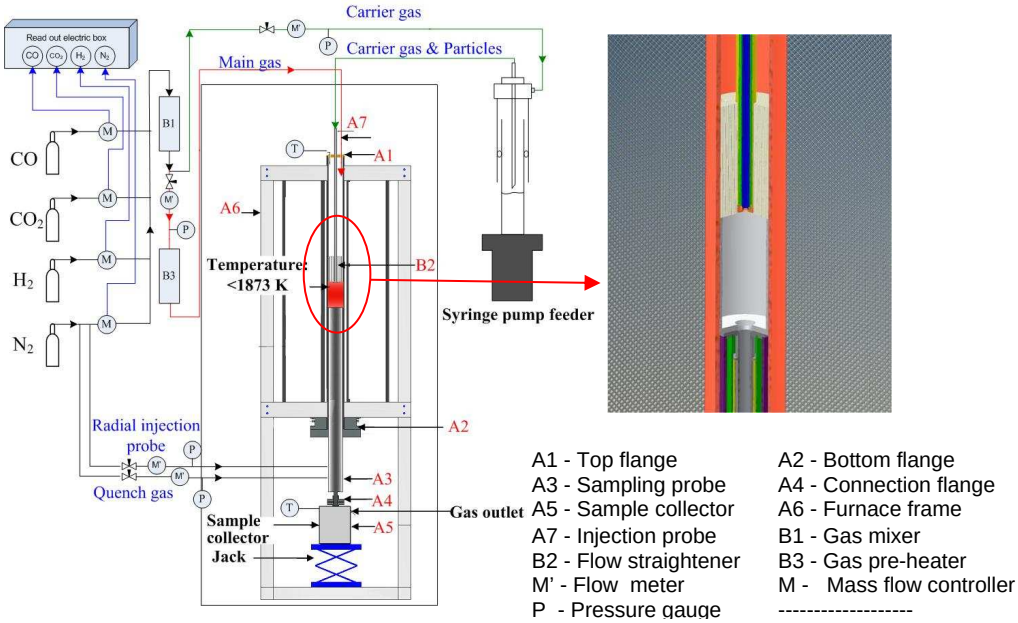

Figure 4.1 Cross-sectional drawing of the HDTF

The HDTF was electrically heated to the required temperature at a low heating rate of 3 K/min to avoid thermal shock to the Alsint reactor tube. During the heating stage and cooling stage, 1 l/min N_2 was guided into the reactor tube as protection gas to prevent the oxidizing reaction between the surface of stainless steel tubes (injection probe and sampling probe) and oxygen in the air. After filling the glass tube of the syringe pump particle feeder with iron ore particles, the top surface of the particle bed was adjusted just below the tip of the capillary tube. When the temperature of the furnace reaches the designated temperature, the quenching N_2 gas injected into the sampling probe was turned on at a flow rate of 3 l/min and the cooling gas was turned on at a low flow rate of 300 ml/min for the sampling probe. Because of the hazardous character of H_2 and CO, a H_2 sensor and a CO sensor were used to detect possible leakage of the experimental set-up during the whole experimental period. After the experiment, the furnace was cooled at the cooling rate of 2 K/min down to room temperature. The reactor and sample collector were cleaned before doing the next experiment.

4.3 Experimental conditions

As shown in Table 4.1, the average experimental temperatures were set to 1550 K, 1600 K, 1650 K, 1700 K and 1750 K. The highest temperatures were measured by

B-type thermocouple in all the experiments and compared with the highest temperatures in the preliminary tests as shown in Chapter 2. The deviation is ±3 K. The post combustion ratios of the reducing gas were set to be 38.9 %, 57.8 % and 80.4 % according to the scenarios of HIsarna process. The amount of post combustion ($CO + O_2$ and $H_2 + O_2$) taking place in the furnace can be represented by post combustion ratio (PCR) which is one of the most important parameters used at the plants of ironmaking to judge the status of the running. The definition of the PCR is given in Eq. 4.1 which is calculated with gas volume percentages. The selected three values are the most meaningful for the smelting cyclone. For each PCR, two gas compositions have been studied: one gas mixture was composed of the four gases: H_2, CO, CO_2, N_2 and the other one was only composed of CO and CO_2.

$$\mathrm{PCR} = \frac{CO_2\%+H_2O\%}{CO_2\%+H_2O\%+CO\%+H_2\%}\times 100\% \tag{4.1}$$

Table 4.1 Experimental conditions

Varieties	**Experimental conditions**	
Temperature (K)	1550; 1600; 1650; 1700; 1750	
Residence time (ms)	210 (t1); 700 (t2); 970 (t3); 1570 (t4); 2020 (t5)	
Particle size (µm)	38-45 (p1); 45-53 (p2); 53-75 (p3); 75-90 (p4);	
Particle feed rate (g/h)	1	
Gas composition	PCR1=38.9 %	10 % H_2 + 45 % CO + 35 % CO_2 + 10 % N_2
	PCR2=57.8 %	8 % H_2 + 30 % CO + 52 % CO_2 + 10 % N_2
	PCR3=80.4 %	8 % H_2 + 10 % CO + 74 % CO_2 + 8 % N_2
	PCR1'=38.9 %	0 % H_2 + 61.1 % CO + 38.9 % CO_2 + 0 % N_2
	PCR2'=57.8 %	0 % H_2 + 42.2 % CO + 57.8 % CO_2 + 0 % N_2
	PCR3'=80.4 %	0 % H_2 + 19.6 % CO + 80.4 % CO_2 + 0 % N_2

The residence time of an iron ore particle in the hot zone could be varied in a wide range from 210 ms to 2020 ms, which is denoted by 't1-t5' and controlled by the gas flow rate. The calculation of residence time is the same as the description in Chapter 3 for the thermal decomposition of iron ore particles in the HDTF. The raw material was prepared at Tata Steel Europe through screening and the particle size was analyzed by the technique of laser diffraction which is on a volume basis to get different particle sizes, and then the sample was dried to remove the water at about 423 K. The studied particle sizes have four grades as shown in Table 4.1 (38-45 µm, 45-53 µm, 53-75 µm, 75-90 µm) which are marked with p1, p2, p3 and p4, respectively. The particle size distribution (PDS) is shown in Figure 4.2. The

median value of particle size generated by laser diffraction was employed to calculate the particle residence time, and used for characterizing the particle size in most cases. Through the analysis based on volume, the median values of the particle size 38-45 µm, 45-53 µm, 53-75 µm and 75 µm-90 µm are 43.3 µm, 50.9 µm, 64.3 µm and 83.0 µm , respectively. The chemical composition of the raw materials is shown in Table 4.2. The content of hematite is as high as 96.08 %. The second highest content is SiO_2 which is 2.38 %.The particle feed rate is 1 g/h.

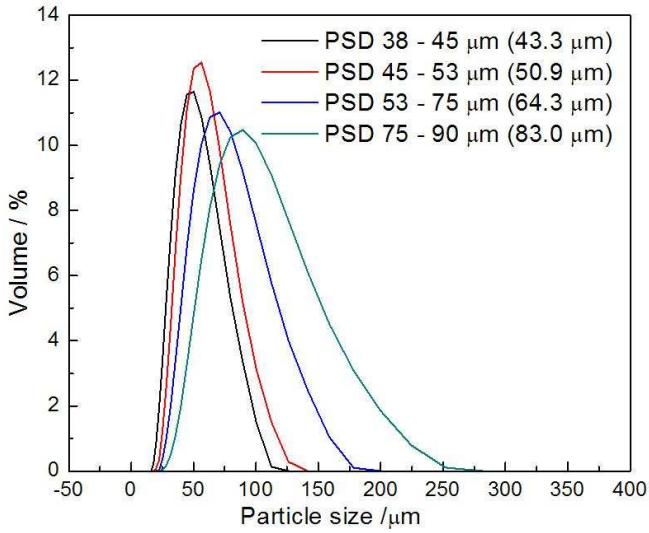

Figure 4.2 Particle size distributions

Table 4.2 Iron ore composition

Composition	wt%	Composition	wt%
Fe_2O_3	96.08	CaO	0.03
SiO_2	2.38	MnO	0.10
MgO	0.06	H_2O	0.67
Al_2O_3	0.40	Rest	0.28

4.4 Experimental objective and strategy

The experimental study of the very fine iron ore reduction is aimed to obtain the reduction mechanism of the individual particle at the selected experimental conditions. It is essential to understand the particle behaviour in the smelting cyclone of the HIsarna process. The reduction degree of iron ore in the smelting cyclone can be affected by many factors. The laboratory study focused on the four most influential factors which are temperature, particle residence time, particle size, and gas composition.

The strategy of the overall laboratory experiment is shown in Figure 4.3. The effect of PCR of reducing gas and the effect of H_2 on the reduction degree of iron ore have been studied at 1650 K. The effect of particle size on the reduction degree of iron ore has been investigated with all the six gas compositions at 1650 K. The effect of temperature on the reaction rate constant has been studied with the gas PCR2' (42.2 % CO + 57.8 % CO_2) and the particle size of 45-53 µm.

For the experimental study of the reduction kinetics of iron ore, mass transfer in the gas film is also possible to be the rate controlling step which determines the reaction rate. Normally in the laboratory study, it could be avoided by increasing the gas flow rate. In order to penetrate into the intrinsic mechanism of iron ore reduction, several tests have been conducted with different gas flow rates, while the other conditions such as residence time, temperature, gas composition and particle size were not changed. The lowest gas flow rate in the tests was 2 l/min. It was found that there was no difference between the results at different gas flow rates. It is probably because the particle feeding rate (1 g/h) compared to the gas flow rate (120 l/h) is too small. The results indicate that the gas flow rate of 2 l/min is already above the limit which causes mass transfer in the gas film to be rate controlling step. Therefore, the mass transfer in the gas film is not a controlling step for the iron ore reduction in the HTDF. The calculation of the reduction degree of iron ore is the same as described in Chapter 3 for the iron ore decomposition in the HTDF.

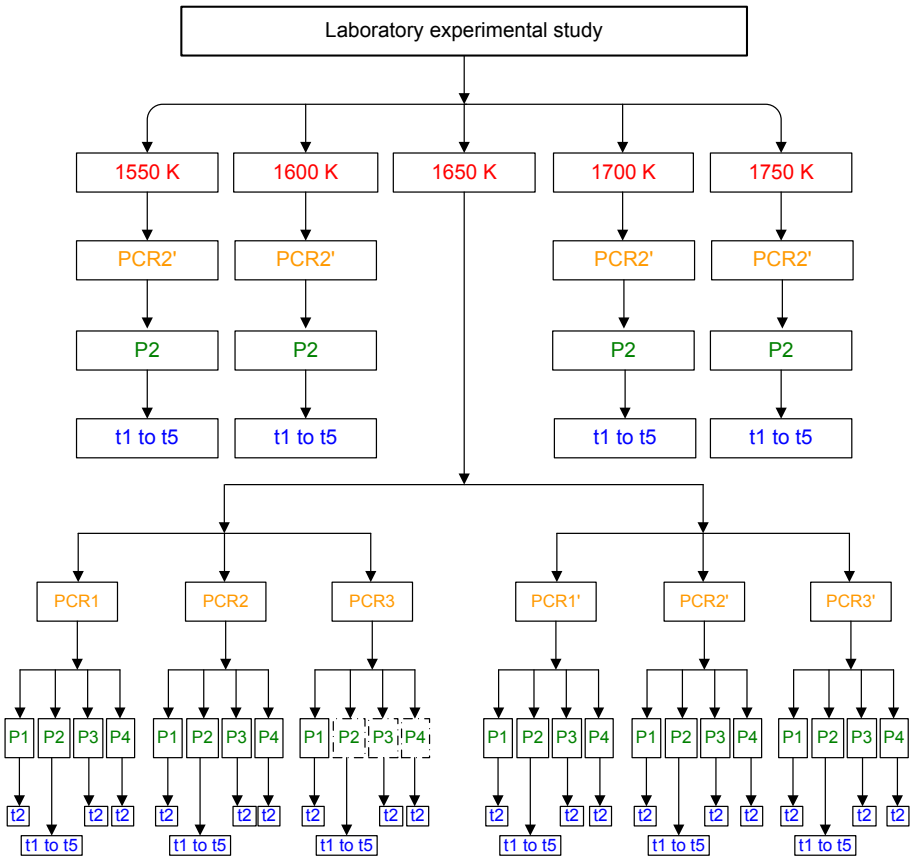

Figure 4.3 Illustration of the laboratory experiment

4.5 Experimental results of the iron ore reduction

4.5.1 Reduction degree of hematite ore

4.5.1.1 Reproducibility testing

In order to make sure that the experimental results with the HTDF are reliable all along the experimental study, a number of experiments have been selected and carried out for three times. According to the temperature, the experiments were divided into 5 groups. For each group, the first experiment was carried out

repeatedly, for example, at 1550 K, five experiments have been conducted and the experiment with residence time 210 ms (t1) was selected. The results are shown in Figure 4.4.

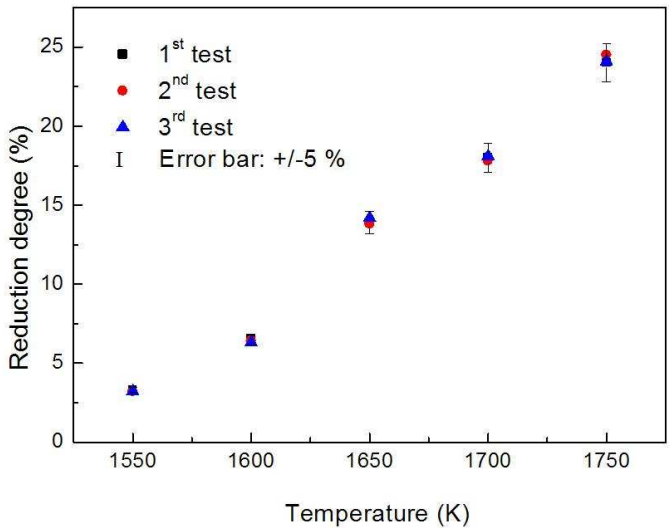

Figure 4.4 Reproducibility of the experiments with HTDF

The particle size used was 45-53 µm. The reducing gas was composed of CO and CO_2 and has the PCR of 57.8 %. The particle residence time was 210 ms. The average deviations are between 0.04-0.2 %. In order to show it clearly in the figure, A error bar is added in the figure, which is ± 5 % based on the first test. Three results at each temperature just have a slight deviation as shown the figure. Therefore the experiments in the HTDF can be considered to be well reproducible. The reduction degree of hematite ore has been analyzed by redox chemical titration which was calibrated by the standard materials. Every time when the new solutions were made, the calibration was conducted. The results showed a high accuracy.

4.5.1.2 Effect of PCR and H_2 content of the reducing gas

Figure 4.5 gives the effect of PCR and particle residence time on the reduction degree. The temperature in the hot zone was 1650 K. The reducing gas was composed of CO, H_2, CO_2 and N_2. The particle size was in the range of 45-53 µm. This particle size is close to the mean particle size used in the pilot plant. The experimental results can be divided into three groups according to the three values of PCR (38.9 %, 57.8 %, 80.4 %). Each group has 5 experiments which were conducted with different particle residence times in the hot zone. From the results, it is found that the reduction degree increases with the increase of residence time,

while the reduction degree decreases with the increase of PCR at the same residence time. The differences of reduction degree between the three groups of experiment are much more obvious at long particle residence times.

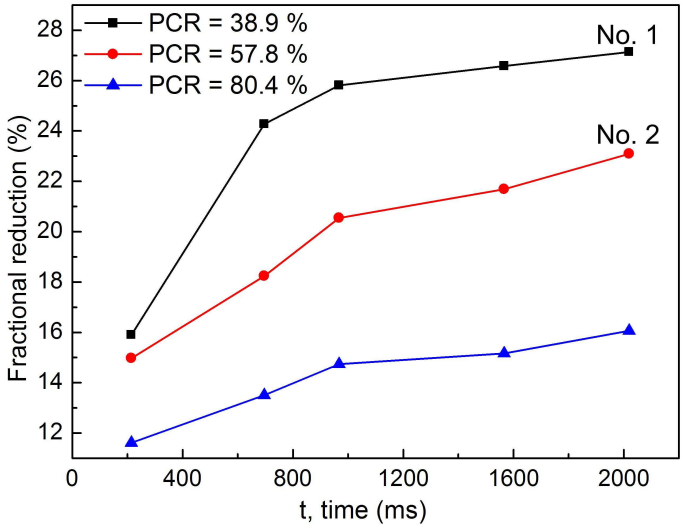

Figure 4.5 Effect of PCR and residence time on the reduction degree of fine iron ore, T = 1650 K, particle size 45-53 μm, gas including H_2 and N_2; the results of No.1 and No.2 were verified at Tata Steel

In Figure 4.5, the experiments No.1 and No.2 have been further analyzed by chemical titration and the technique of XRF, which were conducted at Tata Steel in IJmuiden, the Netherlands. This chemical titration is different from the one used in this study, which could also titrate metallic iron in the partially reduced sample besides Fe^{2+} and Fe_{total}. The Analytical Department of Tata Steel analyzed metallic iron and Fe^{2+} in a sample by dissolving the sample in a bromine-methanol mixture and then filtrate. The metallic iron was in the liquid solution and the Fe^{2+} in the residue. This method uses the reagent of Bromine and the bromine-methanol mixture. The results are shown in Table 4.3. It is assumed that the iron element is in two forms in the iron oxides: Fe_2O_3 and FeO. Through the analysis, it is found that there is no metallic iron generated in the collected iron ore samples which were reduced by the gas PCR1 (38.9 %) and PCR2 (57.8 %). However, the temperature of 1650 K is not the highest temperature in this study. Therefore, the other two experiments were conducted at 1800 K with the reducing gases PCR1 and PCR2, respectively. Theses two experiments were named No.3 and No.4 in the context. The temperature of 1800 K is higher than the highest experimental temperature in the plan and if there is no metallic iron generated in the sample No. 3 and No. 4, metallic iron would not generated in all the experiments planed in this study. The results show that there is no metallic iron in the collected samples. The

reducing gas of PCR3 (80.4 %) has lower reduction ability than the gases of PCR1 (38.9 %) and PCR2 (57.8 %). Therefore, it can be assumed that metallic iron is not possible to be generated in the all the reducing gases.

Table 4.3 Composition of partially reduced iron ore, particle size: 45-53 μm

Composition	**wt% (1650 K)**		**wt% (1800 K)**	
	No. 1 (PCR1)	**No. 2 (PCR2)**	**No. 3 (PCR1)**	**No. 4 (PCR2)**
Fe_total	75.70	74.50	75.40	75.3
Fe	0.00	0.00	0.00	0.00
FeO	77.60	65.30	91.10	74.50
Fe_2O_3	22.00	33.90	6.60	24.90
Al_2O_3	0.27	0.26	0.24	0.27
CaO	0.03	0.03	0.03	0.03
MgO	0.06	0.06	0.06	0.06
MnO	0.06	0.06	0.06	0.06
SiO_2	0.26	0.28	0.29	0.29

By comparison of the composition of unreduced iron ore in Table 4.1 and the reduced iron ore in Table 4.3, it is found that besides the obvious change of iron oxides contents, the percentage of SiO_2 in the four samples has been decreased from 2.38 % to less than 0.30 %. It is because that the following reactions take place during the reduction:

$$SiO_2(s) + H_2 / CO(g) = SiO(g) + H_2O / CO_2(g) \tag{4.2}$$

Part of the solid SiO_2 in the sample was reduced to SiO gas. According to the study of Crowley [1], the minimum reaction temperature of H_2 and SiO_2 is about 1200 K. In the study of Berdnikov [2], it has been proven that in the absence of carbon, SiO_2 is only reduced to silicon monoxide. Therefore, the SiO_2 in the hematite ore must be transferred to SiO gas at such a high temperature. The conclusion can be obtained that not all the weight loss is from the reduction of iron oxides at the temperature higher than 1200 K. If the content of SiO_2 is high in the hematite ore and the reaction temperature is higher than 1200 K, the reduction degree calculated by the weight loss method has low accuracy because it is based on the assumption that there are no weight losses from other compounds except from iron oxides. Therefore, chemical titration was employed in this study to obtain the accurate results.

Figure 4.6 shows the effect of PCR on the reduction degree of iron ore. The reducing gas was only composed of CO and CO_2 without H_2 and N_2. The furnace

was heated up to 1650 K. The particle size was between 45 µm and 53 µm. The reduction degree increases with the decrease of PCR, which is similar to the results as shown in Figure 4.5. However, at the same PCR, e.g. when PCR is 38.9 %, the reduction degree is about 2 % lower without H_2 than the result with H_2. Secondly, the difference in reduction degree without H_2 between two cases: PCR at 38.9 % and PCR at 57.8 % is smaller than the difference including H_2 gas. At PCR of 80.4 % and the residence time of 210 ms, the reduction degree is slightly lower than 11.11 %. It means that a small part of hematite was not reduced to magnetite by assuming that FeO is only generated after the complete consumption of Fe_2O_3. However, whether or not Fe_2O_3 coexists with FeO in one partially reduced sample was further verified by XRD which will be discussed in the following.

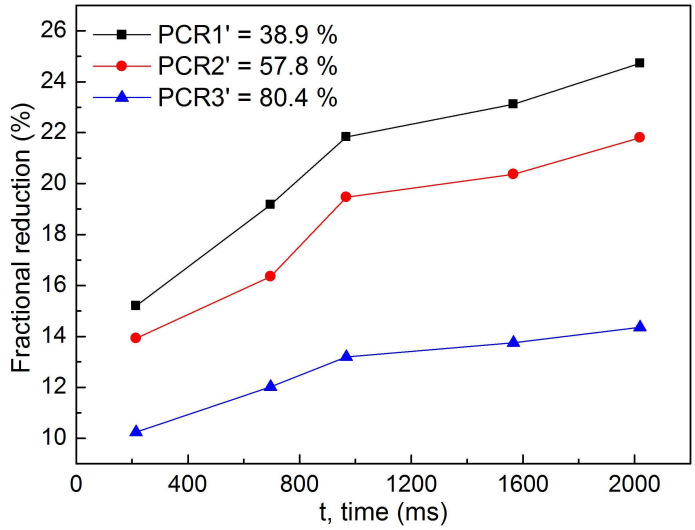

Figure 4.6 Effect of PCR on the reduction degree of iron ore particles, T = 1650 K, Particle size: 45-53 µm, excluding H_2 and N_2

4.5.1.3 Effect of particle size

Figure 4.7 gives the effect of particle size on the reduction degree of iron ore. Four average particle sizes were tested: 38-45 µm; 45-53 µm; 53-75 µm; 75-90 µm. The temperature of the hot zone in the furnace was 1650 K. In Figure 4.7 (a), the reducing gas as composed of CO, CO_2, H_2 and N_2, while in Figure 4.7 (b), the gas was only composed of CO and CO_2. The results show that the reduction degree of iron ore almost linearly decreases with the increase of particle size. It is also observed that the reduction degree of iron ore is higher with low PCR than with high PCR. At the same PCR, the reduction degrees in Figure 4.7 (b) are slightly lower than the results in Figure 4.7 (a). This phenomenon is the same as that

observed between Figure 4.5 and Figure 4.6. The reason is that the reduction ability of H_2 at high temperature is better than of CO [3].

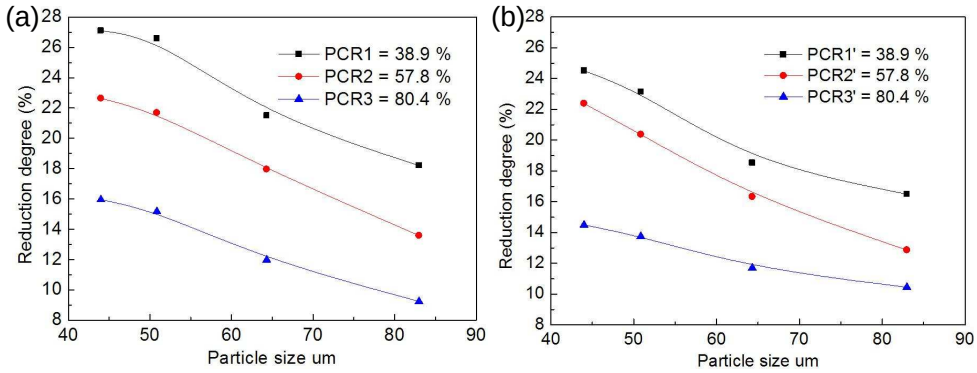

Figure 4.7 Effect of particle size on the reduction degree of fine iron ore with different PCR, T = 1650 K; a) including H_2 and N_2; b) excluding H_2 and N_2

Six linear equations can be derived from the above six lines, which are shown in Table 4.4. The unit of the particle diameter in the equations is 'm'. The formulas could be used to estimate the reduction degree of different particle size at different conditions.

Table 4.4 Reduction degree as a function of particle size at different gas compositions

PCR %	Including H_2 and N_2		Excluding H_2 and N_2	
38.9	$R = 38.1 - 243807.3 d_P$	(4.3)	$R = 33.59 - 213633.9 d_P$	(4.6)
57.8	$R = 33.5 - 239288.0 d_P$	(4.4)	$R = 32.83 - 245189.7 d_P$	(4.7)
80.4	$R = 23.9 - 178716.7 d_P$	(4.5)	$R = 19.04 - 106378.5 d_P$	(4.8)

4.5.1.4 Effect of experimental temperature

More details of the reduction kinetics of iron ore have been investigated with the typical gas composition but at different temperatures as shown in Figure 4.8. It shows the effect of temperature on the reduction degree of hematite ore. The reducing gas (PCR2') was composed of CO and CO_2 and the PCR of the gas mixture was 57.8 %. In these cases, the results only show the reduction ability of CO at different temperatures without the influence of H_2 gas. The step length of the

experimental temperature was fixed at 50 K and the temperature of the hot zone was set to 1550 K, 1600 K, 1650 K, 1700 K and 1750 K, respectively. It is clear that the reduction degree of iron ore goes up with increasing temperature at the same residence time. At 1550 K, the reduction degree of iron ore is quite low in all studied residence times from 210 ms to 2020 ms. Even the highest point (t = 2020 ms) is still lower than 11.11 %. At 1600 K, when the residence time is longer than 970 ms, the reduction degree of iron ore is higher than the level of 11.11 %. For the temperatures above 1600 K, the results of reduction degree of iron ore are all higher than 11.11 % independent of long or short residence times. The difference of the reduction degree of iron ore between 1550 K and 1650 K is larger than the difference between 1650 K and 1750 K. At the two experimental temperatures of 1700 K and 1750 K, the difference between the two values is quite small when the residence time is 2020 ms.

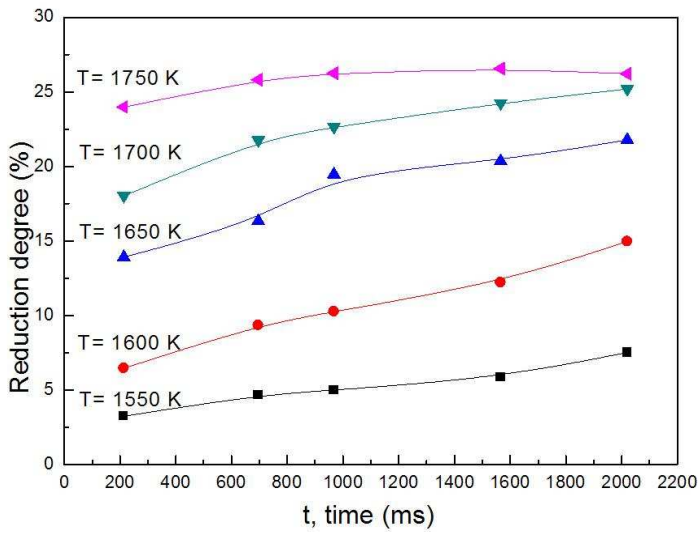

Figure 4.8 Effect of temperature on the reduction degree of fine iron ore, PCR2' (42.2 % CO + 57.8 % CO_2). Particle size: 45-53 μm

4.5.1.5 Discussion

Through analysis of the data in Figures 4.5, 4.6 and 4.8, it can be found that although the experiment was conducted in the shortest residence time of 210 ms, the reduction degrees of iron ore are not close to zero in all cases, e.g. in Figure 4.8, the reduction degree of iron ore in the residence time 210 ms is 3.3 % at 1550 K, while the result is 24.0 % in the same residence time at 1750 K. The average reduction rates in each time period at different temperatures are shown in Figure 4.9. It was found that all the reduction rates after 210 ms are in the range of 0.0-0.1 s^{-1} at all the studied temperatures. However, in the first 210 ms, the

average reduction rates are totally different from that after 210 ms and increases obviously with the increase of temperature. The most important reason is that reduction of hematite takes place accompanied by the thermal decomposition process in the first 210 ms, which is reflected by the fast thermal decomposition of the hematite concluded in Chapter 3. It means that the results of iron ore reduction in the first 210 ms are the combined effects of iron ore reduction and iron ore thermal decomposition (the thermal decomposition degree can be regarded equivalent reduction degree). The combination results caused the high reduction rate in the first 210 ms.

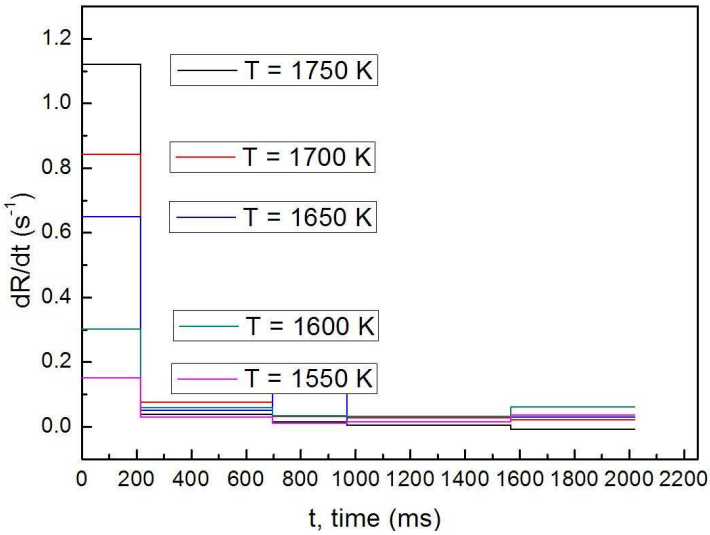

Figure 4.9 Average reduction rates in each time period at different temperatures of 1550-1750 K, by PCR2' (42.2 % CO + 57.8 % CO_2), particle size: 45-53 µm

The experimental study of thermal decomposition of hematite ore is described in Chapter 3. The main conclusion is that the thermal decomposition of hematite ore in CO_2 has a sharp weight loss in a short time at high temperatures. A comparison of thermal decomposition and reduction degrees of hematite ore in CO_2 and reducing gases at different temperatures at the residence time of 210 ms is shown in Figure 4.10. The total reduction degrees at different temperatures at 210 ms are given in the figure. The blue bars represent the reduction degree of iron ore caused by thermal decomposition and the orange bars represent the reduction degree of iron ore caused by reduction. According to the experiments, the thermal decomposition degree was not changed by changing the particle residence time in the hot zone of the HTDF. It means that a portion of hematite in the particles decomposed as soon as the particles were exposed in the hot zone of the HTDF. In the first 210 ms, the thermal decomposition of iron ore contributes much more than reduction to the reduction degree of iron ore, especially at low temperatures.

When the residence time is longer than 210 ms, the further reduction degree of iron ore is almost completely caused by reduction because thermal decomposition does not continue in this period (210-2020 ms) according to the results of thermal decomposition. This implies that the initial stage of thermal decomposition contribute significantly to the total pre-reduction degree.

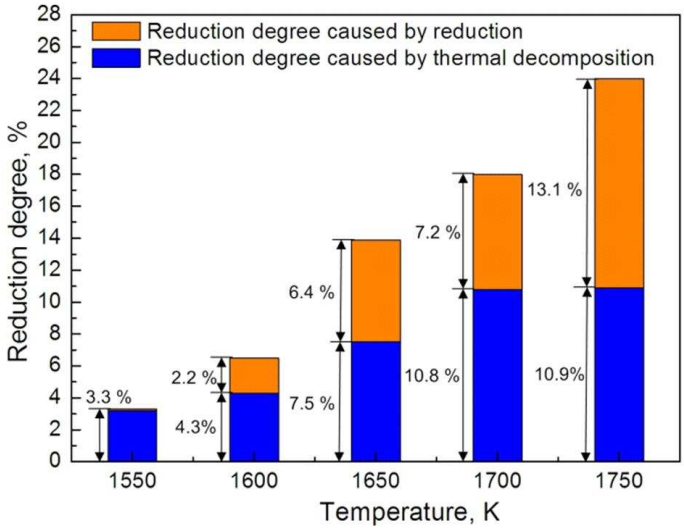

Figure 4.10 Comparison of thermal decomposition degree, reduction degree and total reduction degree of iron ore in the first 210 ms, thermal decomposition in 100 % CO_2, reduction in gas mixture of PCR2' (42.2 % CO + 57.8 % CO_2). Particle size: 45-53 μm

In Figure 4.8, the reduction degree of iron ore at 1750 K keeps constant when the particle residence time is longer than 970 ms and it is slightly lower when the particle residence time is shorter than 970 ms. It indicates that the reduction of iron ore almost reaches the equilibrium state at the current condition when t ≥ 970 ms. This can be confirmed and explained by the Fe-O-C equilibrium diagram as shown in Figure 4.11 made by Biswas [4]. This diagram gives the equilibrium weight percentage of oxygen (wt% O) in wüstite which varies with CO content in the gas and temperature as well as the equilibrium line of Boudouard reaction. According to this study, the reduction degree of iron ore always tends to reach an equilibrium state when the reducing gas has a constant PCR. When the iron oxide is in liquid state above around 1650 K, the equilibrium lines (wt% O) are slightly lower than the values when iron oxide is in solid state. The small deviation can be neglected. The wt% O of 23.2 %, 23.6 %, 24.0 %, 24.4 % and 24.8 % in the diagram were recalculated and converted to reduction degrees of iron ore which are shown in Table 4.5. The CO content in the CO-CO_2 mixture at the vertical axis in the figure is converted to PCR values of the reducing gas. The results in the table directly

present the reduction degree of iron ore as a function of temperature and PCR. For example, if wt% O is 24.8 %, it indicates that the equilibrium reduction degree of iron ore is about 23.26 % based on the conditions that the temperature should be higher than 1320 K and the PCR should be in the approximate range from 70 % to 85 %.

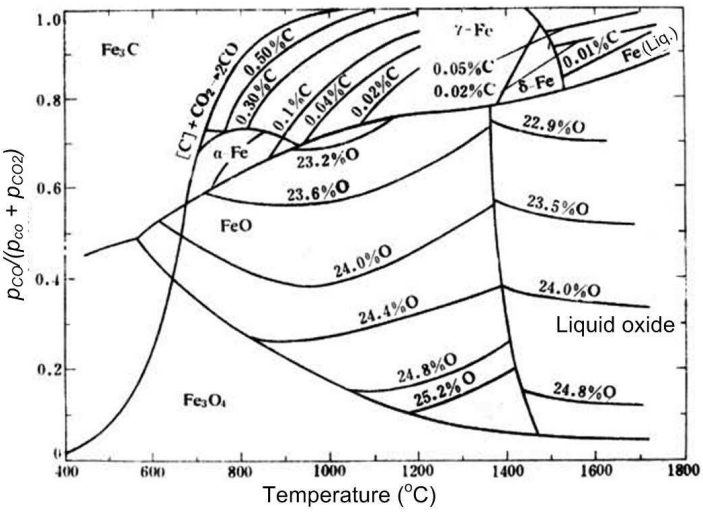

Figure 4.11 Fe-O-C equilibrium diagram including the Boudouard curve as well as degree of oxidation of wüstite in the presence of CO and CO_2 [4]

Table 4.5 Equilibrium reduction degree of iron ore in the field of wüstite

wt% O	PCR, %	T, K	R, %
24.8	70-85	> 1323	23.3
24. 4	60-70	> 1073	24.9
24.0	52-64	> 923	26.5
23.6	43-59	> 953	28.1
23.2	36-55	> 1173	29.7
This study	57.8	1750	26.6

The kinetics study shows that the time for reaching the equilibrium state of reduction becomes shorter and shorter as the temperature increases which can be clearly seen in Figure 4.8. When the PCR of the reducing gas is 57.8 % and the temperature is equal to or higher than 1550 K, the equilibrium wt% O in the final

product would be between 23.6 % and 24.0 %. Therefore, the equilibrium reduction degree of iron ore would be between 26.5 % and 28.1 %. In this study, the reduction degree of iron ore reaches the equilibrium point (26.6 %) in 970 ms at 1750 K (as shown in Figure 4.8). The obtained equilibrium reduction degree of 26.6 % is just in the range of 26.5-28.1 %. Apparently at 1700 K, the reduction degree of iron ore almost reaches the equilibrium state when the residence time is 2020 ms, while the results are far below 26.6 % in 2020 ms at the temperatures lower than 1700 K. The current experimental results are in close agreement with the study of Biswas [4].

4.5.2 Phase changes in the hematite ore

The phase changes from hematite, magnetite, wüstite to metallic iron in the partially reduced iron ore sample contain important information for understanding the reduction mechanism, which could be detected by the technique of XRD. A series of the selected experiments shown in Figure 4.8 were tested by XRD and the XRD patterns are give in the Appendix I. For each temperature, three experiments were selected: t = 210 ms, t = 970 ms, and t = 2020 ms. Semi-quantitative analysis of iron oxides was also obtained by XRD and shown in Table 4.6. X-ray diffraction is often used to semi-quantitatively determine the weight fraction of constituents. By comparing the integrated intensities of the diffraction peaks from each of the known phases, their fraction can be identified. In addition, complex mixtures containing more than two phases also can be quantified. The accuracy of the results is not very high, but the compositions could be compared for one sample relative to the others.

From the figures in APPREDX I and the Table 4.6, it is concluded that the phase of Fe_2O_3 coexists with the phases of Fe_3O_4 and FeO in the partially reduced samples at 1600 K and 1650 K (the gray part in Table 4.6). At 1550 K, the phase of FeO in the partially reduced sample is small and less than 3 %. At 1700 K and 1750 K, the phase of Fe_2O_3 in the partially reduced sample is small and less than 3 %. The phases less than 3 % by semi-quantitative analysis also show weak signal in the pattern of XRD. The composition of the iron ore sample can be calibrated by the analysis of chemical titration as shown in Table 4.6. The analysis by chemical titration also has its advantages and disadvantages. The chemical titration is helpful to obtain the accurate reduction degree of iron ore. However, for the estimation of composition of iron ore, it was based on the assumption that the partially reduced iron ore is only composed of two phases: Fe_2O_3 and Fe_3O_4 or Fe_3O_4 and FeO. As that the iron oxide of Fe_3O_4 can be seen as $FeO{\cdot}Fe_2O_3$ all the Fe^{2+} is assumed in the phase of Fe_3O_4 at low reduction degree, and then the quantity of Fe^{3+} in Fe_3O_4 can be calculated. The rest of the Fe^{3+} is assumed in the form of Fe_2O_3. In this case, the iron ore is composed of Fe_2O_3 and Fe_3O_4. At high reduction degree, it assumes that all the Fe^{3+} is in the phase of Fe_3O_4 and the

quantity of Fe^{2+} in Fe_3O_4 can be obtained. The rest of the Fe^{2+} is in the form of FeO. In this case, the iron ore is composed of Fe_3O_4 and FeO. Therefore, the calculation method with the results of chemical titration is capable to provide more accurate results when the partially reduced iron ore has indeed only two phases or the third phase is so small that it could be ignored according to the XRD results. If the sample has three phases simultaneously: Fe_2O_3 Fe_3O_4 and FeO, the calculation method by chemical titration is meaningless like results shown in the gray part in Table 4.6. For the samples with two phases or the third phase is quite small, the results from chemical titration are much closer to the real values than semi-quantitative analysis.

Table 4.6 Determination of phases in the reduced iron ore samples by XRD and chemical titration (XRD: Semi-quantitative results; CT: Chemical Titration results)

Time (ms)	Phase	Composition (wt %) of the sample at each temperature									
		1550 K		1600 K		1650 K		1700 K		1750 K	
		XRD	CT	XRD	CT	XRD	CT	XRD	CT	XRD	CT
2020	Fe_2O_3	40	33	6	0	0	0	0	0	0	0
	Fe_3O_4	57	67	76	83	44	54	15	38	2	33
	FeO	3	0	17	16	56	46	85	61	98	66
970	Fe_2O_3	60	56	21	8	1	0	1	0	1	0
	Fe_3O_4	39	44	74	91	65	64	33	50	4	33
	FeO	1	0	5	0	34	36	65	50	95	66
210	Fe_2O_3	71	71	53	42	16	0	2	0	1	0
	Fe_3O_4	28	28	45	57	68	87	62	70	27	43
	FeO	1	0	2	0	16	12	37	29	72	56

At 1550 K, a small amount of FeO was generated in all cases. The wt% FeO was only 3 % when the residence time was 2020 ms. It indicates that the main reaction was the reduction from Fe_2O_3 to Fe_3O_4. The decrease of residence time caused the obvious decrease of the generation of Fe_3O_4. At 1600 K, the reduction from Fe_2O_3 to Fe_3O_4 and the reduction from Fe_3O_4 to FeO took place simultaneously when the residence time was longer than 970 ms, while the main reduction from Fe_2O_3 to Fe_3O_4 took place below 970 ms and only a small amount of FeO was generated. The temperature of 1650 K is the other key point. When the residence time was 2020 ms, all the Fe_2O_3 was reduced to Fe_3O_4 and FeO. The wt% Fe_2O_3 was only 1 %, when the residence time was 970 ms. Therefore, at 1650 K, when the residence time was longer than 970 ms, the reduction from Fe_3O_4 to FeO was the main reaction, but when the residence time was lower than 970 ms, the two transitions took place at the same time. At 1700 K and 1750 K, Fe_2O_3 was almost completely reduced to Fe_3O_4 and Fe_3O_4 was partially reduced to FeO in 210 ms.

At the current experimental conditions, the reduction still takes place from hematite to magnetite at 1550 K and there is almost no wüstite generated in the sample

when the residence time is in the range of 210-2020 ms. At 1700 K and 1750 K, the reduction takes place from magnetite to wüstite and the reduction from hematite to magnetite is almost finished within 210 ms. However, at 1600 K when the residence time is longer than or equal to 970 ms and at 1650 K when the residence time is longer than or equal to 210 ms, the reductions from hematite to magnetite and from magnetite to wüstite take place simultaneously. In other words, there are three iron oxides phases in the sample. Combining the reduction degree results in Figure 4.8, it indicates that to achieve 20 % reduction degree in the smelting cyclone of HIsarna process, the average temperature in the reactor should be higher than 1700 K.

4.5.3 Morphological and structural changes during reduction

4.5.3.1 Morphology of reduced particles

The melting behaviour of iron ore particles in the smelting cyclone was the other important aspect which was paid close attention to by people. In this study, the morphology study of the partially reduced particles has been carried out to observe the melting behaviour of the iron ore fines at different temperatures.

The morphology of the reduced particles was mainly observed with the optical microscope and some samples were also selected and investigated with SEM. The particles were scattered uniformly on a tape for optical observation and on a brass sample holder for SEM analysis. Figure 4.12-4.14 (with optical microscope) show the appearances of collected partially reduced ore particles at different temperatures 1550-1750 K. In order to give a comprehensive analysis results, the selected samples for morphology study are from the same experiments with the samples tested by XRD except the three samples in Figure 4.13 (e)-(g), because the melting behaviour of iron ore is directly relevant to phase changes in the particle. It is obvious that the particles almost keep their original shape when the temperature is 1600 K or lower as shown in Figure 4.12. At 1650 K as shown in Figure 4.13 (a)-(c), when the particles experienced a reaction time of 210 ms, the particles still maintain their original shape. However, when the reaction time was longer than 970 ms, a small part of particles were melted down and turned to a spherical shape. Furthermore, when the experimental temperature was increased to 1700 K as shown in Figure 4.14 (a)-(c), a number of particles were still not melted down in the residence time of 210 ms, but for the longer residence times almost all particles were melted down completely. At 1750 K as shown in Figure 4.14 (e)-(g), all the particles were melted down in all studied residence times.

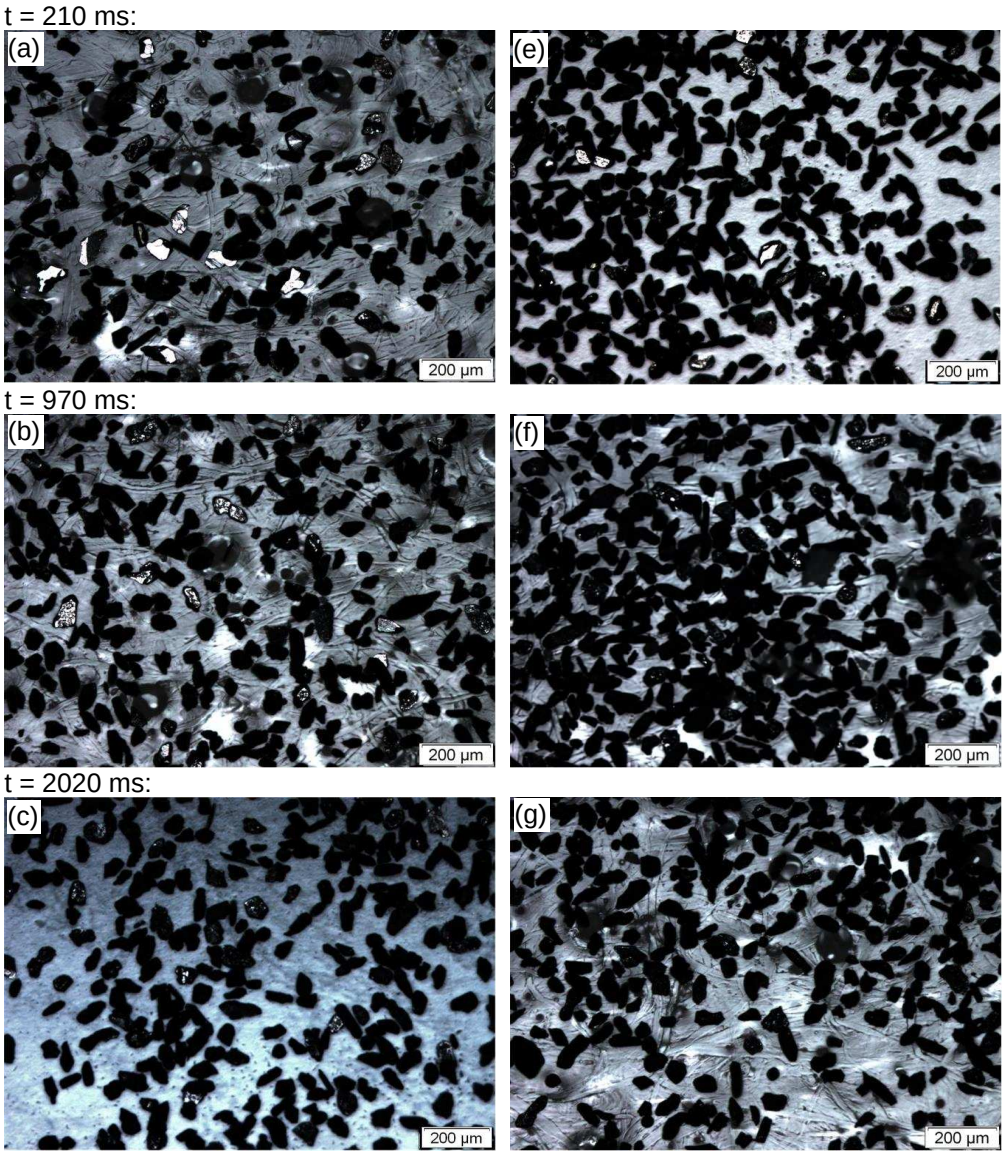

Figure 4.12 Overview of the iron ore particles reduced in the gas PCR2' (42.2 % CO + 57.8 % CO_2); (a), (b), (c): T = 1550 K; (e), (f), (g): T = 1600 K

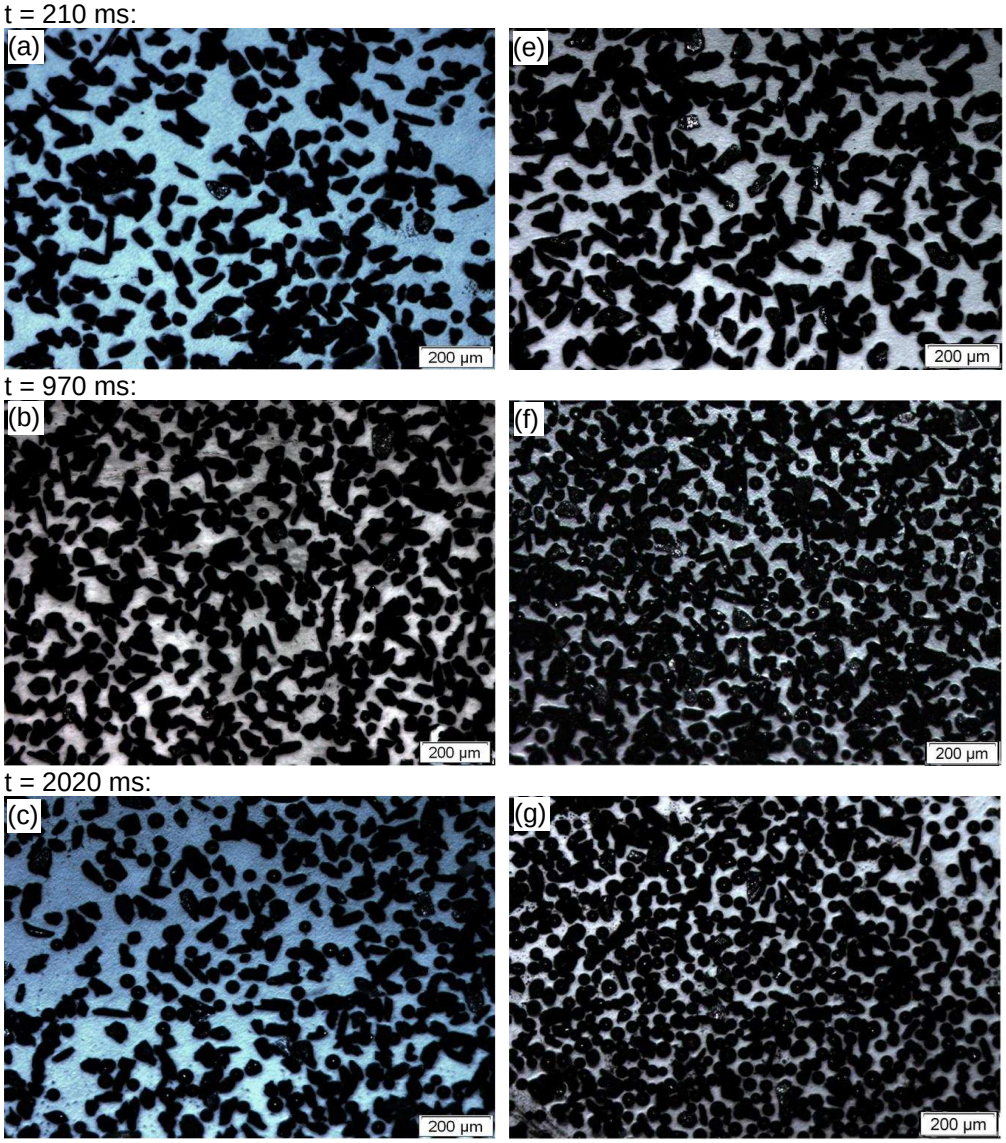

Figure 4.13 Overview of the iron ore particles reduced at 1650 K; (a), (b), (c): gas PCR2' (42.2 % CO + 57.8 % CO_2); (e), (f), (g): gas PCR1' (61.1 % CO + 38.9 % CO_2)

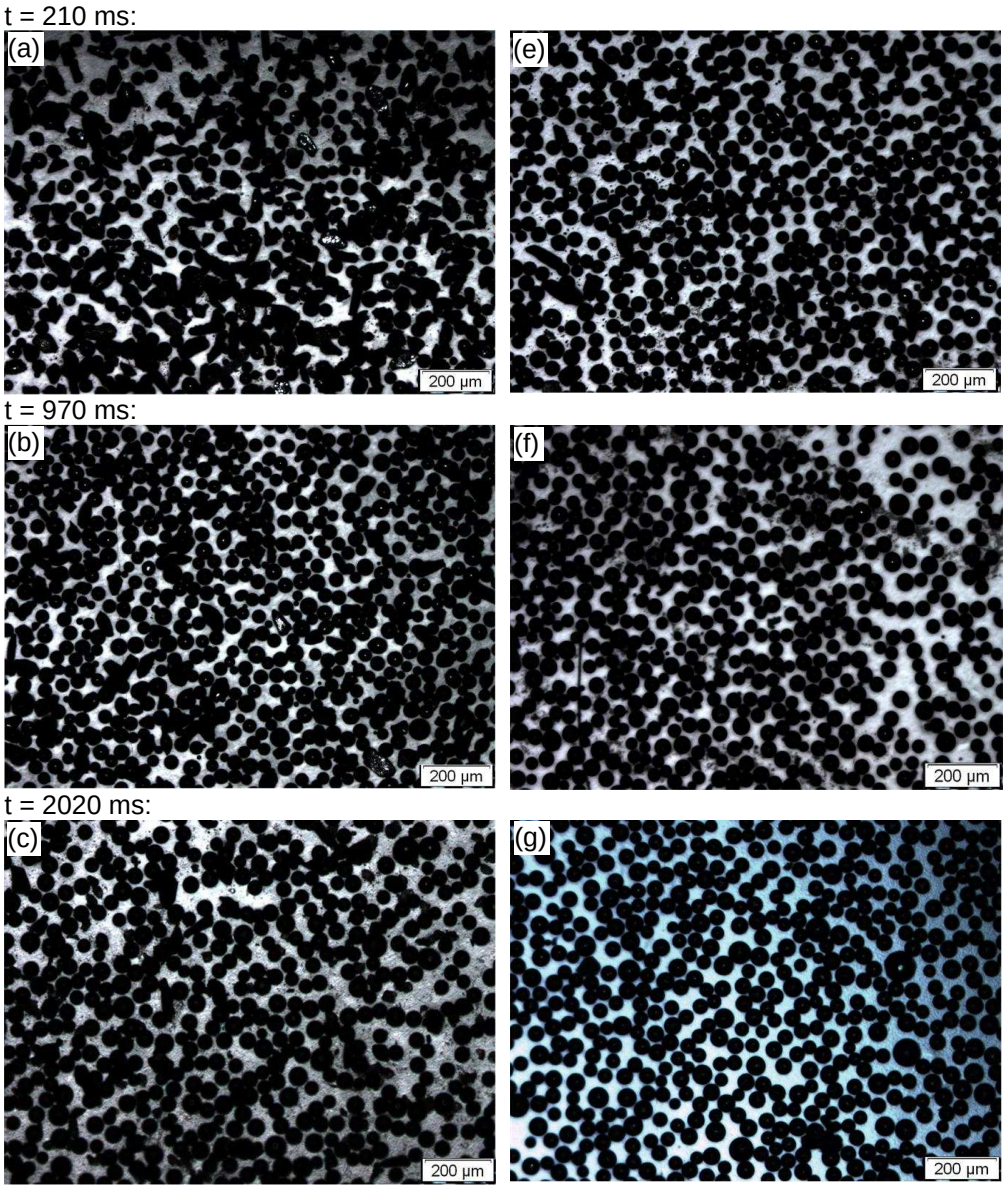

Figure 4.14 Overview of the iron ore particles reduced in the gas PCR2' (42.2 % CO + 57.8 % CO_2); (a), (b), (c): T = 1700 K; (e), (f), (g): T = 1750 K

The temperature of 1650 K is a turning point of the morphological changes of partially reduced particles. Therefore, it is necessary to have more insight into the reduction mechanism at this temperature. Figure 4.13 (a)-(c) give the sample

reduced in the gas mixture with higher PCR (57.8 %), while Figure 4.13 (e)-(g) give the sample reduced in the gas mixture with lower PCR (38.9 %). The number of molten particles in Figure 4.13 (g) is much more than that in Figure 4.13 (c). The same phenomenon is also found in the gas mixture of CO, H_2, CO_2 and N_2. The ratio of molten particles in the collected samples at 1650 K is not only dependent on residence time but also related to gas composition. Through further analysis, it is found that the reduction degree is higher in low PCR gas as discussed previously, and it means that more FeO is generated in the particles. On the other hand, if we integrate this phenomenon with the results in Table 4.6, the temperature of 1650 K is also a turning point of the contents of the iron oxides. The reduced iron ore sample is composed of Fe_2O_3, Fe_3O_4 and FeO in the short reaction time 210 ms. However, the sample is composed of Fe_3O_4, FeO and a small part of Fe_2O_3 in the reaction time 970 ms and there is almost no Fe_2O_3 when the reaction time is longer than 970 ms. The molten particles just appear at the moment of the disappearance of Fe_2O_3. Above all, no matter at what temperatures (1650-1750 K) or in what reducing gas compositions (PCR = 38.9 %, 58.7 %, 80.4 %), it can be concluded that the ratio of the molten iron ore particles is proportional to the low melting FeO content in the partially reduced sample as long as Fe_2O_3 is exhausted.

According to Fe-O diagram (in Figure 1.10) [5], the melting point of pure Fe_2O_3 is about 1838 K, the melting point of pure Fe_3O_4 is about 1870 K and the melting point of FeO is about 1644 K which is the lowest one. The diagram focuses on the type and state of phases as a function of temperature. It shows that the liquidus temperature of the FeO-Fe_3O_4 mixture is from the melting point of FeO 1644 K to the melting point of Fe_3O_4 1870 K and decreases with the increase of the FeO content. This is also the explanation why at 1700 K when the particle residence time is equal to or longer than 970 ms and at 1750 K for all studied residence times, almost all particles were melted down completely even though the content of Fe_3O_4 was still high in the sample. As the individual particles characterized by size, porosity and even composition are different from each other. Therefore, it was not surprise to see that not all the particles were melted down completely in one sample. The composition of the raw materials and the reduced samples we obtained was an average value of a number of particles from one sample.

4.5.3.2 Morphology of a single particle

During the reduction of iron ore fines, morphological and phase changes in particles have a significant influence on the rate of reduction. In order to obtain the details of the reaction, it is essential to focus on a single particle for the observation of its surface and internal structure (through polished sections). Firstly, the images of the surface of the unreduced particles were taken by optical microscopy and SEM as shown in Figure 4.15. It can be seen that the particle has an irregular shape and its surface looks smooth and bright under the light optical microscope.

The image from the SEM further reveals the topography of the particle which has a smooth and close-grained structure.

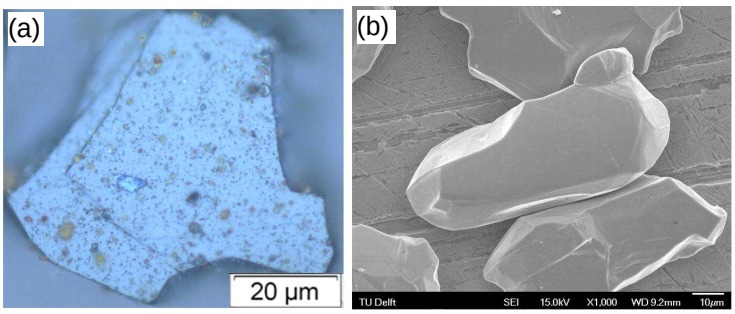

Figure 4.15 Morphological observations of unreduced particle, (a) by optical microscope, (b) by SEM

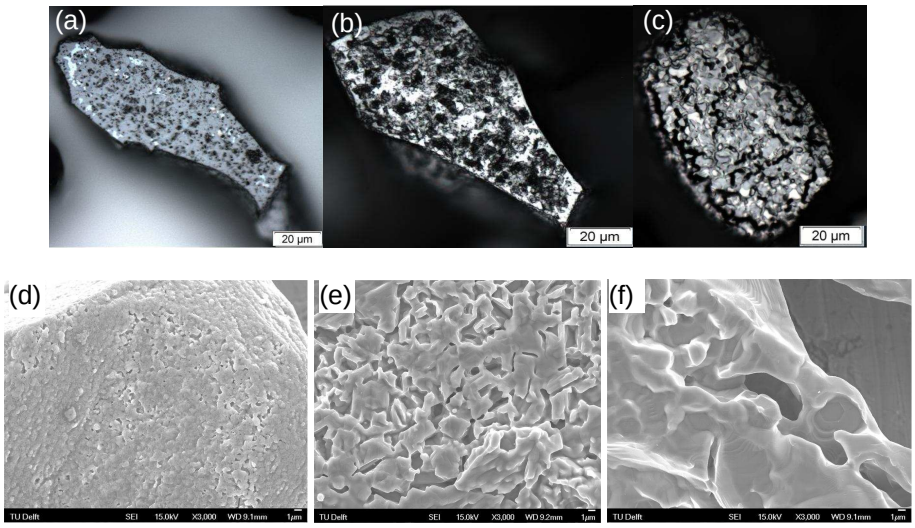

Figure 4.16 Morphological observations of reduced particle at different temperature by optical microscope and SEM, optical microscope: (a) T=1550 K, (b) T=1600 K, (c) T=1650 K; SEM: (d) T=1550 K, (e) T=1600 K, (f) T=1650 K

However, the surface of the reduced particles has a different appearance. Figure 4.16 gives the morphological change of the particles' surface experienced at different temperatures: T=1550 K, T=1600 K and T=1650 K. The residence time of the selected samples shown in the Figure 4.16 was 970 ms. The images (a)-(c) in Figure 4.16 were taken with optical microscope for the entire particles. It can be found that with the increase of temperature, the surface of the reduced particles

becomes coarser and coarser. Big pores can be observed on the particle when the experimental temperature is 1650 K. The magnified images for the part of particles were taken by SEM as shown in Figure 4.16 (d)-(e). The particles were from the same experiment with the particles in (a)-(c), but they were not the same particles. The magnification of the images is 3000x revealing the details of 1 µm. There are not many pores on the particle at the temperature of 1550 K, but the particle already has a rough surface. The size of the micro pores which are formed at 1600 K is smaller than the micro pores which are formed at 1650 K.

At 1700 K and 1750 K, the particles experienced not only reduction but also melted in the hot zone of the HDTF and formed a perfectly spherical shape. The reduction degree of iron ore goes up with the increase of temperature and residence time. For that all the spherical particles produced both at 1700 K and 1750 K have the same appearance, one example at 1750 K is given in Figure 4.17. The details of the surface of the spherical particle are difficult to be photographed by optical microscope as shown in Figure 4.17 (a). However, the SEM can produce very high-resolution images of a sample surface. Due to the very narrow electron beam, SEM micrographs have a large depth of field yielding a characteristic three-dimensional appearance helpful for understanding the surface structure of the particle. There are still a lot of micro pores with a dense distribution on the spherical reduced particles. But the size of the micro pores is much smaller than that shown in Figure 4.16 due to the melting down of the particle.

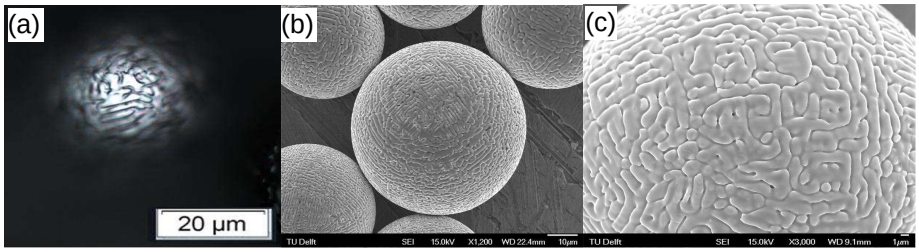

Figure 4.17 Morphological observations of spherical reduced particle at T =1750 K, (a) by optical microscope, (b) by SEM 1200x, (c) by SEM 3000x

The micro pores were formed due to the generation of magnetite and wüstite phases, the loss of oxygen and the particle melting. From the analysis by chemical titration and XRD, it is clear that the main phases in the reduced particle are hematite and magnetite at 1550 K and 1600 K. The main phases are magnetite and wüstite at 1650 K, 1700 K and 1750 K. From Figures 4.15-4.17, it can be found that the micro pores are formed during the chemical reactions and the melting process in iron ore particles. At 1550 K and 1600 K, the micro pores were formed due to the normal swelling that comes from the crystal structure difference between the starting hematite and the formed magnetite. The crystal structure of hematite is close-packed hexagonal while for the magnetite it has an inverse spinal structure.

At 1650 K, 1700 K and 1750 K, reduction rates were higher than that at 1550 K and 1600 K. Hematite was exhausted and magnetite was further converted to wüstite which became the main composition of the partially reduced iron ore particle. Wüstite has an isometric-hexoctahedral crystal structure. Moreover, the liquidus temperature of FeO-Fe_3O_4 mixture moved to the melting temperature of FeO. Therefore, melting process occurred along with the reduction. Finally, the spherical particles were formed after melting down as shown in Figure 4.17. Above all, the morphology of the iron ore particle changes gradually with the increase of reduction degree at high temperatures.

4.5.3.3 Internal structure and phase distribution in a single particle: analysis with optical microscope

The internal structural changes and the phase distribution in a single particle are very important for finding out the reduction mechanism of iron ore. The samples were prepared by putting the particles in a mounting cylinder together with an appropriate amount of resin, and then the samples were polished by the polishing machine. The polished sections of individual particles were observed under the optical microscope. The details of the reduced particles are shown in Figures 4.18-4.22. At 1550 K and 1600 K as shown in Figures 4.18-4.19, topochemical growth of magnetite was found in the individual particles. Combining the results of XRD in Table 4.6, it can be seen that the light areas are the phases of hematite and the dark areas are the phases of magnetite. The light areas decrease with the increase of residence time and temperature. The reduction of hematite to magnetite takes place at a shrinking core interface of the two phases. When temperature was higher than 1600 K, the samples obtained a higher reduction degree and the particles started to present a uniform colour. It means that all hematite was reduced to magnetite and wüstite.

Furthermore, from Figures 4.18 to 4.22, it is found that micro pores generated not only at the surface of particles as shown in Figure 4.15-4.17, but also penetrated into the inner area and core during the reduction process. At the low temperature of 1550 K, the micro pores were formed inside the particle but not too much. The obvious micro pores were formed when the temperature is above 1600 K. At 1650 K and 1700 K, the spherical particles with the big voids in the central part of the particle were generated as shown in Figure 4.21. The voids tended to disappear above 1750 K with the increase of residence time due to melting and generated wüstite. The small size of micro pores distribute uniformly inside the particle as shown in Figure 4.22 (c). It seems that the big voids are composed of a large amount of micro pores or has a phase different from the ring area. The details about the voids in the spherical particles were studied by SEM-EDS in the following part. The formation of micro pores during the reduction process greatly facilitates the diffusion of reducing gases from the outer surface of the particle to the reaction interface.

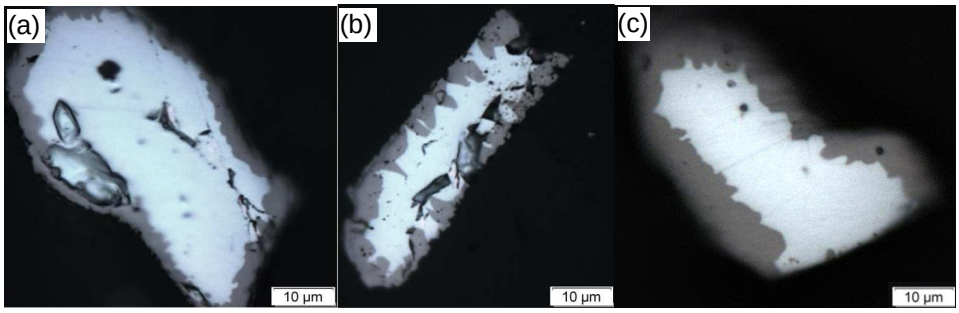

Figure 4.18 Example of polished section of fine iron ore particle at 1550 K, (a) t = 210 ms; (b) t = 970 ms; (c) t = 2020 ms

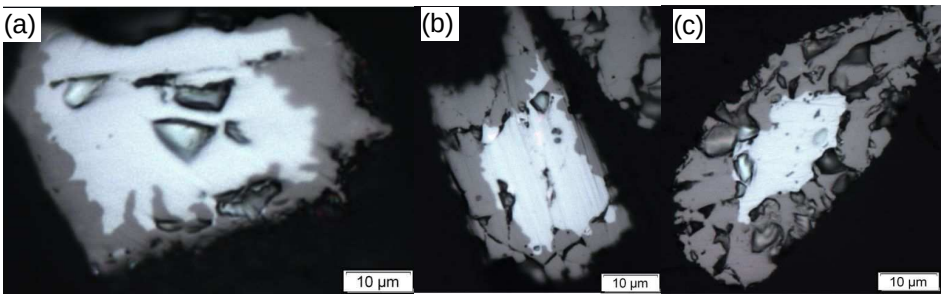

Figure 4.19 Example of polished section of fine iron ore particle at 1600 K, (a) t = 210 ms; (b) t = 970 ms; (c) t = 2020 ms

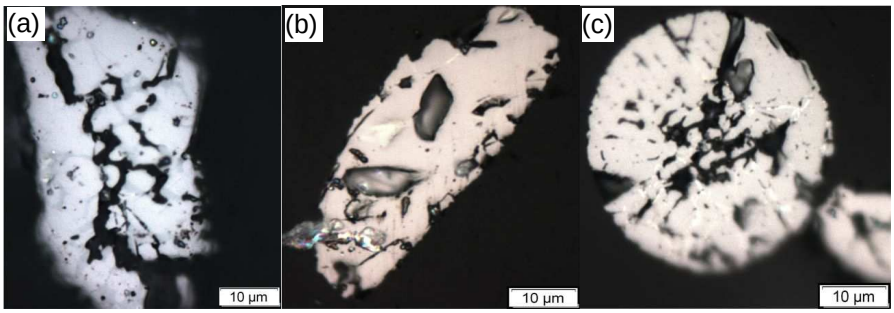

Figure 4.20 Example of polished section of fine iron ore particle at 1650 K, (a) t = 210 ms; (b) t = 970 ms; (c) t = 2020 ms

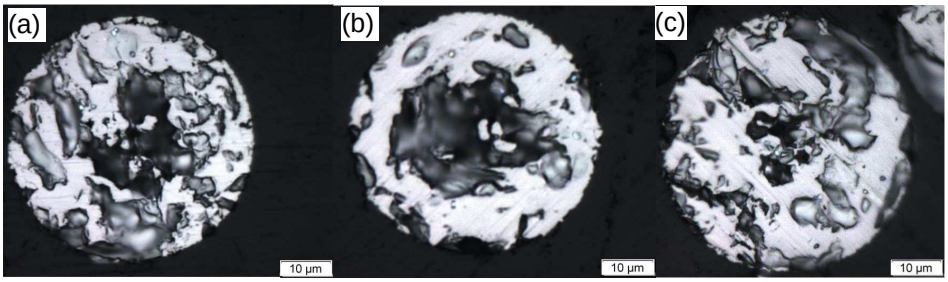

Figure 4.21 Example of polished section of fine iron ore particle at 1700 K, (a) t = 210 ms; (b) t = 970 ms; (c) t = 2020 ms

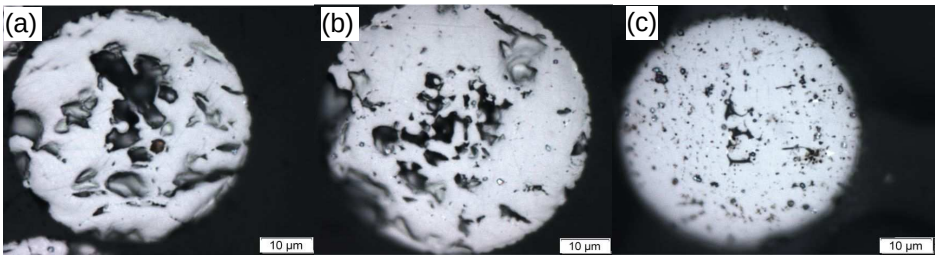

Figure 4.22 Example of polished section of fine iron ore particle at 1750 K, (a) t = 210 ms; (b) t = 970 ms; (c) t = 2020 ms

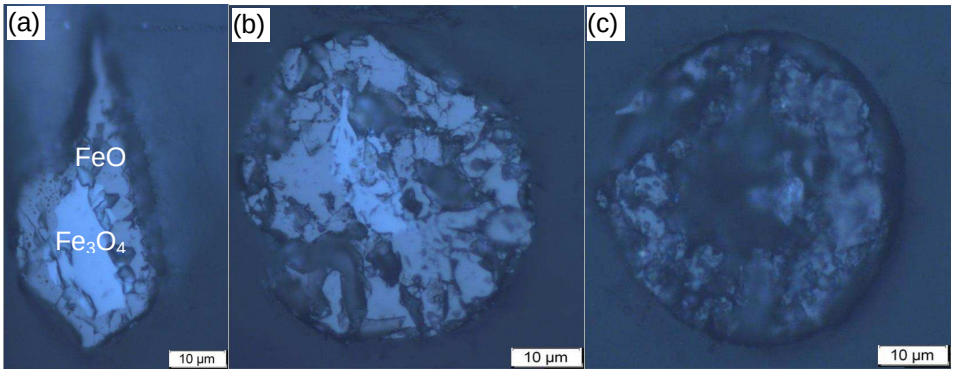

Figure 4.23 Example of optical micrograph of polished section of etched iron ore particle, (a) T= 1650 K; b) T = 1700 K; (c) T = 1750 K

The optical distinction of solid reactant and product phases is quite easy for hematite and magnetite, but the difference between magnetite and wüstite is not clear and the samples had to be etched with an etching solution of a mixture of HCl and ethanol. Three examples are given in Figure 4.23 which shows the etched iron

ore particles reduced in the gas mixture of PCR2' (42.2 % CO + 57.8 % CO_2) and the particle size was in the range of 45-53 µm. The reaction time was 970 ms. It is found that the unreacted shrinking core exists in irregularly shaped particles and in a part of spherical particles. The size of the unreacted core (magnetite) of the individual particles is different depending on their own reduction degree, and becomes smaller with a longer residence time and higher temperature. For example, at 1650 K and 1700 K, after 30 s etching time, the wüstite was heavily attacked the etching solution. Wüstite generated by topochemical growth could be identified in the partial reduced particles. In Figure 4.23 (c), an etched spherical iron ore particle reduced at 1750 K shows nearly complete conversion to wüstite. The results are in agreement with the chemical and XRD analysis shown in Table 4.6.

4.5.3.4 Structural changes and phase distribution in a single particle: analysis with SEM-EDS

The analysis of structural changes of the partially reduced particles by optical microscope shows that an unreacted core was formed during the reduction process. Energy Dispersive Spectroscopy (EDS) of a sample allows one to identify what the particular elements and their relative proportions are. In this study, the EDS results were used to identify the phases on the polished sections of particles in order to confirm the conclusion above by optical microscopy. The analysis of the original hematite ore by EDS is shown in Figure 4.24 and it shows that the Fe element distributes uniformly with a value between 67.4-68.9 wt% on the polished section. Figure 4.25 shows the iron element contents in the polished section of a particle reduced at 1650 K with the gas mixture of PCR2' (42.2 % CO + 57.8 % CO_2) for 2020 ms. It shows clearly that the concentration of Fe element at the core area is lower than that at the ring area of the polished section. It reflects the unreacted shrinking core mechanism and the details of this mechanism have been described in Chapter 1.

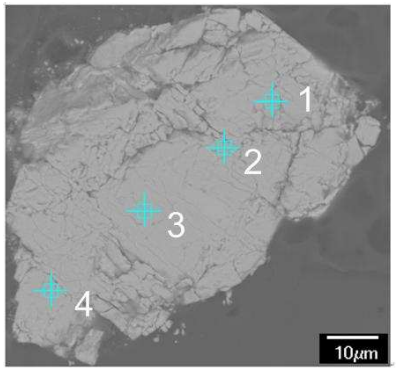

Point	Fe (wt%)
1	67.42
2	68.84
3	67.93
4	68.06

*Weight %

Figure 4.24 Distribution of Fe element at the polished section of the unreduced particle: characterised by EDS

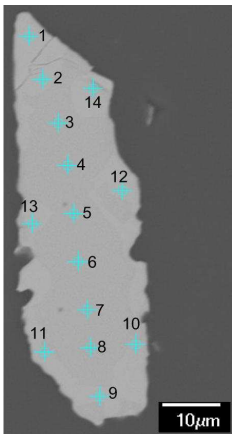

Point	Fe (wt%)	Point	Fe (wt%)
1(ring)	80.26	8(ring)	80.65
2(ring)	80.21	9(ring)	80.68
3(ring)	80.14	10(ring)	81.36
4(core)	78.63	11(ring)	82.97
5(core)	78.66	12(ring)	82.16
6(core)	78.79	13(ring)	80.18
7(ring)	80.51	14(ring)	80.88

*Weight %

Figure 4.25 Distribution of Fe element at the polished section of the particle reduced at 1650 K: characterised by EDS

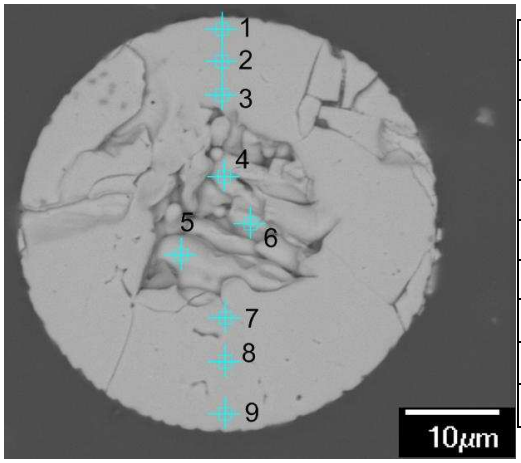

Point	Fe % (wt%)
1(ring)	81.30
2(ring)	82.06
3(ring)	83.67
4(core)	76.89
5(core)	76.05
6(core)	77.87
7(ring)	82.52
8(ring)	82.04
9(ring)	83.00

*Weight %

Figure 4.26 Distribution of Fe element at the polished section of the particle reduced at 1700 K: characterised by EDS

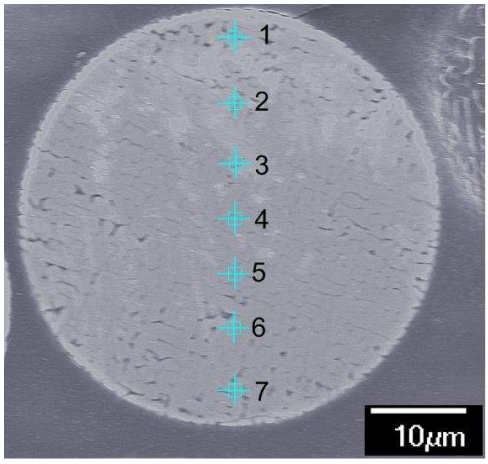

Point	Fe (wt%)
1	82.77
2	82.01
3	82.02
4	81.99
5	81.95
6	82.25
7	81.60

*Weight %

Figure 4.27 Distribution of Fe element at the polished section of the particle reduced at 1750 K: characterised by EDS

Figure 4.26 gives distribution of Fe element at the polished section of the particles reduced at 1700 K, and Figure 4.27 gives similar results at 1750 K. The reaction time of the two particles was 2020 ms. The particles were reduced in the gas mixture, in which PCR equals 57.8 % (PCR2'). At 1700 K, the voids observed by optical microscope at the centre of the particle can be seen clearly by SEM. The weight percentage Fe element at the bottom of the voids (centre area) is significantly lower than in the ring area. In other words, the phase in the voids is different from the phase in the ring area. Combining the above analysis, it can be

concluded that the phase in area of the voids is Fe_3O_4 and the phase in the ring area is FeO. The phenomenon confirms the topochemical growth of wüstite once again. Therefore, the transformation from magnetite to wüstite takes place at the interface between the two phases.

The morphological changes of the very fine iron ore particles during the high temperature reduction process have significant effect on the reaction kinetics. The morphology study is helpful for the construction of the kinetic model of the heterogeneous gas-solid or gas-liquid reactions. Although the fine iron ore particles are smaller than 90 µm, the unreacted shrinking core model is still suitable at the studied experimental conditions. The kinetic modelling is described in chapter 5.

4.6 Conclusions

In order to obtain more details of the iron ore reduction mechanism in the smelting cyclone of the HIsarna process, the reduction kinetics of the individual particles of fine iron ore has been investigated in the HDTF. The experiments have been carried out at different temperatures, in different reducing gas compositions and with different particle sizes. The studied temperature ranged from 1550 K to 1750 K. The post combustion ratio - PCR of the reducing gas is set to 38.9 %, 57.8 % and 80.4 %. The main experiments focused on the particle size of 45-53 um because it is close to the average particle size used in the smelting cyclone. The experimental results reveal the reduction behaviour individual iron ore particles at high temperatures.

From the thermodynamic point of view, the PCR of reducing gas and reaction temperature determine the final state of partially reduced iron ore.

- In the studied PCR values and temperatures, the maximum reduction degree is approximately in the range of 23-30 %.

- In the studied PCR values and temperatures, the final state of partially reduced iron ore can be both solid and molten particle, which depends on how much wüstite is produced in the sample.

From the kinetics point of view, the rate of iron ore reduction is dependent on temperature, gas composition, and particle size.

- The fine iron ore particles could achieve a 20 % reduction degree at a proper temperature and in a suitable gas composition. The reduction degree increases with the increase of temperature, while decreases with the increase of PCR and particle size.

- The morphology study by optical microscope shows molten particles appear at 1650 K in the residence time 970-2020 ms, and the partially reduced particles are fully molten at 1700 K in the residence time of 700-2020 ms and in all the studied residence time at 1750 K.

- The unreacted shrinking cores have been observed during the reduction from hematite to magnetite and from magnetite to wüstite. It means that the reaction takes place at the interfaces between the two adjacent phases. From XRD results, it was found that the three phases of hematite, magnetite and wüstite coexisted in one collected sample at 1600 K in the residence times $t \geq 970$ ms and at 1650 K in the residence time $t = 210$ ms. However, there is no evidence shows that the three phases were found in a single particle by the analysis with both optical microscope and SEM-EDS methods.

- A quantity of micro pores could be formed during the reduction process due to the different crystal structures of hematite, magnetite and wüstite. The micro pores largely facilitate the diffusion of gaseous from the outer surface of particle through the product layer to the reaction interface.

- In the first 210 ms, the thermal decomposition of iron ore contributes much more than reduction to the reduction degree of iron ore, especially at low temperatures. When the residence time is longer than 210 ms, the further reduction degree of iron ore is almost completely caused by reduction.

- The experimental study which uses the typical reaction conditions of smelting cyclone in the pilot plant supplies a good reference to the HIsarna process. The experimental results are helpful on determining the temperature range, gas composition and particle size in the smelting cyclone.

References

[1] Crowley, M. S: Hydrogen Silica Reactions in Refractories, Part II, American Ceramic Society Bulletin 49 (1970) 527-530.

[2] Berdnikov, V.I., Gudim, Yu. A. and Karteleva, M.I., Role of the gas phase in the formation of silicon and calcium carbides, Steel in Translation 38 (2008) 957-960.

[3] Komatina, M., Heinrich, W.G.: The sticking problem during direct reduction of fine iron ore in the fludized bed, Metalurgija – Journal of Metallurgy 2004 309- 328.

[4] Anil K. Biswas, Principles of Blast Furnace Ironmaking, Cootha Publishing House, Brisbane Australia, 1981.

[5] McKewan, W.M., Kinetics of iron oxide reduction, Trans. Met. Soc. AIME, 218 (1962), 2-6.

Chapter 5 Kinetic Modelling of Pre-reduction of Iron Ore Particles

5.1 Introduction

The kinetic mechanism of iron ore reduction is essential for understanding and predicting the reduction process in the smelting cyclone of HIsarna process and is necessary to investigate for optimising the operation of the pilot plant. Therefore, a kinetic model has been built based on the experimental results at the typical operating conditions (particle size: 45-53 µm; Post combustion ratio (PCR): 57.8 %; temperature: 1550-1750 K) in the smelting cyclone, and then the individual rate steps involved in the reaction are discussed to access the rate controlling step to the overall reaction.

The methods used to study iron ore reduction kinetics can be generally grouped into two categories: experimental and computational. The experimental results of morphology study were used to determine the kinetic model, and the computational results were used to determine the rate controlling step and calculate the kinetic data with the experimental results. All the experimental results have been presented in Chapter 4. In order to give a complete story of the kinetic modelling of the iron ore reduction, the main conclusions of morphology study at the typical operating conditions in the smelting cyclone in Chapter 4 are drawn in the following.

The morphology study reveals that the experimental investigation in this study involved both gas-solid particle reduction and gas-molten particle reduction. The gas-solid particle reduction took place at 1550 K, 1600 K in all the studied residence times (210 ms, 700 ms, 970 ms, 1570 ms and 2020 ms) and at 1650 K in the residence times ≤ 970 ms. The molten particles appeared at 1650 K in the residence times > 970, and at 1700 K and 1750 K in all the studied residence times. However, solid partially reduced particles also existed at 1650 K in the residence times 970-2020 ms and at 1700 K in the residence times ≤ 700 ms. Therefore, according to the physical state of the partially reduced particles in the collected sample, the reduction of iron ore was divided into three parts as shown in Figure 5.1: 100 % gas-solid particle reduction, mixed reduction (part of gas-solid reduction and part of gas-molten) and 100 % gas-molten particle reduction.

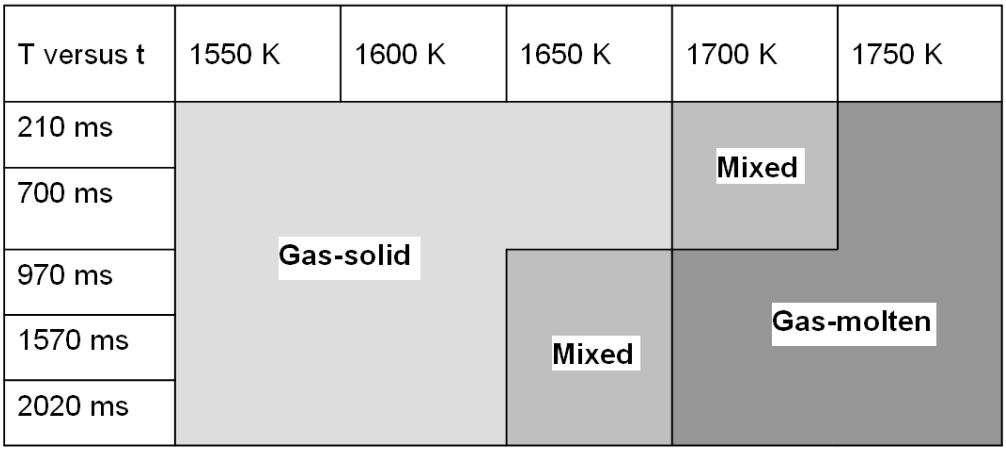

Figure 5.1 Reaction types at 1550-1750 K, particle size: 45-53 µm, reducing gas PCR2' (42.2 % CO + 57.8 % CO_2)

The kinetic model was determined by observing the structural changes inside the partially reduced particles. This method has been widely [1-5] used for the kinetics study of iron ore reduction. In this study, the polished sections of the partially reduced particles of both solid particles and molten particles were observed by optical microscope as shown in Figure 4.18-4.19 and 4.23. The results were confirmed by the measurement with SEM-EDS as shown in Figure 4.25-4.26, which show that the unreacted shrinking core model is applicable for both gas-solid particle reduction and gas-molten particle reduction. It was found that at the temperatures of 1550 K and 1600 K, the peripheral part of hematite particle was reduced to magnetite by reducing gas and the unreacted hematite core remained inside. At the temperature higher than 1650 K, the unreacted core could be observed by etching the partially reduced particle in the diluted hydrochloric acid. In this case, the unreacted core is magnetite phase surrounded by the wüstite phase. Therefore, the reduction of iron ore at the current studied conditions takes place at the topochemical interface of hematite-magnetite or magnetite-wüstite and could be represented by the unreacted shrinking core model.

5.2 Reaction mechanism of iron ore reduction

The details of the reduction kinetics were further studied based on the unreacted shrinking core model. The reduction mechanism of iron ore reduction was obtained and the kinetic data of activation energy and reaction rate constants were

calculated, which could be used for the further mathematical modelling of HIsarna process.

5.2.1 Reduction process

The reduction of hematite takes place in 3 steps at the temperature higher than 843 K according to the Fe-O-C diagram as shown in Figure 4.11. Hematite (Fe_2O_3) is first reduced to magnetite (Fe_3O_4), and then magnetite is reduced to wüstite (FeO), and finally wüstite is reduced to metallic iron. The first two steps ($Fe_2O_3 \rightarrow Fe_3O_4 \rightarrow FeO$) took place in this study and were detected by the analysis with XRD, optical microscope and the chemical titration. According to the XRD results, the three phases of hematite, magnetite and wüstite coexisted in one collected sample at 1600 K in the residence times $t \geq 970$ ms and at 1650 K in the residence time t = 210 ms. However, there is no evidence shows that the three phases were found in a single particle by the analysis with both optical microscope and SEM-EDS methods. It is because that the iron ore particle is so small that hematite is quickly reduced to magnetite before the generation of the wüstite in the particle. Therefore, one interface unreacted shrinking core model was used for describing the reduction behaviour of individual particle. The general knowledge of the unreacted shrinking core model has been presented in Chapter 1 and the special illustration (Figure 5.2) is given here to clarify the reduction process in this study.

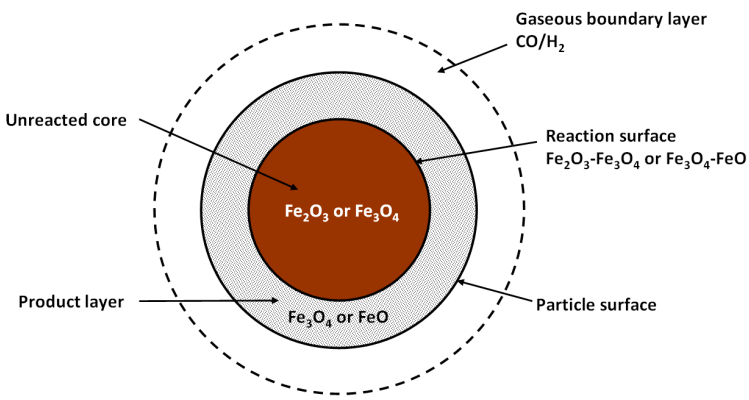

Figure 5.2 Illustration of the unreacted shrinking core model

Generally, in heterogeneous systems, mass transfer (like diffusion from the bulk of the fluid phase towards the interface) and chemical reaction usually proceed in series. If the reaction rate is entirely controlled by the chemical kinetics, the rate is usually called microkinetic. On the other hand, physical phenomena also influence the reaction rate when the diffusion velocity is not much higher than the chemical reaction rate. This reaction rate is usually called macrokinetic, and accounts for

both chemical and physical phenomena [6]. From the point of view of the macrokinetics, iron ore reduction proceeds through the following steps occurring successively during the reaction:

Step 1) Transport of gaseous reactant of CO/H_2 from bulk gas to exterior surface of the iron ore particle through a gaseous boundary layer.
Step 2) Diffusion of gaseous reactant of CO/H_2 through the product layer to the reaction surface hematite-magnetite or magnetite- wüstite.
Step 3) Chemical reduction reaction of iron oxide with CO/H_2.
Step 4) Diffusion of gaseous product (CO_2/H_2O) outward through the product layer.
Step 5) Transport of the gaseous product (CO_2/H_2O) from the exterior surface of the particle to the bulk gas through the gaseous boundary layer.

From the point of view of the microkinetics, the chemical reaction of Step 3) can be interpreted as follows.

Step 3)-(a) Reaction on atomic scale at the interface of hematite-magnetite or magnetite-wüstite:

Hematite-magnetite: $Fe_2O_3 + 3CO = 2Fe^{3+} + 6e^{-1} + 3CO_2$ (5.1)

Magnetite-wüstite: $Fe_3O_4 + 4CO = 2Fe^{3+} + 6e^{-1} + FeO + 4CO_2$ (5.2)

Step 3)-(b) Mass transport of cations (Fe^{3+})and electrons inside the hematite or magnetite matrix along the interfaces of hematite-magnetite or magnetite-wüstite

Step 3)-(c) Nucleation and growth of reaction products at the interfaces of hematite-magnetite or magnetite- wüstite

Hematite-magnetite: $2Fe^{3+} + 6e^{-1} + 8Fe_2O_3 = 6Fe_3O_4$ (5.3)

Magnetite-wüstite: $2Fe^{3+} + 6e^{-1} + 2Fe_3O_4 = 8FeO$ (5.4)

The elementary steps of interfacial chemical reaction of iron oxide reduction have already been proposed by Hayes and Grieveson [7]. Firstly, the reduction gas picks up oxygen and frees the cations and electrons. Then the cations and electrons move inside the hematite or magnetite matrix along the interface. Finally, the nucleation and growth of magnetite or wüstite can take place. The solid state mechanism includes two steps: (Step 3)-(b)) mass transport of cations and electrons inside the matrix along the interfaces and nucleation, and (Step 3)-(c))

growth of reaction products. The mass transport of cations (Fe^{3+}) and electrons inside the hematite or magnetite matrix along the interfaces is also called solid state diffusion. Any step above could be the rate controlling step of iron ore reduction process.

5.2.2 Kinetic analysis

The rate controlling step of the reduction plays an important role in the kinetics analysis, which is the slowest step of the reaction process that determines the rate of the overall reaction. It is very important in deriving the rate equation of the reaction and also very important to the optimization and understanding the reduction process. For the unreacted shrinking core model, the rate controlling step could be either of gaseous diffusion, chemical reaction or mixed control (combination effect of gaseous diffusion and chemical reaction). The rate controlling step has been determined by computational methods including model-fitting method and model-free method, the details of which are given in Chapter 1.

5.2.2.1 Reduction mechanism of gas-solid particle reduction

In this study, firstly, the experimental results of gas-solid reduction (as shown in Figure 5.1: in all the studied residence times at 1550 K and 1600 K, and in the residence time of 210-970 ms at 1650 K) were dealt with model-fitting methods. The mathematical formulations for gaseous diffusion, chemical reaction and mixed control of model-fitting method can be found in Eq.1.41, Eq.1.45 and Eq.1.47. As mentioned in Chapter 1, if the plot of $1 - (1 - R)^{1/3}$ versus t gives a straight line, the rate controlling step is chemical reaction. If the plot of $1 - 2/3R - (1 - R)^{2/3}$ versus t gives a straight line, the rate controlling step is gaseous diffusion. If it is a mixed control, the plot of $t/(1 - (1 - R)^{1/3})$ versus $1 + (1 + R)^{1/3} - 2(1 - R)^{2/3}$ would give a straight line.

The analysis results for gas-solid reduction are shown in Figure 5.2-5.4. The correlation coefficients of each plot are given in Table 5.1, which are used elsewhere [5, 8] to help to judge linear relationship of the kinetic plots. From the results in the figures and table, it found that the kinetic plots of chemical control at the three temperatures have the best linear relationship compared to gaseous diffusion control and mixed control. Therefore, the rate controlling step of gas-solid particle reduction is the chemical reaction control.

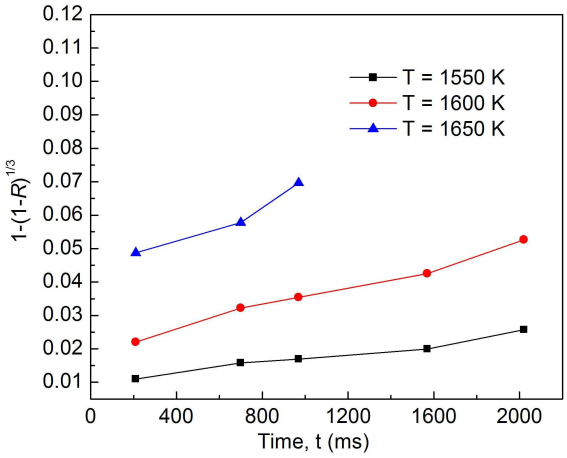

Figure 5.2 kinetic plots of chemical control of gas-solid reduction, particle size: 45-53 µm, reducing gas PCR2' (42.2 % CO + 57.8 % CO_2)

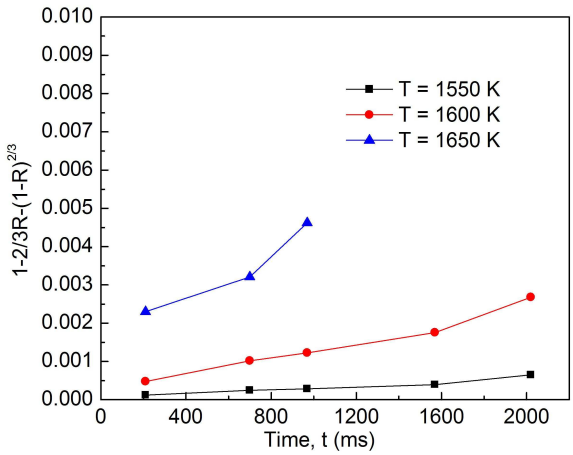

Figure 5.3 kinetic plots of gaseous diffusion control of gas-solid reduction, particle size: 45-53 µm, reducing gas PCR2' (42.2 % CO + 57.8 % CO_2)

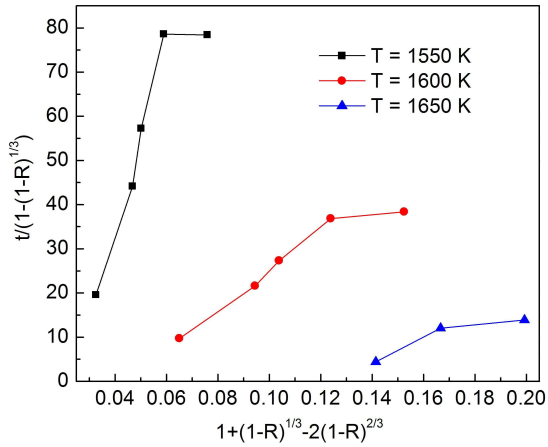

Figure 5.4 kinetic plots of mixed control of gas-solid reduction, particle size: 45-53 µm, reducing gas PCR2' (42.2 % CO + 57.8 % CO_2)

Table 5.1 Correlation coefficients of the kinetic plots for gas-solid reduction (particle size: 45-53 µm, reducing gas PCR2' (42.2 % CO + 57.8 % CO_2))

T (K)	Chemical control	Diffusion control	Mixed control
1550	0.9832	0.9667	0.9171
1600	0.9921	0.9840	0.9594
1650 (0-970 ms)	0.9720	0.9560	0.9162

The reaction rate constants (*k*) were further calculated based on the rate controlling step from the slopes of the plots. The straight plots of $1 - (1 - R)^{1/3}$ versus *t* are drawn with least square method. From the experimental results of particle composition analyzed by chemical titration and XRD method, the collected samples have three iron oxides especially at 1600 K in the residence time of 970-2020 ms and at 1650 K in the residence 0-210 ms (Table 4.5). It is difficult to study the two reduction steps respectively: from hematite to magnetite and from magnetite to wüstite, due to the very fast reaction rate. Therefore, the calculated reaction rate constants at the three temperatures are the average reaction rate constants of the iron ore reduction in the studied residence times. The results of gas-solid reduction are shown in Figure 5.5. It shows that the reaction rate constant goes up with the increase of temperature. At 1550 K, the result is $k = 0.75 \times 10^{-2}\ s^{-1}$. The value turns to more than twice at 1600 K, where $k = 1.60 \times 10^{-2}\ s^{-1}$. At 1650 K the reaction rate constant $k = 2.67 \times 10^{-2}\ s^{-1}$ are more than 3 times as big as the result at 1550 K.

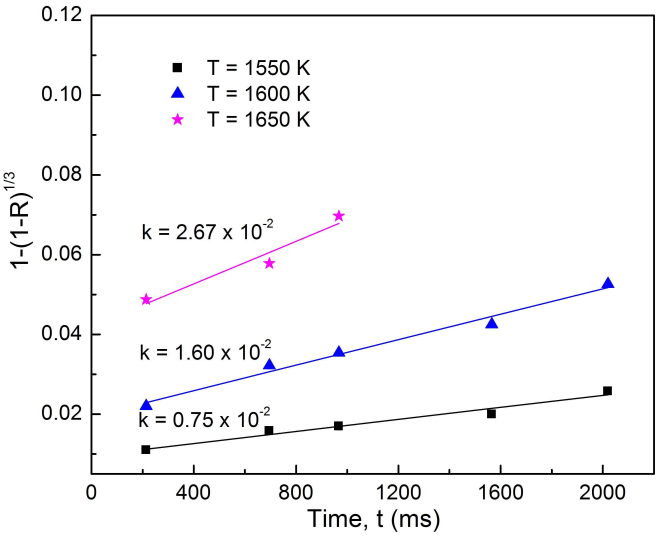

Figure 5.5 Reaction rate constants of gas-solid particle reduction, particle size: 45-53 µm, reducing gas PCR2' (42.2 % CO + 57.8 % CO_2)

The effect of temperature on the reaction rate constant is expressed by the Arrhenius equation (Eq.1.30) which can be converted to Eq.5.5. The Arrhenius equation is obtained from experimental data at different temperatures by calculating the pre-factor (*A*) and activation energy (E_a). Activation energy is the minimum energy required for a chemical reaction to take place.

$$\ln k = \frac{-E_a}{R_g T} + \ln A \tag{5.5}$$

The plot of *lnk* versus *1/T* is drawn in Figure 5.6, with which the pre-factor (*A*) is calculated from the intercept and the activation energy (E_a) from the slope.

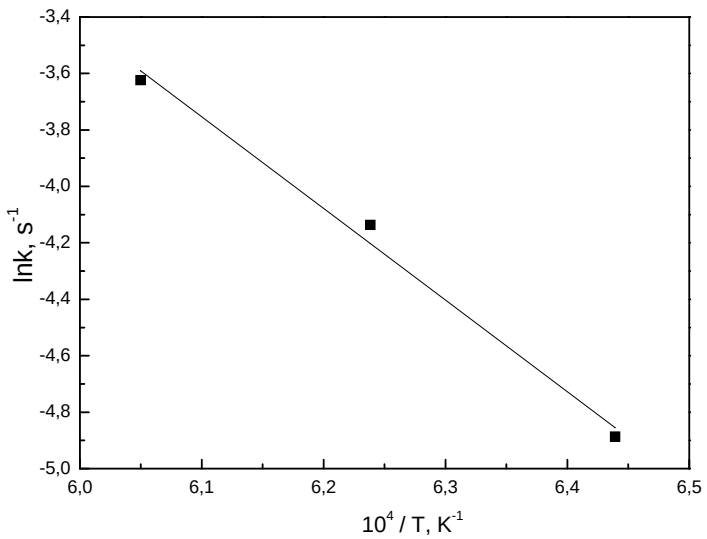

Figure 5.6 Arrhenius plot for calculation of overall activation energy

The activation energy E_a is calculated to be 270.0 kJ/mol and the pre-exponential factor A = 9.36 x 10^6 s^{-1}. Finally, the reaction rate constant can be expressed by Eq.5.6. With this equation, the reaction rate constants of gas-solid reduction at the temperatures 1550 ≤ T≤ 1650 K could be estimated.

$$k = 9.36\times10^{6}\exp\left(\frac{-270000}{R_g T}\right) \tag{5.6}$$

In order to give more evidence for the reaction mechanism of gas-solid reduction, the activation energy is also calculated by the Friedman's method that belongs to model-free method (given in Chapter 1). With the results of reduction degree of gas-solid particle reaction shown in Figure 4.8, the corresponding relationship between the natural logarithmic rate of reduction (*dR/dt*) and the reciprocal of absolute temperature (*1/T*) (according to Eq. 1.54) is drawn in Figure 5.7. The activation energy calculated from the slope of the plot is 271 kJ/mol which is slight higher than the result 270 kJ/mol calculated from model-fitting method.

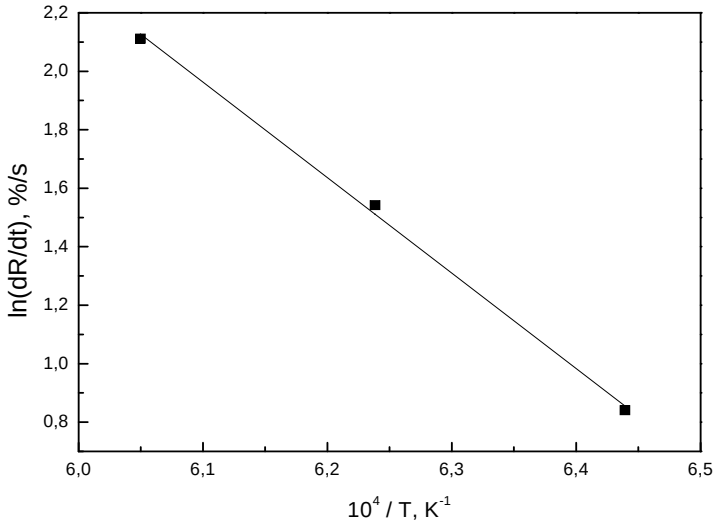

Figure 5.7 Plot of ln(*dR/dt*) versus (1/T), particle size: 45-53 µm, reducing gas PCR2' (42.2 % CO + 57.8 % CO_2)

The activation energy values for iron ore reduction have been calculated by many investigators. The typical ranges of activation energy of different rate controlling steps have been summarized by Strangway [9], which gives that when the activation energy is larger than 90 kJ/mol, the rate controlling step is the solid state diffusion (Step 3)-(b)). The activation energy is normally smaller than 90 kJ/mol, if the rate controlling step is chemical reaction control, gaseous diffusion control or mixed control. A summary of activation energy values regarding chemical control, gaseous diffusion control and mixed control of iron ore reduction process reported in the literature is shown in Table 5.2. In the study of Tabirou [10], it is stated that the activation energy of mass transport of cations and electrons inside the hematite matrix along the hematite-magnetite interfaces could be as high as 400 kJ/mol at some reaction conditions. William [11] gives some examples of the mass transport of Fe atoms: the activation energy of Fe in α-Fe is 251 kJ/mol, the activation energy of Fe in γ-Fe is 284 kJ/mol. The mass transport of cations or electrons is closely related to the defect structure of the solid reactant and the mass transport in the solid is slow under the following conditions:

- Closed-packed structures,
- High melting temperature materials,
- Materials with covalent bonding
- Large atoms
- High density materials

The activation energy of 270 kJ/mol in this study is far higher than 90 kJ/mol, so that the rate controlling step is chemical reaction control. From the microkinetics point view, the rate controlling step is the mass transport of cations and electrons at the reaction interface.

Table 5.2 Summary of activation energy values regarding chemical control, gaseous diffusion control and mixed control of iron ore reduction process reported in the literature

Source	Reduction step	Reduction mechanism	E_a, kJ/mol	Experimental method
Itaya [12]	$Fe_2O_3 \rightarrow Fe$	Ore A: Chemical control	69.1	Fluidized bed
		Ore B: Diffusion control	47.3	973-1073 K Fine iron ore
El-GEASSY [13]	$Fe_2O_3 \rightarrow Fe$	1st stage: mixed control	39.29	Isothermal TGA
		2nd stage: gas diffusion control	12.96	1023-1273 Pellet
Nasr [14]	$Fe_2O_3 \rightarrow Fe$	1st stage: mixed control	28.92	Isothermal TGA
		2nd stage T < 1173: gaseous diffusion control	23.81	1273-1373 K Pure hematite compact
		2nd stage T > 1273: gaseous diffusion control	14.98	
Mohamed [9]	$Fe_2O_3 \rightarrow Fe$	Chemical reaction control	69.5	Isothermal 1173-1473 Pure hematite compact

5.2.2.2 Reduction mechanism of mixed reduction and gas-molten particle reduction

In pilot plant of HIsarna process, the molten iron ore particles are collected on the water-cooled side wall of the cyclone reaction and form a liquid layer. The reduction takes place between the gas and liquid layer. Currently, for mathematical modelling of cyclone reaction, it is assumed that no further reaction takes place after that the molten iron ore particles are collected on the side wall of the reactor. But for the scientific aim, the kinetic reduction mechanism of mixed reduction and gas-molten particle reduction are discussed here.

As shown in Figure 5.1, the mixed reduction (part of gas-solid particle reduction and part of gas-molten particle reduction) takes place at 1650 K in the residence times 970-2020 ms and at 1700 K in the residence times 210-700 ms. The fully molten particles are obtained at 1700 K in the residence times 700-2020 ms and at 1750 K in all the studied residence times. But the reduction degree reaches the equilibrium state at 1750 K, therefore the rate controlling step can not be determined at this temperature. The reduction degrees at 1650 K and 1700 K for the particle size 45-53 µm reduced by gas composition PCR2' (42.2 % CO + 57.8 % CO_2) were also dealt with model-fitting methods based the unreacted shrinking core model. The chemical reaction control fits the experimental data better than gaseous diffusion control and mixed control. The chemical reaction is seen as the rate controlling step of both mixed reduction and gas-molten reduction. The reaction rate constants were calculated from the straight plots of $1 - (1 - R)^{1/3}$ versus t as shown in Figure 5.8.

At 1650 K, the reaction rate constant of mixed reduction is 0.85 x 10^{-2} s^{-1} which is smaller than the reaction rate constant of gas-solid reduction of 2.67 x 10^{-2} s^{-1} as shown in Figure 5.5 (at the same experimental conditions). At 1700 K, the plot of $1-(1-R)^{1/3}$ versus t gives two straight lines which meat at the turning point at the residence time of 700 ms. It is clear that the reaction rate constant of mixed reduction (200-700 ms) is higher than 100 % gas-molten reduction (700-2020 ms). It can be seen that the reaction rate of gas-solid particle reduction is higher than the gas-molten particle reduction rate. However, the reaction rate constant of 1.04 x 10^{-2} s^{-1} of the 100 % gas-molten particle reaction at 1700 K is still higher than the reaction rate constant (0.85 x 10^{-2} s^{-1}) of the mixed reduction at 1650 K (red line in Figure 5.8). The reaction rate constant in the mixed reduction stage at 1700 K is 2.98 x 10^{-2} s^{-1} which is 3 times as large as the kinetic constant (0.85 x 10^{-2} s^{-1}) at 1650 K. Therefore, temperature has significant influence on the reaction rate constant besides the particle physical state.

The activation energy of the gas-molten particle reaction and mixed reduction cannot be calculated directly from the obtained experimental data. For that, on one hand, the reduction at 1750 K reaches its equilibrium state as shown Figure 4.8. Moreover, at the stage of mixed reduction, the reaction mechanism is the combination effect of gas-solid particle reduction and gas-molten particle reduction. It cannot be regarded as gas-molten particle reduction. However, it is clear that before reaching the equilibrium, the reaction rate constant still goes up with the increase of temperature, while it goes down with the increase of molten particle ratio in the sample.

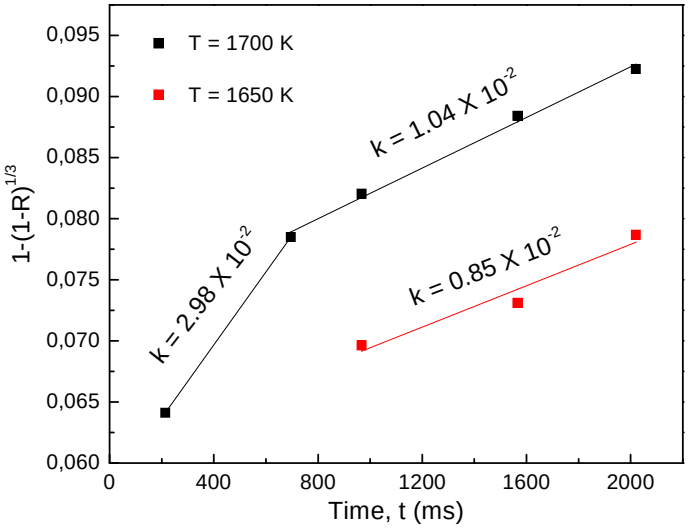

Figure 5.8 Kinetic plots for fine iron ore reduction at 1700 K, reducing gas: CO and CO_2 particle size: 45-53 µm, reducing gas PCR2' (42.2 % CO + 57.8 % CO_2)

5.2.2.3 Effect of partial pressure of reducing gas on the reaction rate constant

The effect of partial pressure of reduction on the reduction kinetics is necessary to be studied for helping to fix a suitable gas composition in the smelting cyclone. At 1650 K, the experiments have been conducted in six different gas compositions with the particle size 45-53 µm. With the morphology study, it is found that the gas-solid particle reduction takes place in the residence time ≤ 970 ms in all the studied gas compositions at 1650 K. The straight plots of $1-(1-R)^{1/3}$ versus t are presented in Figure 5.9. The results of the reduction degree of iron ore versus time at these conditions were given in Figures 4.5 and 4.6. In Figure 5.9 (a), the reducing gases were composed of CO, H_2, CO and CO_2 and had a PCR value of 38.9 %, 57.8 % and 80.4 %, respectively. In Figure 5.9 (b), the reducing gases were composed of CO and CO_2 and had the same values of PCR. The six lines in Figure 5.9 are all characterized by the turning points at the residence time of 970 ms which divide the lines into two stages: 210 ms-970 ms and 970 ms-2020 ms. The first stage results from the gas-solid particle reaction, while the second stage results from the combination effect of gas-molten particle reaction and gas-solid particle reduction. The results in the figure further prove that reduction mechanism between gas-solid particle reaction and gas-molten particle reaction is different.

The reaction rate constants k (s^{-1}) of each group of experiments have been calculated from the slopes of the kinetic plots in Figure 5.9 with the least square method. At the first stage (gas-solid particle reaction), the reaction rate constant

increases with the decrease of PCR at both experimental condition as shown in Figure 5.9 (a) and Figure 5.9 (b). For the influence of molten particles generated in the second stages, the rate constants are much lower than the rate constants at the first stage. The rate constants at the second stage (mixed reduction: 970-2020 ms) also increase with the decrease of PCR from 80.4 % to 57.8 %. However, at the condition of PCR1 = 38.9 % (Figure 5.9 (a)), the rate constant decreases to a very low value of k = 0.52 x 10^{-2} s^{-1} which is lower than the rate constant when PCR2 = 57.8 %. This is because the reduction at this condition is quite close to its equilibrium state at the second stage, which can also be deduced from Figure 4.5. The line in the figure shows that the reduction degree decreases slightly with the decrease of residence time. The highest reduction degree of iron ore at this condition is about 27 % which approximately equals the equilibrium value (~28 %) at this condition.

By comparison of the reaction rate constants in the two figures, it is found that although the PCR of the reducing gas has the same value, the reaction rate constants when the reducing gas contains H_2 (Figure 5.9 (a)) are slightly higher than when the reducing gas does not contain H_2 gas (Figure 5.9 (b)), except for the second stage where the PCR of the reducing gas equals 38.9 %. That is because the reduction ability of H_2 is higher than CO at high temperature, which is also found in Chapter 4. However, it can be seen that a H_2 content lower than 10 % in the gas mixture does not have a significant influence on the reaction rate constant.

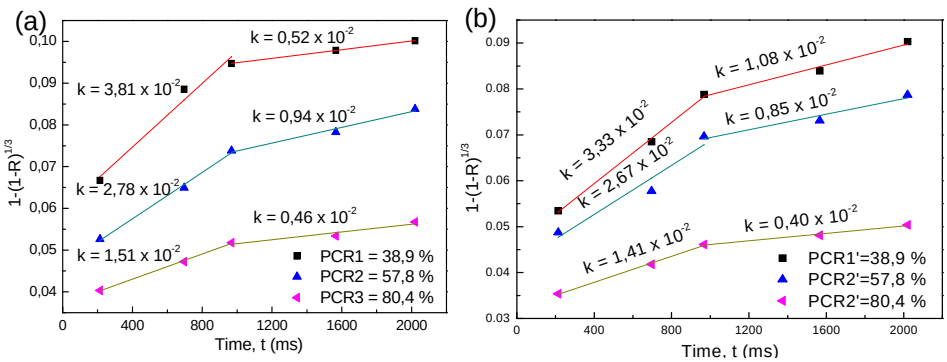

Figure 5.9 Kinetic plots for fine iron ore reduction at 1650 K, reducing gas: (a) CO, H_2, CO_2, N_2; (b) CO and CO_2

Figure 5.10 gives the influence of partial pressure of reducing gas (H_2 and CO) on the reaction rate constant at the gas-solid reduction stage of the experimental study at 1650 K. Figure 5.10 (a) shows the cases where iron ore particles were reduced in the gas mixture of CO, H_2, CO_2 and N_2. The partial pressure of reducing gas is the sum of partial pressure of H_2 and CO. Figure 5.10 (b) shows the cases where iron ore particles were reduced in the gas mixture of CO and CO_2. The particle size was 45-53 µm. The reaction rate constant linearly increases with the

increase of the partial pressure of the reducing gas in every investigated gas mixture.

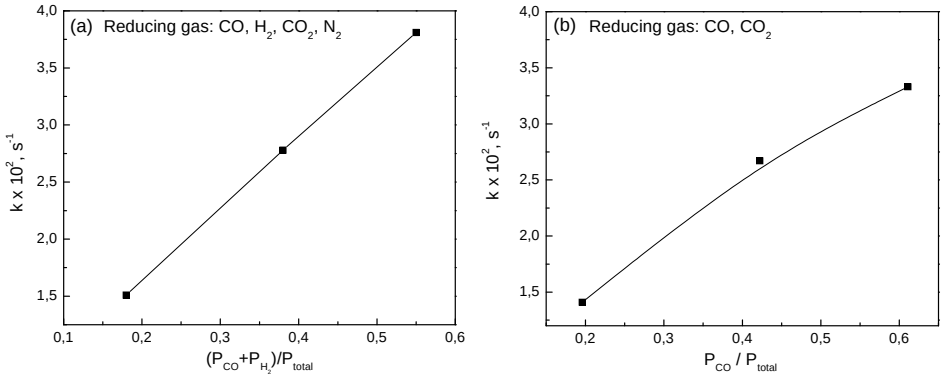

Figure 5.10 Influence of partial pressure of the reducing gas on the reaction rate constant: gas-solid reduction stage (210-970 ms) at 1650 K

Two equations of reaction rate constant as a function of reducing gas partial pressure are obtained from the two lines, respectively, which are listed as follows,

$$k = 0.40\times10^{-2} + 6.22\times10^{-2}\,\frac{p_{CO} + p_{H_2}}{p_{tot}} \tag{5.7}$$

$$k = 0.56\times10^{-2} + 4.66\times10^{-2}\,\frac{p_{CO}}{p_{tot}} \tag{5.8}$$

The results at the stage of mixed reduction of the experimental study at 1650 K are shown in Figure 5.11. In the reducing gas mixture of CO, H_2, CO_2, and N_2, the reaction rate constant goes up first and then goes down with the increase of partial pressure of reducing gas. It is because the reduction almost reaches its equilibrium state in the long residence times when PCR equals 38.9 %. However, in the reducing gas mixture of CO and CO_2, the plot still shows a straight line which mathematically can be represented by the following Eq.5.9:

$$k = 0.10\times10^{-2} + 1.65\times10^{-2}\,\frac{p_{CO}}{p_{tot}} \tag{5.9}$$

According to the studied experimental conditions, when the reducing gas is composed of H_2, CO, CO_2 and N_2, the validity range of the ratio of reducing gas ($(p_{CO}+p_{H2})/p_{tot}$) in Eq.5.7 is from 0.18 to 0.55. When the reducing gas is composed

of CO and CO_2, the validity range of the ratio of reducing gas (p_{CO}/p_{tot}) in Eqs.5.8-5.9 is from 0.196 to 0.611. The typical reducing gas ratio in the in-situ smelting cyclone of HIsarna process is included in these ranges.

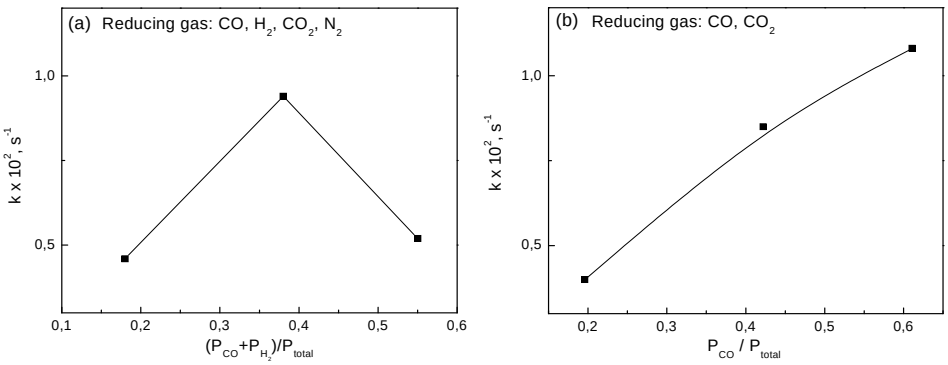

Figure 5.11 Influence of partial pressure of reducing gas on the reaction rate constant: mixed reduction stage (970-2020 ms) at 1650 K

5.2.2.4 Forward reaction rate constant

For more in-depth research, the forward reaction rate constants based on the unreacted shrinking core model has been calculated, which could be used directly in the rate formulas in the mathematical modelling of smelting cyclone.

From Eq.1.39, the specific rate constant k of a first order reversible reaction can be expressed as follows,

$$k = \frac{k_f (1+K_e)(C^0{}_{CO} - C^e{}_{CO})}{K_e \rho_O r_0} \tag{5.10}$$

The forward reaction rate constant k_f is calculated. For the existence of H_2 in the reducing gas the equilibrium constant K_e is calculated by Eq.5.11 [12].

$$K_e = X_{CO+CO_2} K_{CO} + X_{H_2+H_2O} K_{H_2} \tag{5.11}$$

Where,

X_{CO+CO_2} – Sum of mole concentration of CO, CO_2;

$X_{H_2+H_2O}$ – Sum of mole concentration of H_2, H_2O;

K_{CO} – Equilibrium constant of reduction by CO;

K_{H_2} – Equilibrium constant of reduction by H_2;

$$K_{CO} = \exp(3.35 + 553.6/T) \tag{5.12}$$

The equilibrium constant of reduction by CO from magnetite to wüstite is taken from literature [15]. The equilibrium constant of reduction by H_2 in the gas mixture of CO, H_2, CO_2 and N_2 is calculated by Eq.5.13 taking into consideration the water-gas shift reaction.

$$K_{H_2} = K_{CO} \times K_{wg} \tag{5.13}$$

Where the equilibrium constant of the water-gas shift reaction K_{wg} is calculated by Eq.5.14 [16].

$$K_{wg} = \exp\left(-4.33 + \frac{4577.8}{T}\right) \tag{5.14}$$

In this investigation, the resistance offered by the boundary layer of stagnant gas around the sample was negligible. Consequently, C_{CO}^{0} and C_{CO2}^{0} equal the bulk gas concentration and can be considered to remain constant throughout the experiments. C_{co}^{e} is calculated by Eq.5.15.

$$C_{CO}^{e} = \frac{C_{CO}^{0} + C_{CO_2}^{0}}{1 + K_{CO}} \tag{5.15}$$

The forward chemical reaction rate constants (k_f) for gas-solid particle reduction at different temperatures are calculated and shown in Table 5.3. The particle size is in the range of 45-53 µm. The PCR of the gas equals 57.8 %. From Table 5.3, it can be found that the forward reaction rate constant increases with increasing temperature. At 1550 K, k_f = 0.53 x 10^{-2} m/s. However, as the temperature increased to 1600 K and 1650 K, the forward reaction rate constants are twice and four times as big as the value at 1550 K, respectively.

The forward chemical reaction rate constant (k_f) for the mixed reduction and gas-molten particle reduction at the temperatures which are ≥ 1650 K are shown in Table 5.4. The particle size is in the range of 45-53 µm. The PCR of the gas equals to 57.8 %. The reaction rate constants at mixed reduction stage (970-2020 ms) at 1650 K and at 1700 K (210-700 ms) reflect the average value of mixed reactions (gas-molten particle reaction and gas-solid particle reaction). At gas-molten particle

reduction stage of the experimental study at 1700 K (700-2020 ms), the forward reaction rate constant can be seen as the reaction rate constant of pure gas-molten particle reduction. The reaction rate constant of gas-molten particle reduction is much lower than the gas-solid particle reaction constant.

Table 5.3 Reaction rate constants of gas-solid particle reduction, particle size: 45-53 µm; Gas composition (42.2 % CO + 57.8 % CO_2)

Temperature, K	k x 10^2 , s^{-1}	k_f x 10^2 , m/s
1550	0.75	0.53
1600	1.60	1.17
1650	2.67	2.01

Table 5.4 Reaction rate constants of mixed reduction and gas-molten particle reduction, particle size: 45-53 µm; Gas composition (42.2 % CO + 57.8 % CO_2)

Temperature, K	k x 10^2 , s^{-1}	k_f x 10^2 , m/s
1650 mixed reduction	0.85	0.64
1700 mixed reduction	2.98	2.32
1700 gas-molten reduction	1.04	0.81

5.3 Conclusions

The reaction mechanism of iron ore reduction at high temperatures has been investigated through the kinetic model analysis. The reduction of iron ore particles at the studied conditions can be divided into three stages according to the physical state of the collected particles: gas-solid particle reduction, mixed reduction and gas-molten particle reduction. The kinetic model has been determined by the morphology study, the results of which show that the un-reacted shrinking core model could be applied to both gas-solid particle reaction and gas-molten particle reaction. The rate controlling step of gas-solid particle reduction at the typical operating condition of smelting cyclone has been obtained by the model-fitting method and then confirmed by the model-free method. The activation energy of the gas-solid particle reaction is about 270 kJ/mol. The results reveal that the reaction rate controlling step of gas-solid reduction is chemical control from macrokinetics

point of view, and the rate controlling step is the mass transport of cations and electrons inside the hematite or magnetite matrix along the interfaces from the microkinetics point of view. The reduction rate controlling step of gas-molten particle reduction is also chemical control.

At 1650 K, the reaction rate constants of the gas-solid particle reaction are greater than that of the mixed reduction, and at 1700 K, the reaction rate constant of mixed reduction are greater than gas-molten particle reaction. Before reaching the reduction equilibrium state, the rate constant linearly increase with the increase of partial pressure of the reducing gas. The results of kinetic analysis offer a good understanding of the iron ore melting and reduction behaviour in the smelting cyclone and provide kinetic data for the further mathematical modelling study. It will eventually help in the scaling up the pilot plant of HIsarna process, together with the CFD reactor model of the plant. The rate controlling step determines the iron ore reduction rate in the smelting cyclone. According to the identified rate controlling step in this study, the operating parameters of the smelting cyclone could be adjusted to intensify the reduction process.

References

[1] Takeuchi, N., Nomura, Y., Ohno, K., Maeda, T. Nishioka, K. and Shimizu, M.: Kinetic analysis of spherical wüstite reduction transported with CH_4 gas, ISIJ International 47 (2007) 386-391.

[2] Turkdogan, E.T., and Vinters, J.V.: Gaseous reduction of iron oxides: Part I. Reduction of hematite in hydrogen, Metallurgical transctions 2 (1971) 3175 -3188.

[3] ET-Tabirou, M., Dupre, B., and Gleitzer, C.: Hematite single crystal reduction into magnetite with CO-CO_2, Metallurgical transactions B 19B (1988) 311-317.

[4] Weiss, B. Sturn, J., Voglsam, S., Strobl, S., Mali, H.,Winter, F. and Schenk, J.: Structual and morphological changes during reduction of hematite to magnetite and wüstite in hyfrogen rich reduction gases under fluidised bed conditions, Ironmaking and Steelmaking 38(2011) 65-73.

[5] Khawam, A., and Flanagan, D.R.: Solid-state kinetic Models: Basics and mathematical fundamentals, J. Phys. Chem. B, 110 (2006) 17315-17328.

[6] R. Rota: Microkinetics versus macrokinetics: the role of transport phenomena in determining reaction rates, Fundamental of Chemistry 2.

[7] Hayes, P. and Grieveson, P.: Microstructural changes on the reduction of hematite to magnetite, Metallurgical transactions B 12 (1981) 579-587.

[8] Piotrowski, K., Mondal, K., Wiltowski, T., Dydo, P., and Rizeg, G.: Topochemical approach of kinetics of the reduction of hematite to wüstite, Chemical Engineering Journal, 131 (2007) 73-82.

[9] Khedr, M.H.: Isothermal reduction kinetics of Fe_2O_3 mixed with 1-10 % Cr_2O_3 at 1173 – 1473 K, ISIJ International 40 (2000) 309-314.

[10] TABRIOU, M.E., DUPRE, B. and GLEITZER, C.: Hematite single crystal reduction into magnetite with CO-CO_2, Metallurgical transaction B, 19B (1988) 311-317.

[11] William, D. C.: Fundamentals of materials science and engineering, Department of Metallurgical Engineering, University of Utah, United States of America, 2001.

[12] Itaya, H., Sato, M. and Tagychi, S.: Circulation and Reduction Behaviour of Iron Ore in a Circulating Fluidized Bed, 39 (1994) 393-400.

[13] EL-GEASSY, A. A., NASR, M.I., KHEDR, M.H., ABDEL-HALIM, K.S.: Reduction behaviour of iron ore fluxed pellets under load at 1024-1273 K, ISIJ International 44 (2004) 462-469.

[14] Nasr, M.I., Omar, A.A., Hessien, M.M., and El-Geassy, A.A.: Carbon-monoxide reduction accompanying swelling of iron-oxide compacts, ISIJ International 36(1996) 164-171.

[15] Acevedo, C.M.U.: Mathematical modelling and control of the blast furnace process, PhD thesis, 1981, Purdue University, Lafayette.

[16] Byron, S.R.J., Loganathan, M. and Shantha, M.S.: A review of the water gas shift reaction kinetics, International Journal of Chemical Reactor Engineering 8 (2010) 1-32.

Chapter 6 Conclusions and Outlook

6.1 Conclusions

The HIsarna technology has long-term potential to replace conventional blast furnaces, coke ovens and sinter plants and is today the most promising alternative ironmaking process in the field of smelting reduction. It is expected to reduce carbon-dioxide emissions from ironmaking by more than 50 % if combined with Carbon Capture and Storage (CCS). The first HIsarna pilot plant campaign, executed in spring 2011, proved that a plant using this breakthrough technology can operate in practice, and not merely in theory. The second campaign has been conducted in autumn 2012 and lasted about six weeks. The technology is still at a very early pilot stage and the conditions in the reactors are very complicated.

The reduction mechanism of individual iron ore particles in the reducing gas as existing in the HIsarna cyclone at high temperature has been investigated in this project. The laboratory study aims to provide significant information for primarily understanding the process which will also be useful for scaling up the pilot plant. The partially reduced iron ore from the smelting cyclone has around 20 % reduction degree as a consequence of thermal decomposition and gas reduction.

The thermal decomposition behaviour of hematite ore has been studied by theoretical and experimental methods. The experimental study has been carried out with a TGA-DSC analyzer and a high temperature horizontal furnace with long reaction times. The kinetics of the individual particle thermal decomposition behaviour has been investigated in the High-temperature Drop Tube Furnace (HDTF) at different conditions. The results show that in the inert gas, the lowest start thermal decomposition temperature of Fe_2O_3 could be around room temperature when p_{O2} is close to 0 Pa. If p_{O2} is lower than the equilibrium pressure of oxygen (82 Pa) at 1473 K, the intensive thermal decomposition takes place at the temperatures 1473-1573 K. The lowest start temperature of thermal decomposition of Fe_3O_4 is also around room temperature when p_{O2} is 0 Pa. If p_{O2} is lower than the equilibrium pressure of oxygen (1.7 Pa) at 1773 K, the thermal decomposition of Fe_3O_4 is speeded up slightly above 1773 K. Fe_2O_3 is the most unstable iron oxide among the three iron oxides, while FeO is the most stable one. The thermal decomposition of magnetite was not as intensive as hematite during the studied reaction times. From the experimental results in the horizontal tube furnace, the high accurate results of thermal decomposition degree of hematite at a certain temperature and holding time were obtained. The thermal decomposition degree of hematite ore increases with the increase of temperature. However, there is no significant difference between the results at 1673 K and 1773 K. The thermal

decomposition degree at 1873 K is much higher than the result at 1773 K in same holding time. It indicates that the thermal decomposition of magnetite was accelerated at 1873 K. In the HDTF, the effects of particle size, residence time, temperature, and gas composition on the thermal decomposition degree have been investigated. It was found that the sharp weight loss stage which was observed in the TGA–DSC experiments was partly achieved in the HTDF especially in the CO_2 gas. The fine iron ore particles were heated up faster in CO_2 gas than in N_2 gas due to the strong radiation properties (emission and absorption) of CO_2 gas. Also for this reason, in the HDTF, the thermal decomposition degree of fine iron ore particles in N_2 gas increases with the increase of temperature and particle residence time. Because CO_2 is the main gas in the smelting cyclone, more experiments have been conducted in CO_2 gas. The thermal decomposition degree in CO_2 gas also increases with the increase of temperature. However, no significant influence of particle size and residence time on the thermal decomposition degree was observed, when the particle diameter is smaller than 250 µm.

The reduction mechanism of hematite ore in the smelting cyclone has been investigated in the HTDF. The experiments have been carried out at different temperatures, in different reducing gas compositions and with different particle sizes. The studied temperature was ranged from 1550 K to 1750 K. The post combustion ratio PCR of the reducing gas was set to 38.9 %, 57.8 % and 80.4 %. The main experiments focused on the particle size 45-53 um because this particle size is most close to the average particle size used in the smelting cyclone. The experimental results reveal the individual particle reduction behaviour at high temperature. The PCR of the reducing gas and the reaction temperature determine the final equilibrium state of partially reduced iron ore. In this study, the maximum reduction degree is in the range of 23-30 %. The iron ore could reach its equilibrium state in a short time at high temperature and low PCR of reducing gas. During the first selected reaction time of 210 ms, both thermal decomposition and reduction contributed to the reduction degree. Combining the results of thermal decomposition of hematite ore, it is found that in the first 210 ms, thermal decomposition of hematite ore was the main reaction at low temperature, while gas particle reduction played an important role in the reduction degree at high temperature. The morphology study by optical microscopy shows gas-solid particle reaction took place in all the studied residence times at 1550 K and 1600 K. It also took place when residence time $\leqslant$ 970 ms at 1650 K. Gas-molten particle reaction took place at 1700 K in the residence times of 700-2020 ms and at 1750 K in all the studied residence times. The unreacted shrinking cores have been found during the reduction from hematite to magnetite and from magnetite to wüstite. It means that the chemical reaction takes place at the interfaces between the two adjacent phases. From XRD results, it was found that the three phases of hematite, magnetite and wüstite coexisted in one collected sample at 1600 K in the residence times $t \geq 970$ ms and at 1650 K in the residence time $t = 210$ ms. However, there is no evidence shows that the three phases were found in a single particle by the

analysis with both optical microscope and SEM-EDS methods. Therefore, one interface unreacted shrinking core model was employed in this study. A number of micro pores were formed during the reduction process due to the different crystal structure of hematite, magnetite and wüstite.

The reaction mechanism of iron ore reduction at high temperature was revealed through the kinetic analysis. The rate controlling step of gas-solid particle reaction has been obtained by the model-fitting method and confirmed by model-free method. The rate controlling step of mixed reduction and gas-molten particle reaction has been determined by the model-fitting method. The unreacted shrinking core model was applied to both gas-solid particle reaction and gas-molten particle reaction. The reaction rate controlling step of gas-solid particle reaction, mixed reduction and gas-molten reaction is chemical reaction control from macrokinetics point of view. Furthermore, it is found that the reaction rate controlling step of gas-solid particle reaction is the mass transport of cations and electrons inside the matrix along the interfaces from microkinetics point of view. Before reaching the reduction equilibrium state, the rate constant linearly increases with the increase of partial pressure of the reducing gas.

6.2 Outlook

This study has presented a fundamental understanding of the individual iron ore particle reduction kinetics in the smelting cyclone of HIsarna process. However, many new questions about the reactions and the reactor systems have been raised at the same time. In a closer relation to the HIsarna process and reactor optimisation, extended and new research topics are recommended for research, which could fulfil the current study and act as a bridge among the current obtained kinetic equations. Finally, a more perfect theoretical framework could be obtained from the insights and experimental results and the equations for the reduction and melting rates developed in that framework should be applicable in (commercial) CFD software.

In the smelting cyclone, fine ore and flux are fed together with oxygen. The iron ore particles experience a series of chemical and physical changes, like heating up, thermal decomposition, reduction and melting down. The molten iron ore particles land on the water-cooled side wall of the cyclone reactor. A liquid layer is formed and flows down the wall to the smelt reduction vessel SRV under gravity. Firstly, in this study, the kinetics study focused on the particle size of 45-53 μm and the effect of particle size has been studied at 1650 K in different gas compositions. In the following study, bigger particle sizes reduced at different temperatures should be tested to build a whole kinetic story. Secondly, during the flying time of iron ore particles, some particles form a swarming flow. The reduction behaviour of the ‘particle swarms’ should be studied next to that of individual particles. This could be

done by increasing the particle feed rate by the current experimental set-up. Thirdly, the thermal decomposition of hematite ore should be further studied with different oxygen partial pressures. Finally, the particles' collision behaviour as well as the particles' trajectories with different carrier gas flow rate is not known yet. A cold model could be used to observe the particles' collision behaviour and trajectories in the smelting cyclone. On the other hand, the capture efficiency in the smelting cyclone of HIsarna process could be estimated.

SUMMARY

The HIsarna is a coal-based smelting reduction process for ironmaking to drastically reduce CO_2 emission and is one of the most promising alternative ironmaking processes under development in the world. The furnace consists of two inter-connected reactors: i) a smelting cyclone, ii) a smelting reduction vessel. The smelting cyclone is expected to provide about 20 % pre-reduction degree through thermal decomposition and reduction. However, as a new technology still at its development stage, the iron ore behaviour in the smelting cyclone is not well studied. Three HIsarna pilot plant campaigns have been conducted successfully during the years of 2011-2013 at the Tata Steel site in IJmuiden, the Netherlands. The laboratory study has been carried out in the same period at Delft University of Technology as part of the research programme of the Matrials innovation institute M2i, to focus on the thermal decomposition and reduction kinetics of individual particles in the smelting cyclone of the HIsarna, forming the main part of this thesis.

In this study, a special experimental set-up has been designed and commissioned: the high temperature drop tube furnace (HTDF). The HTDF was used to investigate the reduction mechanism at high temperature of individual ore particles without agglomeration. The reaction gas is a mixture of CO, CO_2, H_2 and N_2, and the composition is controlled with mass flow controllers. The gases are firstly guided into a gas mixing station and form a flow of gas mixture. And then the gas mixture is split up into two flows. A small flow of the gas mixture enters the syringe pump feeder as particle carrier gas. The other flow is preheated to 773 K through a pre-heat furnace before entering the electrically heated furnace. The particle feed rate is controlled by a syringe pump feeder. The individual iron ore particles from the syringe pump feeder pass through a water-cooled injection probe before entering the hot zone. The iron ore reduction takes place during the flying time of the particle in the hot zone. The off-gas and the partially reduced particles are received by a water-cooled sampling probe. Finally, the iron ore particles are collected by a sample collector.

The study of the thermal decomposition behaviour of hematite ore started with a theoretical evaluation. The experimental study has been conducted with the TGA-DSC analyser and in a high temperature horizontal furnace at a steady state. The individual particle thermal decomposition behaviour has been investigated in the HDTF under different conditions. The theoretical evaluation shows that, in the inert gas environment, the lowest start thermal decomposition temperature of Fe_2O_3 could be room temperature when the partial pressure of oxygen is close to zero bar. The thermal decomposition of Fe_2O_3 can be accelerated when the temperature is higher than 1473 K. The thermal decomposition of pure Fe_3O_4 can also take place at room temperature when the partial pressure of oxygen is close to zero bar and the thermal decomposition can be accelerated when the temperature is higher than 1673 K. These results have been confirmed by the following experimental studies.

From the TGA-DSC analysis, it was found that a sharp weight loss in a short time appears on the TG curve. However, the weight loss is quite small during the time elapsed after the sharp weight loss stage. The experimental study in the horizontal furnace provided accurate results of the thermal decomposition degree of hematite ore at different temperatures and holding times by chemical titration. The thermal decomposition degree of iron ore increases with the increase of temperature. At the same temperature, the thermal decomposition degree of iron ore increases slowly with the increase of holding time (1 h, 2 h and 3 h). In addition, no significant difference was observed between the results at 1673 K and 1773 K. Furthermore, whether the sharp weight loss stage occurs and how much of the thermal decomposition degree could be achieved in the smelting cyclone has been further tested with the HTDF. The effects of different inert gases: N_2, Ar, CO_2 (CO_2 is the primary gas in the pilot plant besides CO), temperature, residence time, and particle size on the final thermal decomposition degree were studied. It was found that the sharp weight loss stage observed in the TGA-DSC experiments can be mostly achieved in the HTDF in the CO_2 gas rather than N_2 and Ar. For example, at 1750 K in CO_2 gas, the thermal decomposition degree of iron ore in the HTDF is around 10.8 % which is slightly lower than the value of 12.6 % obtained in the horizontal furnace. This is because the fine iron ore particles could be heated up faster in CO_2 gas than in N_2 and Ar gas due to the strong radiation properties (emission and absorption) of CO_2 gas. Temperature plays an important role in determining the iron ore thermal decomposition which dramatically goes up with the increase of temperature. However, there is no significant influence of particle size and residence time on the thermal decomposition degree observed, when the particle diameter is smaller than 250 µm. It indicates that the thermal decomposition of iron ore quickly takes place in the first 210 ms.

Based on the results of thermal decomposition of iron ore particles, the individual particle reduction mechanism of hematite ore in the smelting cyclone has been investigated with the HTDF. Under the studied experimental conditions, the maximum reduction degree of iron ore particle is in the range of 23-30 %. Before reaching the reduction equilibrium state, the reduction degree of iron ore goes up with the increase of residence time and temperature, and decreases with the increase of Post Combustion Ratio ($CO_2 + H_2O$)/($CO + CO_2 + H_2 + H_2O$). The gas-solid particle reaction takes place in all the studied residence times at 1550 K and 1600 K, and at 1650 K in the residence times of 210-970 ms. The 100 % gas-molten particle reduction takes place at 1700 K in the residence times of 700-2020 ms and in all the studied residence times at 1750 K. The reduction degree of iron ore in the first 210 ms is the combined result of reduction and thermal decomposition. During the reduction process, quantities of micro pores were formed due to the different crystal structures of hematite, magnetite and wüstite. The micro pores could accelerate the reduction process.

The reaction mechanism of iron ore reduction at high temperature has been revealed through the kinetic analysis. The kinetic model was determined by

microscopic examination. The unreacted shrinking core model was applied to both gas-solid particle reaction and gas-molten particle reaction. The rate controlling step of gas-solid particle reduction was obtained by the model-fitting method and confirmed by the model-free method, and the rate controlling step of gas-molten particle reduction and mixed reduction was obtained by the model-fitting method. The reaction rate controlling step was found to be the chemical control for gas-solid particle reduction, mixed reduction and gas-molten particle reduction from a macrokinetics point of view. Through further study, the rate controlling step of gas-solid particle reduction was found to be mass transport of cations and electrons inside the matrix along the interfaces from a microkinetics point of view.

The most typical operating conditions of the smelting cyclone of the HIsarna process have been studied in this study and the fundamental understanding of the reduction kinetics of the individual iron ore particle is presented in this thesis. At the same time, new questions about the reactions and the reactor systems have been raised like the reduction mechanism of bigger particle size, reduction behaviour of ‘particle swarms’, the particles’ collision behaviour and so on. The further laboratory study seems significant for future development of the HIsarna process.

SAMENVATTING

Het HIsarna proces is een op kolen gebaseerd smeltreductie proces ontwikkeld om de CO_2 uitstoot te verminderen en is een van de meest veelbelovende alternatieve ijzer bereidingsprocessen die in de wereld in ontwikkeling zijn. De oven bestaat uit twee onderling verbonden reactoren: i) een smeltcycloon, ii) een smeltreductie vat. De verwachting is dat de smeltcycloon ongeveer 20 % voorreductie zal bereiken door thermische ontleding en reductie. Echter, voor deze nieuwe technologie in een vroeg stadium van ontwikkeling is het gedrag van ijzererts in de smeltcycloon nog niet goed begrepen. Drie campagnes met de HIsarna proeffabriek zijn met succes uitgevoerd in de jaren 2011-2013 bij Tata Steel in IJmuiden. De laboratorium studie is in dezelfde periode uitgevoerd aan de Technische Universiteit Delft in het research programma van het Materials innovation institute M2i, gericht op de thermische ontleding en de reductie kinetiek van individuele deeltjes in de smeltcycloon van HIsarna, en vormt het hoofdonderwerp van dit proefschrift.

In deze studie is een speciale proefopstelling ontworpen en gebouwd, die de naam heeft gekregen van “high temperature drop tube furnace (HTDF)”. De HTDF is gebruikt om bij hoge temperatuur het reductie mechanisme te onderzoeken van individuele ijzererts deeltjes zonder samenklontering (agglomeratie). Het reactie gas is een mengsel van CO, CO_2, H_2 en N_2, en de samenstelling wordt geregeld door middel van massa stroom regelaars. De gassen worden eerst door een gas mengstation geleid en vormen een stroom van menggas. Dit gasmengsel wordt in twee stromen opgesplitst. Een kleine gasstroom wordt de spuit doseerpomp ingevoerd als draag gas voor de deeltjes. De andere stroom wordt voorverwarmd tot 773 K door een voorverwarmoven voordat het gas de elektrisch verwarmde oven wordt binnen geleid. De doseersnelheid van de deeltjes wordt geregeld door de spuit doseerpomp. De individuele ijzererts deeltjes van de doseerpomp gaan door een water gekoelde injectie buis voordat ze de hete zone binnentreden. De ijzererts reductie vindt plaats tijdens de vluchtduur van het deeltje in de hete zone. Het uittredende gas en de gedeeltelijk gereduceerde deeltjes worden opgevangen in een water gekoelde monsterbuis. Tenslotte worden de ijzer deeltjes opgeslagen in een monster verzamelaar.

Het onderzoek van de thermische ontleding van hematiet is begonnen met een theoretische berekening. De experimentele studie is uitgevoerd met een TGA-DSC analyse apparaat en een hoge temperatuur horizontale buis oven in evenwichtssituatie. Het thermische ontledingsgedrag van individuele deeltjes is onderzocht in de HDTF onder verschillende omstandigheden. De theoretische berekening laat zien dat, in een inerte gas omgeving, de laagste temperatuur waarbij Fe_2O_3 begint te ontleden kamertemperatuur kan zijn als de zuurstofpotentiaal dicht bij 0 bar ligt. De thermische ontleding van Fe_2O_3 kan versneld worden als de temperatuur hoger is dan 1473 K. De thermische ontleding

van zuiver Fe_3O_4 kan ook plaatsvinden bij kamertemperatuur als de partiële druk van zuurstof dicht bij 0 bar is en de thermische ontleding kan versneld worden als de temperatuur hoger is dan 1673 K. Deze resultaten zijn bevestigd door de volgende experimentele onderzoeken. Bij TGA-DSC analyse is een scherp gewichtsverlies in een kort tijdsbestek gevonden op de TG curve. Het gewichtsverlies is daarentegen gering in de periode na de fase met scherp gewichtsverlies. Experimenteel onderzoek in de horizontale oven heeft door chemische titratie nauwkeurige resultaten opgeleverd van de thermische ontledingsgraad van hematiet erts bij verschillende temperaturen en reactietijden. De thermische ontledingsgraad neemt toe met toenemende temperatuur. Bij gelijk blijvende temperatuur neemt de thermische ontledingsgraad langzaam toe met toenemende reactietijd (1 uur, 2 uur en 3 uur). Daarbij is geen significant verschil gemeten tussen de resultaten bij 1673 K en 1773 K.

Verder is in de HTDF onderzocht of de scherpe gewichtsdaling ook optreedt en hoe veel van de thermische ontleding bereikt zou kunnen worden in de smeltcycloon. De invloed van verschillende inerte gassen: N_2, Ar, CO_2 (CO_2 is het primaire gas in de proeffabriek naast CO), temperatuur, verblijftijd en deeltjesgrootte op de uiteindelijke thermische ontledingsgraad is onderzocht. Geconstateerd is dat de fase met het scherpe gewichtsverlies in de HTDF vooral bereikt kan worden in CO_2 gas en minder in N_2 en Ar. Bij voorbeeld bij 1750 K in CO_2 gas is de thermische ontledingsgraad in de HTDF ongeveer 10.8 % wat iets lager is dan de waarde van 12.6 % zoals verkregen in de horizontale oven. Dit wordt verklaard doordat de fijne ijzerertsdeeltjes sneller kunnen worden verhit in CO_2 gas dan in N_2 en Ar gas hetgeen veroorzaakt wordt door de sterke stralingseigenschappen (emissie en absorptie) van CO_2 gas.

De temperatuur speelt een belangrijke rol in het bepalen van de thermische ontleding van ijzererts die dramatisch stijgt met stijgende temperatuur. Er is echter geen significante invloed van deeltjesgrootte en verblijftijd op de thermische ontledingsgraad gemeten als de deeltjesgrootte kleiner is dan 250 µm. Het duidt erop dat de thermische ontledingsgraad van ijzererts snel plaatsvindt in de eerste 210 ms.

Gebaseerd op de resultaten van thermische ontleding van ijzererts deeltjes is het individuele reductiemechanisme van hematiet in de smeltcycloon onderzocht met de HTDF. Onder de bestudeerde experimentele condities ligt de maximale reductiegraad van ijzerertsdeeltjes in het bereik van 23-30 %. Voordat de reductie evenwichtstoestand wordt bereikt neemt de reductiegraad van ijzererts toe met toename van de verblijftijd en temperatuur, en neemt af met de toename van de naverbrandingsgraad $CO_2/(CO+CO_2)$. De reactie tussen gas en vast deeltje vindt in alle onderzochte verblijftijden plaats bij 1550 K en 1600 K, en bij 1650 K bij verblijftijden van 210-970 ms. De 100 % gas-gesmolten deeltje reductie vindt plaats bij 1700 K in verblijftijden van 700-2020 ms en in alle onderzochte verblijftijden bij 1750 K. De reductiegraad van ijzererts in de eerste 210 ms is het

gecombineerde resultaat van reductie en thermische ontleding. Gedurende het reductieproces worden micro poriën gevormd door de verschillende kristalstructuren van hematiet, magnetiet en wüstiet. Deze micro poriën zouden het reductieproces kunnen versnellen.

Het reactiemechanisme van ijzererts reductie bij hoge temperatuur is ontrafeld door een analyse van de kinetiek. Het kinetische model is bepaald door microscopisch onderzoek. Het model van de niet gereageerde krimpende kern is toegepast op zowel de gas-vaste deeltje en de gas-gesmolten deeltje reductie. De snelheidsbepalende stap van de gas-vaste deeltje reductie is verkregen door de model-aanpassing methode en bevestigd door de model-vrije methode, en de snelheidsbepalende stap van de gas-gesmolten deeltje reductie en gemengde reductie is verkregen door de model-aanpassing methode. Vanuit een macro kinetisch standpunt is gevonden dat de chemie de snelheidsbepalende stap is voor gas-vast deeltje reductie, gemengde reductie en gas-gesmolten deeltje reductie. Door verder onderzoek is vastgesteld dat massa transport van kationen en elektronen in de matrix langs de grensvlakken de snelheidsbepalende stap is voor gas-vaste deeltje reductie vanuit een micro kinetisch standpunt.

De meest kenmerkende bedrijfsomstandigheden van de smeltcycloon van het HIsarna proces zijn bestudeerd in dit onderzoek en het fundamentele begrip van de reductiekinetiek van de individuele deeltjes is in deze dissertatie gepresenteerd. Tegelijkertijd zijn nieuwe vragen over de reacties en de reactiesystemen opgeworpen zoals het reductie mechanisme van grotere deeltjes, het reductie gedrag van zwermen deeltjes, het botsingsgedrag van deeltjes en dergelijke. Verder laboratorium onderzoek lijkt significant voor de verdere ontwikkeling van het Hisarna proces.

APPENDIX A: XRD Pattern

Gas mixture: CO and CO_2, PCR = 57.8 %

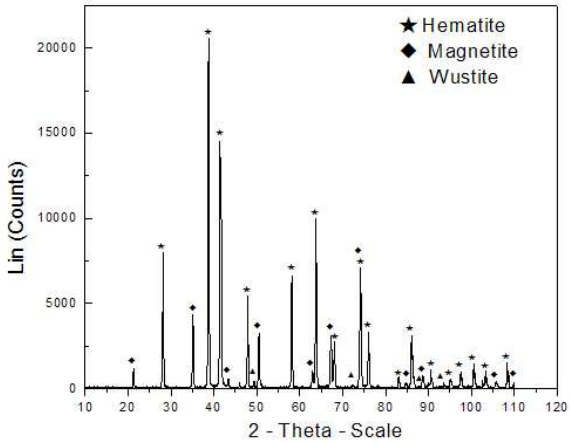

Figure A-1 XRD pattern of reduced particle at 1550 K, t = 210 ms

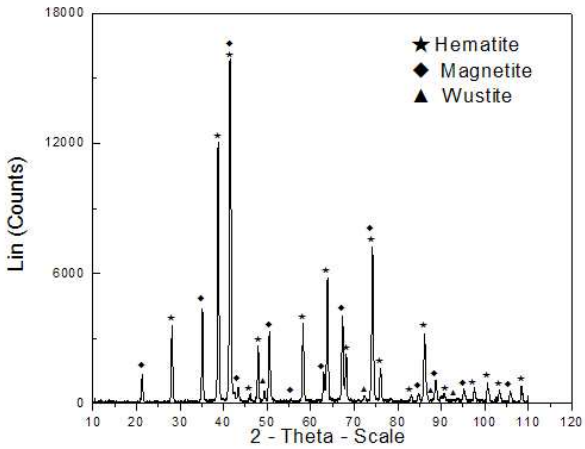

Figure A-2 XRD pattern of reduced particle at 1550 K, t = 970 ms

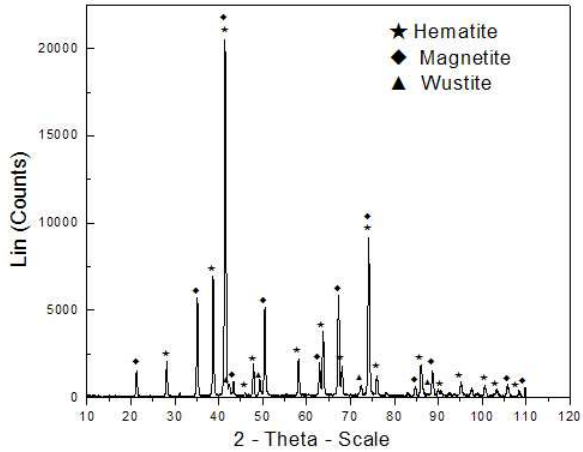

Figure A-3 XRD pattern of reduced particle at 1550 K, t = 2020 ms

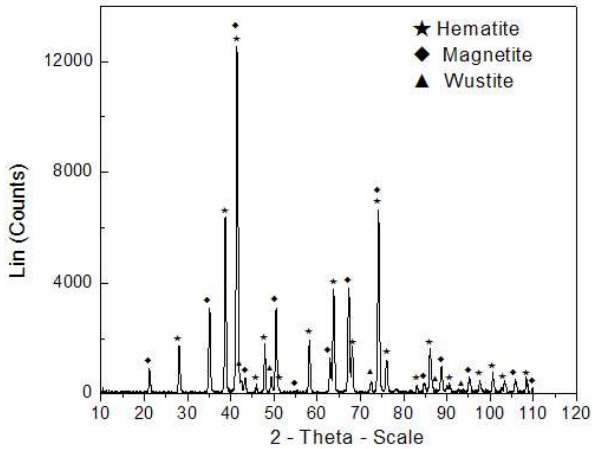

Figure A-4 XRD pattern of reduced particle at 1600 K, t = 210 ms

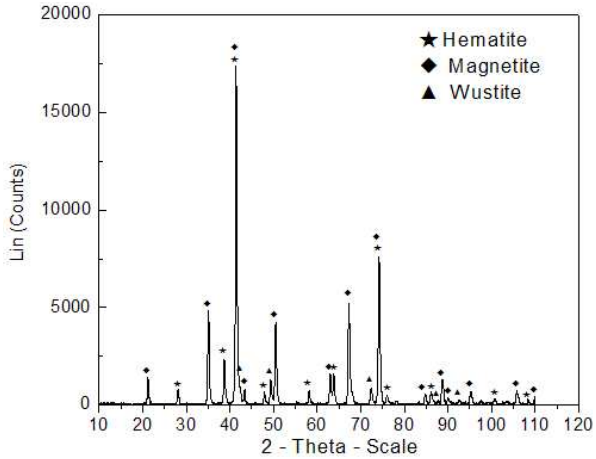

Figure A-5 XRD pattern of reduced particle at 1600 K, t = 970 ms

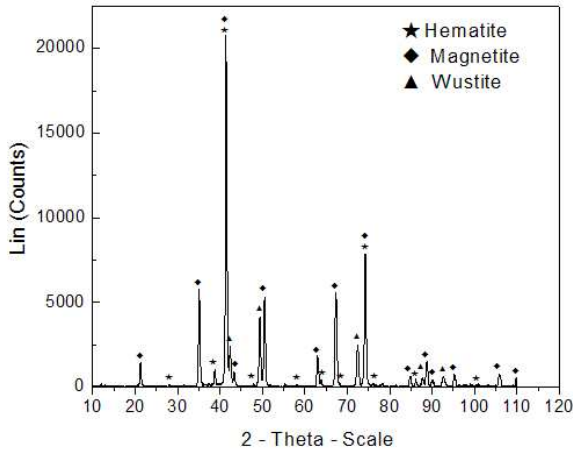

Figure A-6 XRD pattern of reduced particle at 1600 K, t = 2020 ms

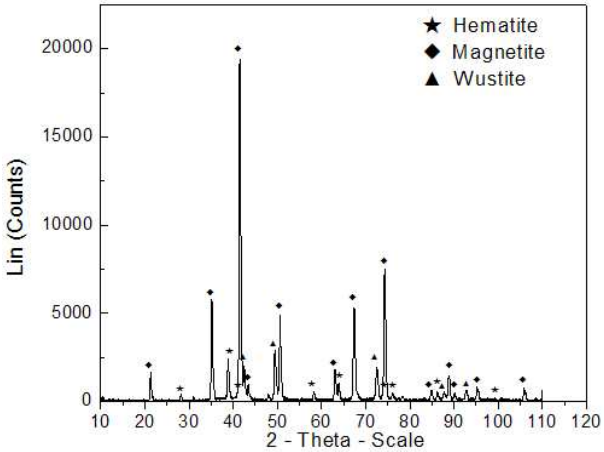

Figure A-7 XRD pattern of reduced particle at 1650 K, t = 210 ms

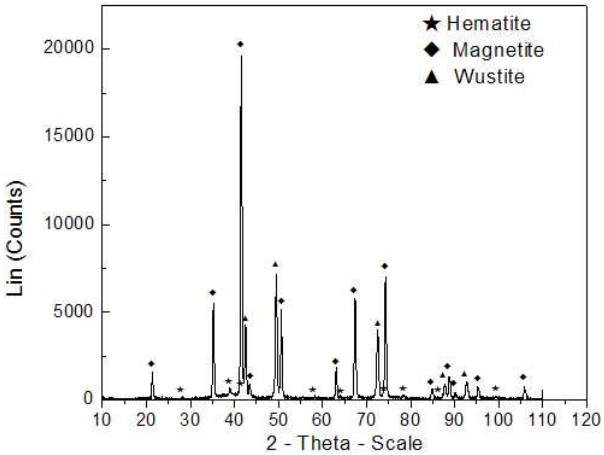

Figure A-8 XRD pattern of reduced particle at 1650 K, t = 970 ms

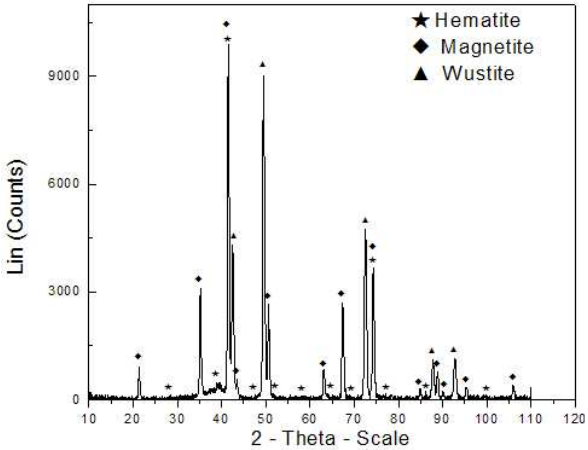

Figure A-9 XRD pattern of reduced particle at 1650 K, t = 2020 ms

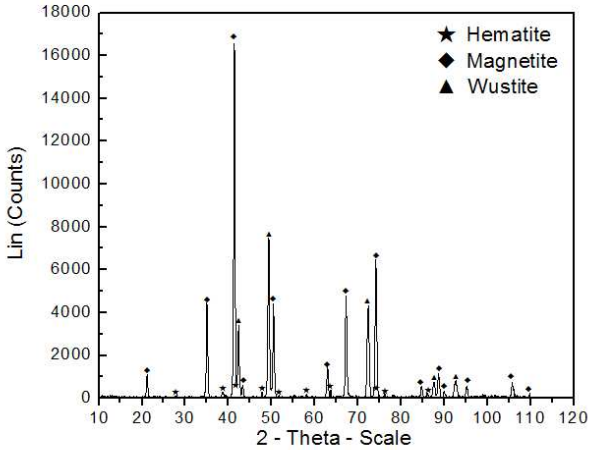

Figure A-10 XRD pattern of reduced particle at 1700 K, t = 210 ms

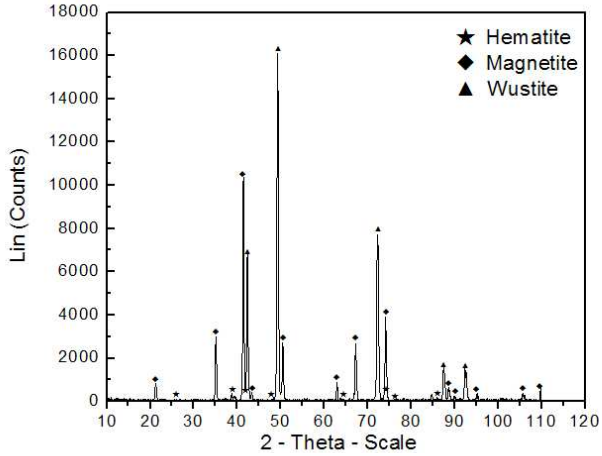

Figure A-11 XRD pattern of reduced particle at 1700 K, t = 970 ms

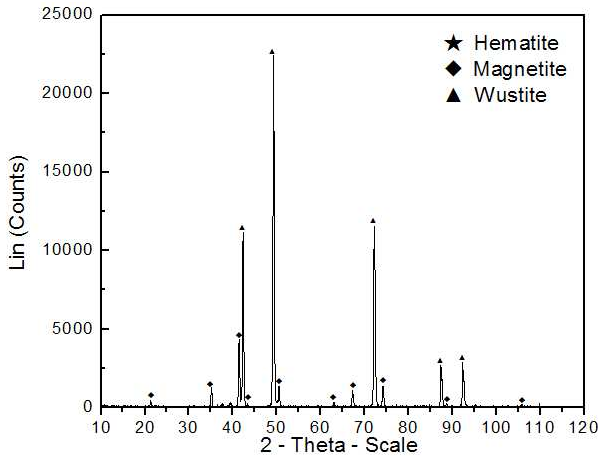

Figure A-12 XRD pattern of reduced particle at 1700 K, t = 2020 ms

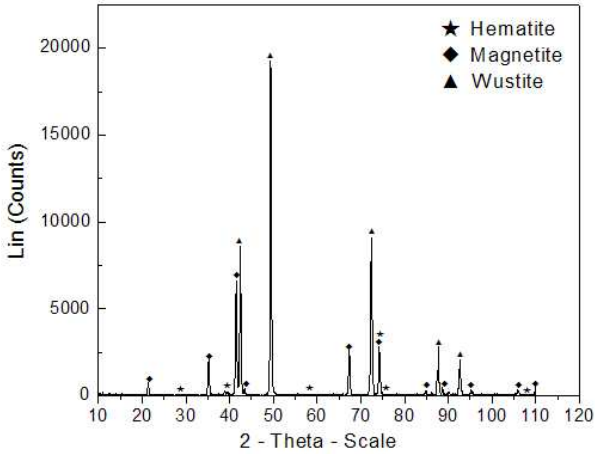

Figure A-13 XRD pattern of reduced particle at 1750 K, t = 210 ms

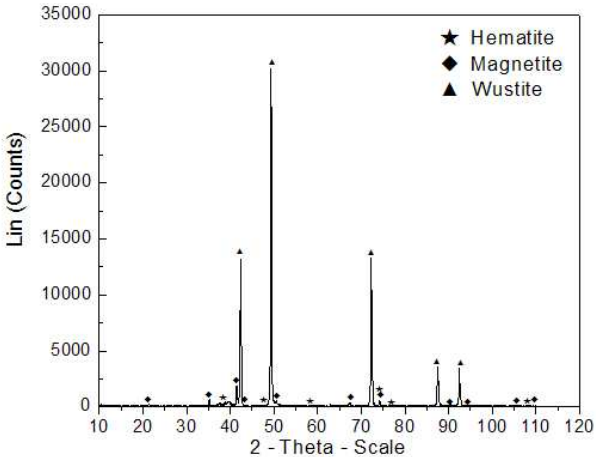

Figure A-14 XRD pattern of reduced particle at 1750 K, t = 970 ms

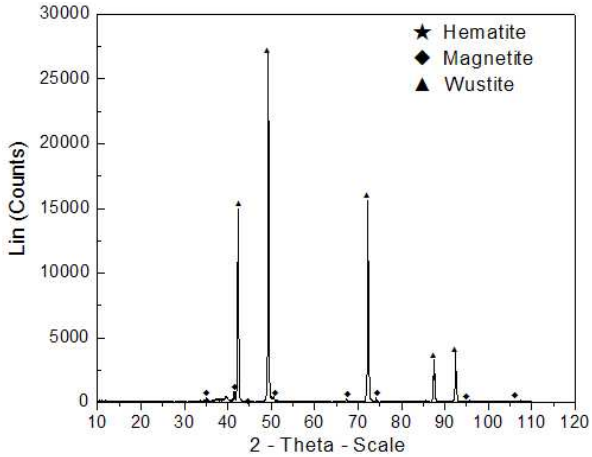

Figure A-15 XRD pattern of reduced particle at 1750 K, t = 2020 ms

ACKNOWLEDGEMENTS

The past four and a half years study will definitely be one of the most memorable periods in my life. The most important academic achievements could be expressed by words in this thesis, but the greatest fortune in my heart is the study process, during which I have got a lot of sincere help and support from my supervisors, colleagues, industrial partner and my family. This project couldn't be done without their kind help. I would like to express my deepest gratitude to all the people who helped me.

First of all, I would like to thank my promoter Prof. dr. Rob Boom, and co-promoter and daily supervisors Associate Prof. dr. Yongxiang Yang for their tremendous guidance and encouragement. Prof. Boom impressed me as a supervisor with great humor and wisdom. When I need his help, Prof. Boom has always been patient, enthusiastic and helpful to me. He is an outstanding teacher, for that he could always use a simple example to let me understand a complicated theory and sometimes use his humor. Prof. Yang has provided a great support for me. He was always there, whenever I met difficulties. When I was off the track on my way to success, he was always the person who takes me back. Without his kind help, I couldn't complete the project so quickly. The other person who deserves special thanks is Dr. Yanping Xiao who shared her rich experience of laboratory experiment with me. In addition, her encouragement gave me a great sense of uplift at every time when I get depressed.

I would like to express my thankful to Prof. Zongshu Zou who was my supervisor in Northeastern University when I was a graduate student for Master's degree. I learned a lot from him and with his guidance I became to get interested in metallurgy field. I would also like to thank Prof. Xiaoming Wang who is the other financial supporter besides Prof. Zongshu Zou when I study abroad. Without their great support, I couldn't get the opportunity of PhD study in TU Delft. Prof. Nan Wang accompanied with me when I came to the Netherlands for the first time. I could never forget the talk that evening. She told me how to study and live abroad. I appreciate her very much. I also thank Dr. Zhiguo Luo and Dr. Qiang Li for their help when I studied in Northeastern University.

Sincerely thanks to Mrs. Olga Wens-van Swol for her kind help during my PhD life. I would also like to thank our technician John van den Berg for his kind support to my experiments. The other person deserving my special thank is Henk Jansen who is working at Brooks instrument in the Netherlands. In the following days, he always tried his best to help me to solve the problems of the mass flow meters I met. He is always ready to help others. When I was designing my experimental set-up, Steve van Herk gave me a lot of help. Sincerely thanks to him.

Our industrial partner Tata steel fully supported our research. Their participation and contribution are greatly appreciated. Dr.Christiaan Zeilstra, Ir. Koen Meijer, Ir. Jan van der Stel and Dr. Ir. Jeroen Link, thank you very much for your valuable comments and suggestions.

In my PhD life, I was lucky to work with many very kind colleagues. I want to express my particular appreciation to Qingshi Song, Zhan Zhang, Guoliang Zhu, Liang Zhang, Allert Adema, Yulia Meteleva-Fischer who are enthusiastic and generous persons. They give me a lot of supports to my experiments. I will never forget the happy time shared with them. They always provided helps at any time when I needed.

I would like to appreciate some special friends met in The Netherlands, Dongjuan Xiao, Hong Liu, Lei Zu, Chongxin Yuan, Huajun Fan, Chuangxin Zhao, Zhiguang Huan, He Gao, Xuhong Qiang, Xu Jiang, Xiwen Liu, Mo Zhang, Fei Cao, Xiaoyan Yang, Xiaoye Zhuang, Hu Liang, Weixin Zhang, Tao Xu, Yang Xu etc. We had a lot of fun time together.

I appreciate the hospitality of our university and the Materials innovation institute. This research was carried out under project number M41.5.09327 in the framework of the Research Program of the Materials innovation institute M2i (www.m2i.nl). I also would like to thank China Scholarship Council for providing the scholarship for the PhD study at TU Delft.

Last but not least, I want to express my sincerest appreciation to my family. Firstly, I would like to thank my father Shaode Qu. Thank him for bringing me to this wonderful world and giving me his great love. Although he has been to the other world for many years, I feel that he is always with me. I would like to thank my mother Shuqin Shao. She is the most important person and the first teacher in my life. With her love and protection, I have such a wonderful and happy life. Thank my little sister Yingchun, she acts as not only a little sister but also a good friend. I would also like to thank my husband, Dapeng, for his support and love!

Yingxia Qu

CURRICULUM VITAE

Yingxia Qu

Born on 14th June, 1983
In Donggang, Liaoning Province, China

BSc. (2002-2006)

Materials Science and Metallurgical Engineering, Northeastern University, Shenyang, China. Supervisor: Prof. dr. Zongshu Zou.

MSc. (2006-2008)

Materials Science and Metallurgical Engineering, Northeastern University, Shenyang, China. Supervisor: Prof. dr. Zongshu Zou.

PhD. (2008-2013)

Materials Science and Engineering, Delft University of Technology, the Netherlands. Supervisors: Prof. dr. Rob Boom and Dr. Yongxiang Yang.